Prague Medical REPORT

(Sborník lékařský)

Multidisciplinary Biomedical Journal
of the First Faculty of Medicine,
Charles University

Vol. 126 (2025) No. 3

Prague Medical Report (Prague Med Rep) is indexed and abstracted by Index-medicus, MEDLINE, PubMed, EuroPub, CNKI, DOAJ, EBSCO, and Scopus.

Abstracts and full-texts of published papers can be retrieved from the World Wide Web (https://pmr.lf1.cuni.cz).

Development, Implementation, Pharmacokinetic and Safety Evaluation of an Immunotherapeutic Treatment for COVID-19: Double-blind Randomized Placebo-controlled Trial

Guillermo Alberto Keller[1,2,3], Silvia Miranda[3], Adolfo Rafael De Roodt[1], Roxana Salvi[2], Ivana Colaianni[2], Elizabeth García[2], Guillermo Bramuglia[3], Leandro Calderón[1], Diego Mazza[1], Laura Lanari[1], Oscar Perez[1], Matias Fingermann[1], Guillermo Temprano[1], Guillermo Di Girolamo[3], Claudio Bonel[1], José Cristian Dokmetjian[1]

[1] Administración Nacional de Laboratorios e Institutos de Salud "Dr. Carlos G. Malbrán" (ANLIS-Malbrán), Instituto Nacional de Producción de Biológicos (INPB), Buenos Aires, Argentina;
[2] Hospital General de Agudos Donación Francisco J. Santojanni, Buenos Aires, Argentina;
[3] Instituto Alberto C. Taquini de Investigaciones en Medicina Traslacional (IATIMET), Facultad de Medicina, Universidad de Buenos Aires, Buenos Aires, Argentina

Received January 21, 2025; Accepted August 27, 2025.

Key words: Immune sera – Antitoxin – Antibodies – SARS-CoV-2 – Immunoglobulin fragments – Immunotherapy – Equine immune sera

Abstract: Passive immunotherapy has been evaluated in many infections. The present study aims to evaluate purified $F(ab')_2$ fraction of equine hyperimmune IgG (anti-SARS-CoV-2) in the treatment of coronavirus lung disease. Patients with coronavirus disease of 2019 (COVID-19) with World Health Organization (WHO) score 3, 4 or 5 up to 72 hours of evolution from the onset of symptoms were included. They were randomly assigned to anti-SARS-CoV-2 or placebo. Follow-up was performed for 28 days to assess efficacy, safety, pharmacokinetics, detection of anti-horse antibodies, circulating cytokines and determination of anti-SARS neutralizing activity. The 20 initial patients (44±14 years) were included. On the third day of treatment there was an improvement (P=0.02) in arterial saturation (95±1.6 vs. 93±2.5%) with increasing differences over time between treatments (day 8: 97±0.1 vs. 94±0.3%). The length of oxygen therapy treatment was 2±0.8 vs. 3±0.9 (0.048) in patients falling within WHO 5 category (no difference to WHO 4). Mean hospitalization was 13±2.5 vs. 14±0.8 days (P=0.095) and time to clinical improvement was 2±0.5 vs. 3±0.9 days (P=0.048) in patients with initial 5 WHO category, with no differences to patients who started with WHO stage 4. The time to nasal swab negativization was 10±2.1 vs. 12±0 day (P=0.015). No adverse reactions or intercurrences were detected. All patients presented heterophile antibodies without clinical correlate. The new treatment shows improvement in arterial saturation (days 3 to 12), and a decrease on detectable viral RNA (days 8 to 11) with good pharmacokinetic and safety profile.

This study was supported by the Instituto Nacional de Producción de Biológicos and ANLIS-Malbrán, a public state administration that groups the national health institutes.

Mailing Address: Prof. Guillermo Alberto Keller, MD., PhD., Administración Nacional de Laboratorios e Institutos de Salud "Dr. Carlos G. Malbrán" (ANLIS-Malbrán), Instituto Nacional de Producción de Biológicos (INPB), Av. Vélez Sarsfield 563, C1282AFF Ciudad Autónoma de Buenos Aires, Argentina; Phone: +54 9 11 3751-8048; e-mail: gkeller@anlis.gob.ar

https://doi.org/10.14712/23362936.2025.20

Prague Medical Report / Vol. 126 (2025) No. 3, p. 121–138

Introduction

The coronavirus pandemic caused damages in social, economic and health terms. Meanwhile, even after a decade of coronavirus research, there are still no licensed therapeutic agents. In early January 2020, Kruse (2020) advocated for therapeutic strategies in an outbreak scenario to treat the novel coronavirus originating from Wuhan. He recommended starting with options based on knowledge of immunology, to combat SARS-CoV-2 (severe acute respiratory syndrome linked to Coronavirus type 2) and treat patients under compassionate use, while conducting formal clinical trials, including the use of convalescent plasma as a potential therapy for COVID-19 (Bloch et al., 2020).

Passive immunotherapy is a well-established historical procedure introduced by von Behring in 1890, as a cure for diphtheria and tetanus using antibodies isolated from horse blood (Klein, 1894). Von Behring received the Nobel Prize in Physiology and Medicine in 1901 for his work. This approach was used with success in other major epidemics, such as the Spanish flu in 1918 (McGuire and Redden, 1918), the 1934 measles epidemic in the United States of America (le Fleming, 1937), most recently during the Middle East Respiratory Syndrome (MERS) epidemic in the Middle East in 2012 (Ko et al., 2018), SARS of viral etiology (Mair-Jenkins et al., 2015) and against Ebola in 2015 (Racine et al., 2019; Fischer et al., 2020). The strategy of using convalescent plasma in SARS-CoV-2 infection is based on the same therapeutic principle of passive immunization to neutralize the virus (Abolghasemi et al., 2020).

Immunology clearly demonstrates that antibodies in blood or plasma fraction recognize epitopes of pathogens (e.g. viruses). They neutralize or reduce the virus load along with cellular responses to prevent or eventually cure disease; therefore, antibodies are very efficient endogenous molecules to start the healing process in the human body.

For more than 100 years, the extraction and transference of specific antibodies directed against certain antigens to infected people as a passive immunization is an established therapeutic alternative for many diseases such as diphtheria, rabies, tetanus, and the Ebola virus (Fischer et al., 2020).

Although in some infectious diseases such as influenza, the most recent clinical studies did not show evidence of benefit with passive immunotherapy (Beigel et al., 2019; Davey et al., 2019). A subsequent analysis has shown that these studies presented some methodological and conceptual errors (Kanjilal and Mina, 2019). For example, both studies used material (immunoglobulins or plasma) from healthy individuals, with no history of recent infection, and therefore possibly possessing lower antibody titters, raising the necessity of the assessment of neutralizing activity. Beigel's study evaluated plasma defined as "high titter" (1:80) and Davey's study evaluated the use of high-titter immunoglobulin (quantified as amount of immunoglobulins or by affinity to viral components but not by neutralizing activity). The latter showed benefit against influenza B, against which it had higher affinity, showing that the immunoglobulin concentration is not a good unit of measurement to correlate with the neutralizing activity. Further, inhibition titters are generally considered protective if they are much higher than 1:80, with some evidence indicating that values higher than 1: 50,000 are necessary. For the periodic viral infections, the quality, rather than the quantity of antibodies, is more likely to drive efficacy (Kanjilal and Mina, 2019). Several studies have pointed out the importance of evaluating the preparations used in passive immunization through neutralization activity with a neutralizing titter ≥ 1:80 (FDA, 2023), being neutralization by ELISA IgG a valid substitute (Ko et al., 2018).

SARS-CoV-2 is a new coronavirus that poses a global threat and places unprecedented burdens on healthcare providers and the healthcare system. Until now, there is no specific and effective antiviral therapy against COVID-19 disease. From an immunological point of view, antibodies collected from patients who have recovered from COVID-19 show neutralizing activity (NAb). Passive immunization represents an alternative treatment until other drugs become available (Bloch et al., 2020). Meanwhile, the rebirth of passive immunization could be a bridge technology until effective drugs or active immunization are available (Chen et al., 2020; Duan et al., 2020; Keith et al., 2020; Roback and Guarner, 2020; Tanne, 2020; Tiberghien et al., 2020; Ye et al., 2020). Shen C. and colleagues from China were the first to report that convalescent plasma could be a treatment option for COVID-19 patients with respiratory failure (Bloch et al., 2020). Passive immunization improved the clinical situation in 5 patients where antiviral drugs or steroids were not effective. The patient's viral load decreased and became negative within 12 days after the transfusion (Bloch et al., 2020). One problem with this report was that all patients received antiviral drugs and steroids before receiving their convalescent plasma. The last treatment was done as compassionate use as no other treatment therapy worked. Therefore, the results are very difficult to interpret. Within days of this initial report, a case report from Korea showed that 2 elderly patients improved after convalescent plasma application (Ahn et al., 2020). One of the patients was a 71-year-old

man with no underlying medical conditions who was initially treated with antimalarial drugs and who needed respiratory assistance for severe pneumonia. His condition improved when he was treated with convalescent plasma from a young patient, along with steroids. The second patient, a 67-year-old woman, did not respond to initial treatments that included chloroquine, remdesivir, and oxygen therapy. She began to recover after receiving plasma and steroid therapy at the same time. A study (Duan et al., 2020) in 10 severely ill SARS-CoV-2 individuals who were transfused with 200 ml of convalescent plasma with specific neutralizing antibody titters greater than 1:640 in addition to standard supportive care, showed that the therapy was well tolerated, and it could improve clinical outcomes by neutralizing viremia. In a case series from Wuhan, 1–3 convalescent plasma infusions were also well tolerated and effective, in addition to being associated with negative pharyngeal swab (Klein, 1894; Bloch et al., 2020).

The Food and Drug Administration (FDA) has approved convalescent plasma as a treatment option for critically ill patients with COVID-19 (Tanne, 2020). The optimal dose and time point of application, as well as the clinical benefit of convalescent therapy, needs further investigation in larger, well-controlled trials. Even so, the administration of convalescent plasma has some drawbacks, such us availability of plasma and donors, the risks inherent in any transfusion (circulatory overload, acute lung injury, allergic and anaphylactic reactions, transmission of infections, non-hemolytic febrile reactions, red cell alloimmunization, transfusion hemolytic reaction), some donors develop low neutralizing antibody titters (material received from different individuals is not homogeneous). Similarly, there is no clear guideline of the minimum neutralizing value with verifiable clinical efficacy, although the FDA recommends: "When the measurement of neutralizing antibody titters is available, we recommend neutralizing antibody titters of 1:160. A 1:80 titter may be considered acceptable if an alternative matching unit is not available" (FDA, 2023).

High-dose polyclonal human immunoglobulin (25 grams per day) was also used, obtaining improved respiratory function in a case series (Cao et al., 2020). As an alternative approach (Wang et al., 2005; Luo et al., 2007; Zhou et al., 2007), antibodies of equine origin, with known safety and pharmacological properties (Klein, 1894; McGuire and Redden, 1918; Bal et al., 2015), present some advantages: greater availability, higher neutralizing titter, better homogeneity, avoiding the risk of transmission of various pathogens (human immunodeficiency virus – HIV, hepatitis B or C, etc.), and reducing the incidence of adverse reactions associated with the product after enzymatic digest which cleave the Fc fragment.

This study aims to evaluate the initial safety, pharmacokinetics, and efficacy of a hyperimmune equine serum with neutralizing activity against the SARS-CoV-2 virus.

Material and Methods

Trial design and investigational product

An adaptive phase 2/3, double-blind, parallel (1:1), placebo-controlled, multicenter clinical trial that analysed the pharmacokinetics, safety and efficacy of a sterile injectable solution product of purified $F(ab')_2$ fraction of horse IgG anti-SARS-CoV-2 (investigational product), manufactured under Good Manufacturing Practices (GMP) conforming to the guidelines recommended by ANMAT (National Regulatory Authority or National Drug Regulatory Agency), in the ANLIS Production Factory approved by ANMAT. The equine hyperimmune serum was generated from antigenic stimulation with the SARS-CoV-2 receptor binding domain (RBD) purified protein.

Participants

Hospitalized adult patients were eligible if they presented: (1) over 18 years old and under 80 years old; (2) positive results by RT-PCR for SARS-CoV-2; (3) clinical picture compatible with respiratory compromise in the form of pneumonia attributed to COVID-19 – stage 3, 4 or 5 according to the World Health Organization (WHO) scale – lasting up to 72 hours from the onset of symptoms to their evaluation to be incorporated into the study; (4) patients with good disposition towards the study and that signs the informed consent.

Exclusion criteria were: (1) patients with clinical disease corresponding to mild/asymptomatic forms (absence of radiological infiltrate and risk factors, with normal auscultation and arterial saturation of oxygen [$SatO_2$] greater than 95%); (2) patients with clinical disease corresponding to severe forms (severe pneumonia: presence of severity criteria [according to American Thoracic Society and Infectious Diseases Society of America – ATS/IDSA], one of two major or three minor criteria); (3) patients who have received other therapeutic strategies in the framework of an experimental study that make it difficult to evaluate the results obtained; (4) pregnant or lactating women; (5) women of childbearing potential not using an effective contraceptive method; (6) history of severe anaphylactic reaction with the administration of equine plasma; (7) patients with comorbidities that

Prague Medical Report / Vol. 126 (2025) No. 3, p. 121–138

justify a risk of high mortality from causes independent of SARS-CoV-2 infection (e.g. stage IV cancer); (8) patients who do not consent to participate.

Although the clinical study is designed as multicenter, the initial phase of the study (first twenty subjects) was carried out in a single care center (data were collected in Emergency Department of Hospital Santojanni).

Interventions

The "treatment group" received the administration of two doses of 10 ml of an investigational product (sterile injectable solution with neutralizing activity of SARS-CoV-2 not less than 1/5120), by slow intravenous infusion (10 ml diluted in 100 ml of physiological solution, administered during 50 to 60 minutes by slow drip), at time 0 when incorporated into the study – initial dose – and after 48 hours – second dose.

The "control group" received the administration of 10 ml of a sterile injectable saline or physiological solution with no-neutralizing activity of SARS-CoV-2 (also manufactured under Good Manufacturing Practices conforming to the guidelines recommended by ANMAT [National Regulatory Authority], in the ANLIS Production Factory approved by ANMAT), administered in similar conditions.

Outcomes

The primary objective was to demonstrate the efficacy and safety of the purified $F(ab')_2$ fraction of equine hyperimmune serum (anti-SARS-CoV-2). The primary efficacy endpoint was the change in time needed to clinical improvement, during 28 days after the assignment (time).

Secondary outcome measures include: (1) change in the number of patients in each (WHO) ordinal scale category (0 to 8 being 0 better and 8 worse) (days 7, 14 and 21 post-inclusion); (2) change in mortality rate (28 days); (3) change in mechanical ventilation requirement rate (28 days); (4) change in duration of oxygen treatment requirement (28 days); (5) change in length of hospitalization (28 days); (6) change in frequency of nosocomial infections (28 days); (7) change in lymphocyte cell count (28 days); (8) change in viral RNA negativization rate on nasopharyngeal swab test (at 7, 14, 21, and 28 days); (9) description of adverse events type and frequency (28 days); (10) requirement of additional treatments for adverse drug reactions (28 days); and based on quantification of purified $F(ab')_2$ anti-SARS-CoV-2 on different times (basal, 1, 3, 6, 24, 48, 49 and 96 hours, and on days 7, 14, 21 and 28) describing the pharmacokinetics in terms of (11) area under the curve (AUC); (12) maximum plasma concentration (C_{max}); (13) elimination half-life (t1/2); (14) elimination constant (Ke) (16).

Safety outcome measures included: number and type of adverse events, seriousness classification occurred during the 28-day follow-up period, discontinuation or suspension of infusions, and laboratory values abnormalities.

Sample size

The original sample size was determined as 200 patients (100 individuals for each group), which will allow reaching a statistical power (1-beta) of 80% with a level of significance (2 tails) of alpha = 0.05, to detect an 8-day change in time to clinical improvement in the intervention group (Grasselli et al., 2020; Onder et al., 2020). The study will be a phase 2/3 adaptive research. First, 20 subjects (1:1 ratio) were staggered, one patient at a time, so that no new patient should be included until at least 24 hours after the second administration of the last patient included. The Data Monitoring Committee for Patient Safety (CMDSP) review the safety data and interim analysis was proposed after 20, 50, 100 and 150 patients have been included in the study (given the 1:1 randomization in blocks of 10, it will correspond to the incorporation of 25, 50, and 75 patients for each branch). The current manuscript presents the partial results corresponding to the first 20 subjects of the adaptive study, where the pharmacokinetic study was carried out.

Randomization

Sequence generation: permuted block randomization to receive active treatment (purified $F[ab']_2$ fraction of equine hyperimmune serum with anti-SARS-CoV-2 neutralization activity) or placebo was performed for each block of 10 patients with a mixed 1:1 allocation. Randomization was performed through an allocation system based on random manual draw. Based on randomization, the study medication was prepared in such a way that each treatment (numbered from 1 to 200) had an indistinguishable label in terms of its content (active treatment or placebo) and with a label that clearly details the clinical study for which it will be used, the name of the producing laboratory and the number of the patient who should receive it. The patients were incorporated successively following the numerical order and receiving the treatment that was previously assigned by their number through a random mechanism.

Allocation concealment mechanism: treatment allocation was kept hidden from the professionals involved in the treatment of the patients. An envelope sealed with security sealing wax was kept in the health center guarded by a person not linked to patient care

so that in the event of an eventual need to unmask treatment in an emergency, it could be carried out.

Implementation: random allocation sequence was generated by independent personnel caring for patients. The blinded enrolment and allocation of treatment was carried out by the research team.

Blinding

The treatment was blinded for the patients, the researcher, his team and all the professionals involved in the care of the patients, as well as the personnel who carried out the determinations in laboratory samples. Active treatments (investigational product: sterile injectable solution with purified $F[ab']_2$ fraction of equine hyperimmune serum with anti-SARS-CoV-2 neutralization activity) and placebo (control solution: sterile injectable saline or physiological solution without neutralizing activity for SARS-CoV-2) were prepared in similar volumes, vials of the same characteristics and labelled in such a way that the presence or absence of the active treatment cannot be differentiated.

Ethics and trial evaluation

The study was approved by the hospital's independent ethics committee (registry identifier PRIISA.BA 2578), authorized by the National Drug Regulatory Agency (ANMAT DI-2021-2196-APN-ANMAT#MS), registered in the National Registry of Health Research (identifier: RENIS IS003268), and clinicaltrials.gov (NCT04913779).

Study procedures

After the detection of a case that meets the inclusion criteria, information was presented to the candidate in a clear way, with simple language, providing space for questions and giving the necessary time to make the decision to enter the study or not.

In the case of accepting to participate, and after signing the informed consent, a sequential number of participations in the study was assigned, immediately correlative to the last assigned number, which would determine, according to the previously designed randomization table, the treatment (blind) received for each patient. The treatment was blind for the patient, investigator and the treating medical team, who only had access to the medication previously labelled for that assigned patient number. Baseline clinical and laboratory variables were obtained and lung X-ray and/or tomography performed. Treatment was administered as infusion of a vial of 10 ml of treatment diluted in 100 millilitres of physiological solution to pass intravenously in a slow drip for 1 hour. The vial could correspond (blinded treatment) to 10 ml of placebo or control solution or 10 ml of investigational product. A second dose of treatment, with the same posology, was administered 48 hours after the first. Once the first administration was finished, the participating research subject was checked again frequently during the following 6 hours and the corresponding samples were extracted from the first 20 subjects (at time 0 min, 1 h, 3 h, 6 h, 24 h, 48 h, 49 h, 96 h, 7 days, 14 days, 21 days and 28 days) for kinetic analysis. After the treatment, the participating research subject was closely monitored by the research staff evaluating: 1) clinical status of the patient according to ordinal point scale, vital signs and general clinical assessment, laboratory analysis, existence of intercurrences/complications and their description, and development of adverse events (with special emphasis on the appearance of symptoms compatible with anaphylaxis and/or later serum sickness). At 24 h, 48 h, 49 h, 96 h, 7 days, 14 days, 21 days and 28 days, a blood sample was drawn to measure the neutralizing activity of SARS-CoV-2 and to quantify horse $F(ab')_2$ in the first 20 study participants. On days 7, 14, 21 and 28, if the patient was still hospitalized, the detection of viral RNA detected in the nasopharyngeal swab sample was evaluated. If a patient is discharged from hospital before day 28, the day was recorded, and the follow-up continued by telephone (landline/cell phone), mail and/or personal (home visit) aimed at maximizing the permanence of the subject in the study in order to record the evolution, clinical status, and adverse reactions at least until day 28 after the start of treatment.

Determination of pharmacokinetic parameters

Plasma concentration of the $F(ab')_2$ equine therapeutic product ("P") was monitored at basal conditions (pre-infusion) and at different times post-first infusion (1 h, 3 h, 6 h, 24 h, 48 h) and post second infusion (49 h and 7, 14, 21 and 28 days) in all patients. To this aim, a double antibody ELISA was carried out. High binding ELISA polystyrene plates (Corning) were coated with 2 µg of rabbit anti-equine IgG unconjugated as capture antibody (Novus Biologicals™) at pH 9.0 during 2 hours at 37 °C. Plates were blocked with 2% bovine serum albumin (BSA) in phosphate buffered saline (PBS) for 12 h at 37 °C and washed. As standard, "P" was loaded in a range of concentrations between 51,870 and 0.405 mg/l, which fit the required linearity of the assay (r^2>0.98). Standard and samples were loaded in duplicate and incubated during 1.5 h at 37 °C. Then, plates were washed with PBS-Tween 0.05% and incubated with rabbit anti-equine IgG, human-adsorbed, horseradish peroxidase (HRP) conjugated as detection antibody (Novus

Prague Medical Report / Vol. 126 (2025) No. 3, p. 121–138

Biologicals™). Tetramethylbenzidine (TMB, Invitrogen) was used as developer and HCl 1N as stopper. Finally, optical density was assessed at 450 nm. The standard (St) curve was plotted as the best fit curve of absorbance for 5 serial sample dilutions. Plasma equine $F(ab')_2$ concentrations were interpolated from the St curve and the mean results of two independent assays were expressed as mg/l. Data processing was performed using the GraphPad Prism program, version 6.0 for Windows.

From the results at the different sampling times, the following variables were calculated: AUC_{0-t}: area under the serum concentration curve between time 0 and time t (last extraction performed); $AUC_{0-\infty}$: area under the serum concentration curve, resulting from the extrapolation between time 0 and time ∞; C_{max}: maximum serum concentration; T_{max}: time in which the maximum serum concentration is reached.

Immunogenicity assessment

The detection of circulating antibodies anti horse $F(ab')_2$ and their titters were carried out in all patients at basal conditions, 14 and 28 days post first infusion employing an indirect ELISA. High binding ELISA polystyrene plates (Corning) were coated at pH 9.0 and 37 °C during 2 hours with 2 µg of an intermediate pepsin digestion product with the purpose of detecting antibodies anti equine $F(ab')_2$ but also with specificity towards possible traces of contaminants. After blocking with 3% skim milk in PBS at 37 °C for 2 h and washing with PBS, diluent (in blank wells) or samples were loaded in duplicate from 1/150 to 1/2,400 dilutions (range that fit the linearity of the assay with a r^2>0.98) and incubated at 4 °C overnight. After washing with PBS-Tween 0.05%, goat anti human IgG, horse-adsorbed, HRP conjugated (Invitrogen) was added. TMB (Invitrogen) was used as developer and HCl 1N as stopper and finally optical density was assessed at 450 nm. Then, the best fit curve of absorbance/dilutions was plotted for each sample. Titters of antibodies anti equine $F(ab')_2$ were expressed as the mean AUC of two independent assays. Data processing was performed using the GraphPad Prism program, version 6.0 for Windows.

Cytokine plasma levels

Plasma concentrations of IL-6, TNFα and IFNα were assessed by a magnetic bead multiplex assay employing the human cytokine panel HCYTOMAG-60K, in a Magpix® equipment (all Merck-Millipore). The assay was performed according to the manufacturer's instructions. Standard curves and samples were tested in duplicate. The standard curve detection ranged from 3.2 to 10,000 pg/ml for all analytes. Standards were plotted and concentrations were determined using xPONENT® software version 4.2 and expressed in pg/ml.

Statistical methods

The original sample size was determined as 200 patients (100 individuals for each group or arm), which will allow reaching a statistical power (1-beta) of 80% with a level of significance (2 tails) of alpha = 0.05, to detect a change of 8 days in time to clinical improvement in the group subject to the intervention, assuming that the control group will have an average time of 20 days and 60% will achieve clinical improvement.

Interim analysis for safety and efficacy was planned when: 20, 50, 100, and 150 patients were achieved. The patient safety control committee evaluates the result of each analysis performed to recommend the continuation or interruption of the study.

The epidemiological characteristics of the included patients were described according to the classic methodology of descriptive statistics. The discrete variables were described in percentages with 95% CI (confidence interval) and the continuous ones in means ± standard deviation.

The primary analysis of efficacy was carried out considering intention to treat and will include all patients who have been incorporated into the study and assigned to any of the therapeutic arms. Time to clinical improvement was assessed after all patients had reached day 28.

The secondary objectives related to the proportion of patients in each category of the WHO ordinal scale, the negativization of the swab sample by PCR for SARS-CoV-2 and mortality, were analysed using a Kaplan-Meier graph and compared with a log rank test.

The variables: duration of oxygen therapy (quantified in days required to supply oxygen to achieve arterial saturation greater than 92%), duration of hospital stay (quantified in days from diagnosis of SARS-CoV-2 infection to hospital discharge), and lymphocyte count (integer continuous numerical variable) were expressed as means ± standard deviation. The results obtained with the different treatments were compared with the chi-square test and with the *t*-test.

The frequency of adverse reactions was presented as the absolute risk of adverse reactions associated with each treatment and broken down into serious and non-serious reactions. If the number allows it, they were subclassified according to Medical Dictionary for Regulatory Activities (MedDRA) and discriminated by Class of Organs and Systems, High Level Grade Term and High Level Term. The adverse reactions that had required medical treatment were described individually, and based on their number, they

were grouped to quantify the risk associated with the therapeutic conduct taken as absolute risk for each treatment and relative risk.

The biological activity was evaluated by quantification of the serum neutralization *in vitro* with samples of serum extracted from the first research subjects recruited at the different times. The serum neutralizing activity was analysed as a function of time, obtaining the following pharmacokinetic parameters for each treatment: C_{max}, T_{max}, AUC_{0-t} (28 days), $AUC_{0-\infty}$, C_{max} (maximum activity equivalent to the maximum concentration found) and T_{max} (time in which maximum activity was obtained), will be obtained directly from the original data set, and AUC_{0-t} was calculated using the linear trapezoidal rule. $AUC_{0-\infty}$, was calculated as AUC_{0-t} + Ct/Ke, where Ct was the last concentration measured and the elimination rate constant, Ke, was calculated by linear regression of the log-linear portion of the serum neutralization-time curve. The half-life (t1/2) will be calculated as ln(2)/Ke.

Statistical comparisons of the titter of heterophilic antibodies at basal conditions between "study" and "control" groups were analysed applying unpaired two-tailed *t*-test using the nonparametric Kruskal-Wallis test, followed by the Mann-Whitney post-test to compare pairs. Data were expressed as medians with interquartile ranges. Statistical comparisons of titter of heterophilic antibodies and cytokine levels among time of study were analysed by one-way ANOVA and Tuckey's multiple comparison test. All analyses were performed using GraphPad Prism 6.0 software package (San Diego, CA, USA) for Windows. A P-value < 0.05 was considered statistically significant.

Results

Clinical and laboratory results

Twenty patients were recruited between 06/15/21 and 08/16/21 (Figure 1). In all cases, the patients were evaluated and received a talk with information about the clinical study individually, they were given a copy of the Informed Consent Form (ICF), they were given at least 30 minutes to read the information from the ICF, and they were offered a space to ask questions and clear up doubts and queries, and they were allowed to reflect on it. Subsequently, the level of understanding of the information provided was evaluated. No patient presented vulnerability criteria. All of them presented a positive result of detection of the SARS-CoV-2 viral genome by PCR in a nasal swab sample at the time of signing the ICF.

The patients did not present significant differences in the general characteristics, vital parameters, laboratory, symptoms at the time of inclusion, and clinical stage according to the WHO score (Table 1).

Monitoring of vital parameters (systolic and diastolic blood pressure, heart rate, respiratory rate, and

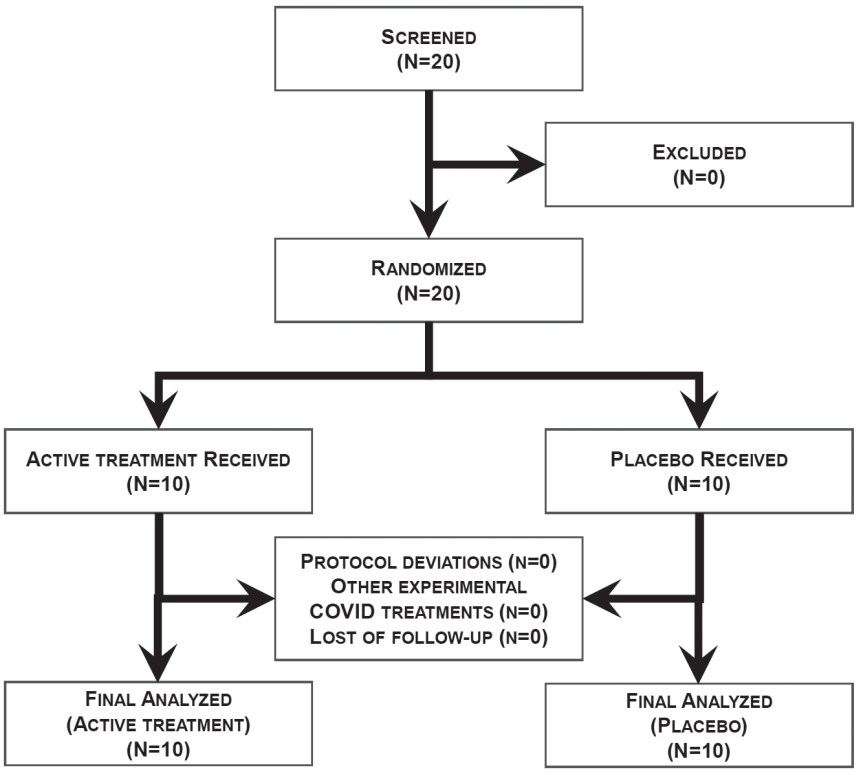

Figure 1: Consort flow-chart.

Prague Medical Report / Vol. 126 (2025) No. 3, p. 121–138

Table 1: Sample characteristics

		Total sample (N=20)	Treatment (N=10)	Control (N=10)
General	Age (years)	44 ± 14 (18–73)	44 ± 13 (26–73)	43 ± 15 (18–60)
	Gender (female)	♀ 6 (30%)	♀ 5 (50%)	♀ 1 (10%)
	Weight (kg)	84 ± 16 (54–109)	80 ± 17 (56–103)	88 ± 15 (54–109)
	Height (cm)	172 ± 9 (151–186)	168 ± 9 (151–185)	176 ± 7 (164–186)
	BMI (kg/m^2)	28 ± 5 (20–38)	28 ± 6 (20–38)	29 ± 5 (20–34)
Vital signs	SBP (mm Hg)	113 ± 12 (100–135)	118 ± 13 (100–135)	109 ± 10 (100–125)
	DBP (mm Hg)	76 ± 13 (60–100)	80 ± 13 (60–100)	72 ± 12 (60–90)
	HR (bpm)	84 ± 16 (60–104)	87 ± 18 (60–104)	81 ± 14 (60–104)
	RR (bpm)	19 ± 3 (16–24)	19 ± 3 (16–24)	20 ± 4 (16–24)
	Temperature (°C)	37 ± 1 (36–38)	37 ± 1 (36–38)	37 ± 1 (36–38)
	$SatO_2$ (%)	89 ± 2 (85–91)	89 ± 2 (86–91)	89 ± 2 (85–91)
Laboratory tests	HCT (%)	35 ± 3 (30–38)	35 ± 3 (32–38)	34 ± 2 (30–38)
	WBC (/mm^3)	7824 ± 1115 (5280–9300)	7888 ± 1213 (5280–9000)	7760 ± 1069 (6240–9300)
	PLT (×10^3/mm^3)	232 ± 70 (124–318)	230 ± 77 (124–318)	235 ± 67 (126–309)
	Glucose (mg/dl)	103 ± 9 (91–119)	101 ± 9 (91–116)	106 ± 10 (91–119)
	Urea (mg/dl)	32 ± 6 (20–41)	31 ± 7 (20–41)	33 ± 5 (26–40)
	Creatinine (mg/dl)	1.0 ± 0.1 (0.8–1.2)	1.0 ± 0.1 (0.8–1.2)	1.0 ± 0.1 (0.9–1.2)
	Prothrombine time (%)	84 ± 12 (71–103)	81 ± 12 (71–103)	87 ± 13 (72–103)
	aPTT (s)	36 ± 6 (28–45)	36 ± 6 (28–45)	36 ± 5 (30–45)
Symptoms	Cough (N, %)	12 (60%)	5 (50%)	7 (70%)
	Fever (N, %)	15 (75%)	8 (80%)	7 (70%)
	Odynophagia (N, %)	16 (80%)	9 (90%)	7 (70%)
	Dyspnoea (N, %)	13 (65%)	6 (60%)	7 (70%)
	Ageusia (N, %)	15 (75%)	7 (70%)	8 (80%)
	Anosmia (N, %)	16 (80%)	9 (90%)	7 (70%)
WHO score	5	9 (45%)	4 (40%)	5 (50%)
	4	11 (55%)	6 (60%)	5 (50%)
	3	0 (0%)	0 (0%)	0 (0%)

BMI – body mass index; SBP – systolic blood pressure; DBP – diastolic blood pressure; HR – heart rate; RR – respiratory rate; $SatO_2$ – arterial oxygen saturation; HCT – hematocrit; WBC – white blood cell count; PLT – platelet count; aPTT – activated partial thromboplastin time; WHO – World Health Organization

temperature) did not show changes of significant clinical interest. Arterial oxygen saturation showed higher values in the treated group between the third and twelfth days (Figure 2). The mean values were compatible with the absence of oxygen therapy requirement from day 3 in the treated group, which was reached in the control group from day 5.

On biochemical parameters, the treatment group presented increased lymphocyte count (day 4), decreased concentration of ferritin (days 4 and 5), and decreased D-dimer (day 4). No other significant changes were observed (Table 2). The PCR for SARS-CoV-2 test on nasal swab showed an earlier negative result in the treated patients, presenting a decrease in it on day 8 to 11, in such a way that the patients treated with anti-SARS-CoV-2 presented a 50% negativization of the swabs, compared to the control group (Table 3).

Individuals in the treatment group presented more frequently lower WHO clinical categories in the 3rd to 5th days of treatment (all the individuals in the treatment group had a WHO score of 3 on day 4, while 30% of the control sample still had a WHO score of 4). Hospitalization time did not present significant differences between the treated groups, although a lower proportion of hospitalized patients can be observed in the treatment group at any time of the study (Table 4).

There were no cases of altered consciousness, impaired ventilatory mechanics, inotropic drug

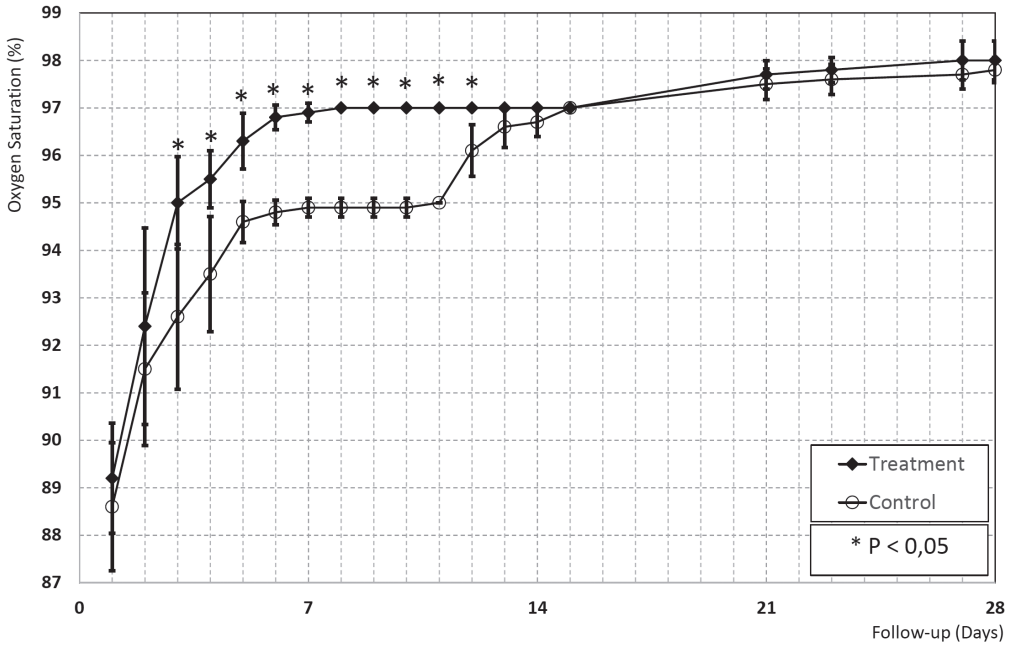

Figure 2: Arterial oxygen saturation follow-up.

Table 2: Laboratory result during follow-up

		Total sample	Treatment (10)	Control (10)	P
Day 01	Lymphocytes (/mm^3)	1060 ± 239 (600–1300)	1020 ± 215 (700–1300)	1100 ± 267 (600–1300)	0.47
	Neutrophils (/mm^3)	2025 ± 297 (1500–2400)	1970 ± 323 (1500–2400)	2080 ± 274 (1600–2400)	0.42
	Urea (mg/dl)	29 ± 7 (20–43)	29 ± 8 (20–40)	29 ± 7 (20–43)	0.95
	LDH (IU/l)	269 ± 86 (100–390)	276 ± 71 (120–370)	262 ± 102 (100–390)	0.73
	CRP (mg/l)	0.35 ± 0.16 (0.13–0.57)	0.29 ± 0.15 (0.13–0.55)	0.40 ± 0.15 (0.13–0.57)	0.11
	Ferritin (ng/ml)	360 ± 79 (210–480)	360 ± 68 (290–480)	360 ± 92 (210–470)	1.00
Day 04	D-dimer (ng/dl)	273 ± 108 (110–460)	276 ± 117 (120–460)	269 ± 104 (110–430)	0.89
	Lymphocytes (/mm^3)	1305 ± 267 (800–1700)	1460 ± 152 (1300–1700)	1100 ± 283 (800–1400)	**0.04***
	Neutrophils (/mm^3)	1885 ± 243 (1600–2300)	1960 ± 288 (1600–2300)	1740 ± 167 (1600–2000)	0.18
	Urea (mg/dl)	33 ± 8 (20–44)	35 ± 6 (27–42)	32 ± 10 (20–43)	0.65
	LDH (IU/l)	213 ± 66 (110–340)	188 ± 52 (110–240)	256 ± 98 (120–340)	0.21
	CRP (mg/l)	0.19 ± 0.07 (0.10–0.28)	0.22 ± 0.04 (0.15–0.26)	0.22 ± 0.08 (0.13–0.28)	0.85
	Ferritin (ng/ml)	345 ± 104 (210–490)	254 ± 77 (210–390)	442 ± 61 (340–490)	**<0.01***
	D-dimer (ng/dl)	213 ± 89 (110–370)	152 ± 28 (110–180)	316 ± 55 (250–370)	**<0.01***
Day 05	Lymphocytes (/mm^3)	1330 ± 258 (900–1700)	1400 ± 274 (1000–1700)	1260 ± 251 (900–1500)	0.42
	Neutrophils (/mm^3)	1920 ± 244 (1600–2300)	1820 ± 192 (1600–2100)	2020 ± 268 (1600–2300)	0.21
	Urea (mg/dl)	32 ± 8 (22–44)	27 ± 5 (22–33)	37 ± 7 (29–44)	0.04
	LDH (IU/l)	203 ± 48 (130–320)	204 ± 11 (190–220)	202 ± 71 (130–320)	0.95
	CRP (mg/l)	0.15 ± 0.06 (0.10–0.26)	0.13 ± 0.03 (0.10–0.19)	0.18 ± 0.07 (0.10–0.26)	0.20
	Ferritin (ng/ml)	341 ± 93 (230–480)	270 ± 39 (230–320)	412 ± 74 (290–480)	**0.01***
	D-dimer (ng/dl)	192 ± 81 (110–320)	152 ± 33 (110–190)	232 ± 97 (110–320)	0.12
Day 09	Lymphocytes (/mm^3)	1650 ± 280 (1300–2200)	1850 ± 265 (1600–2200)	1517 ± 214 (1300–1900)	0.06
	Neutrophils (/mm^3)	1910 ± 311 (1500–2400)	1700 ± 231 (1500–1900)	2050 ± 288 (1600–2400)	0.08
	Urea (mg/dl)	32 ± 7 (25–44)	39 ± 6 (30–44)	28 ± 4 (25–34)	**0.01***
	LDH (IU/l)	186 ± 67 (100–290)	145 ± 47 (100–190)	213 ± 68 (130–290)	0.12
	CRP (mg/l)	0.16 ± 0.03 (0.11–0.21)	0.15 ± 0.04 (0.11–0.19)	0.17 ± 0.04 (0.11–0.21)	0.60
	Ferritin (ng/ml)	276 ± 52 (200–340)	295 ± 65 (200–340)	263 ± 43 (210–340)	0.38
	D-dimer (ng/dl)	134 ± 25 (100–180)	150 ± 22 (130–180)	123 ± 23 (100–160)	0.11

Prague Medical Report / Vol. 126 (2025) No. 3, p. 121–138

		Total sample	Treatment (10)	Control (10)	P
Day 10	Lymphocytes (/mm^3)	1750 ± 284 (1300–2100)	1883 ± 223 (1500–2100)	1550 ± 265 (1300–1900)	0.06
	Neutrophils (/mm^3)	1960 ± 227 (1600–2400)	2050 ± 226 (1800–2400)	1825 ± 171 (1600–2000)	0.13
	Urea (mg/dl)	29 ± 8 (21–43)	30 ± 8 (21–43)	28 ± 10 (22–42)	0.67
	LDH (IU/l)	153 ± 31 (100–210)	142 ± 27 (100–170)	170 ± 32 (140–210)	0.17
	CRP (mg/l)	0.16 ± 0.03 (0.11–0.19)	0.16 ± 0.04 (0.11–0.19)	0.16 ± 0.02 (0.13–0.18)	0.88
	Ferritin (ng/ml)	258 ± 44 (200–330)	242 ± 26 (220–290)	283 ± 59 (200–330)	0.17
	D-dimer (ng/dl)	76 ± 24 (50–120)	75 ± 23 (50–110)	78 ± 30 (50–120)	0.88
Day 22	Lymphocytes (/mm^3)	1925 ± 240 (1600–2300)	1940 ± 196 (1700–2300)	1910 ± 288 (1600–2300)	0.79
	Neutrophils (/mm^3)	2035 ± 289 (1500–2400)	1970 ± 298 (1500–2400)	2100 ± 279 (1700–2400)	0.33
	Urea (mg/dl)	33 ± 8 (20–44)	33 ± 10 (20–44)	34 ± 6 (26–44)	0.83
	LDH (IU/l)	151 ± 33 (100–190)	156 ± 31 (110–190)	145 ± 35 (100–190)	0.46
	CRP (mg/l)	0.15 ± 0.02 (0.11–0.19)	0.14 ± 0.03 (0.11–0.19)	0.15 ± 0.02 (0.11–0.17)	0.56
	Ferritin (ng/ml)	194 ± 29 (150–240)	191 ± 29 (150–240)	196 ± 30 (150–240)	0.71
	D-dimer (ng/dl)	74 ± 15 (50–90)	71 ± 15 (50–90)	77 ± 16 (50–90)	0.40
Day 28	Lymphocytes (/mm^3)	1950 ± 278 (1600–2300)	1950 ± 284 (1600–2300)	1950 ± 288 (1600–2300)	1.00
	Neutrophils (/mm^3)	2030 ± 303 (1600–2400)	2010 ± 338 (1600–2400)	2050 ± 280 (1700–2400)	0.78
	Urea (mg/dl)	31 ± 8 (20–44)	36 ± 7 (25–44)	26 ± 5 (20–35)	**<0.01***
	LDH (IU/l)	145 ± 31 (100–190)	145 ± 38 (100–190)	144 ± 24 (110–180)	0.94
	CRP (mg/l)	0.14 ± 0.03 (0.10–0.19)	0.13 ± 0.03 (0.10–0.19)	0.15 ± 0.02 (0.11–0.17)	0.07
	Ferritin (ng/ml)	197 ± 30 (150–240)	207 ± 24 (170–240)	187 ± 33 (150–240)	0.14
	D-dimer (ng/dl)	71 ± 15 (50–90)	71 ± 14 (50–90)	71 ± 16 (50–90)	1.00

*statistically significant differences; LDH – lactate dehydrogenase; CRP – C-reactive protein

Table 3: Percentage of positivity of nasal swabs throughout the follow-up

Day	Total	Treatment	Control
Basal	20 (100%)	10 (100%)	10 (100%)
4	20 (100%)	10 (100%)	10 (100%)
8	15 (75%)	5 (50%)	10 (100%)
12	0 (0%)	0 (0%)	0 (0%)
15	0 (0%)	0 (0%)	0 (0%)
21	0 (0%)	0 (0%)	0 (0%)
28	0 (0%)	0 (0%)	0 (0%)

requirements, mechanical respiratory support requirements, or other criteria for moving to an intensive care unit in any of the groups arms.

No adverse reactions were reported in any of the research subjects studied through the 28-day follow-up. Adverse reactions were actively investigated through questioning, laboratory controls, and spontaneous reports, not registering any type of event.

There were no differences regarding the total duration of hospitalization, time to clinical improvement or time required for supplemental oxygen therapy. A shorter time was found for nasal swabs to become negative in the treatment group. A disaggregated analysis based on severity at patient admission showed that those with greater severity (WHO score 5) had less time to obtain clinical improvement, and less time on oxygen therapy (Table 5).

Neutralizing activity

The samples obtained from blood after the administration of the product did not present detectable neutralizing activity by means of the method used in any of the post-administration times.

Safety controls

Patients were evaluated by physical examination and questioning daily during hospitalization and periodically

Table 4: WHO clinical category classification and hospital discharge follow-up comparison between groups

Day	Treatment				Control			
	hospitalized			ambulatory	hospitalized			ambulatory
	WHO 5	WHO 4	WHO 3	WHO <3	WHO 5	WHO 4	WHO 3	WHO <3
Basal	4 (40%)	6 (60%)	–	–	5 (50%)	5 (50%)	–	–
1	4 (40%)	6 (60%)	–	–	5 (50%)	4 (40%)	1 (10%)	–
2	1 (10%)	5 (50%)	4 (40%)	–	1 (10%)	7 (70%)	2 (20%)	–
3	–	2 (20%)	8 (80%)	–	1 (10%)	5 (50%)	4 (40%)	–
4	–	–	10 (100%)	–	–	3 (30%)	7 (70%)	–
5	–	–	10 (100%)	–	–	1 (10%)	9 (90%)	–
6	–	–	10 (100%)	–	–	–	10 (100%)	–
7	–	–	10 (100%)	–	–	–	10 (100%)	–
8	–	–	10 (100%)	–	–	–	10 (100%)	–
9	–	–	10 (100%)	–	–	–	10 (100%)	–
10	–	–	10 (100%)	–	–	–	10 (100%)	–
11	–	–	6 (60%)	4 (40%)	–	–	10 (100%)	–
12	–	–	5 (50%)	5 (50%)	–	–	10 (100%)	–
13	–	–	5 (50%)	5 (50%)	–	–	9 (90%)	1 (10%)
14	–	–	5 (50%)	5 (50%)	–	–	9 (90%)	1 (10%)
15	–	–	4 (40%)	6 (60%)	–	–	2 (20%)	8 (80%)
16 to 28	–	–	–	10 (100%)	–	–	–	10 (100%)

WHO – World Health Organization

Table 5: Time to different parameters of clinical improvement

		Total	Treatment	Control	P
Length of hospitalization (days)	total	13 ± 1.9 (10–15)	13 ± 2.5 (10–15)	14 ± 0.8 (12–15)	0.095
	WHO 5	14 ± 1.8 (10–15)	13 ± 2.4 (10–15)	14 ± 0.5 (14–15)	0.209
	WHO 4	13 ± 2.1 (10–15)	13 ± 2.7 (10–15)	14 ± 0.9 (12–14)	0.389
Time to clinical improvement (days)	total	8 ± 5.4 (2–15)	8 ± 5.7 (2–15)	9 ± 5.4 (2–14)	0.968
	WHO 5	3 ± 0.9 (2–4)	2 ± 0.5 (2–3)	3 ± 0.9 (2–4)	**0.048**
	WHO 4	13 ± 2.1 (10–15)	13 ± 2.7 (10–15)	14 ± 0.9 (12–14)	0.389
Time to nasal swab negativization (days)	total	11 ± 1.8 (8–12)	10 ± 2.1 (8–12)	12 ± 0.0 (12–12)	**0.015**
	WHO 5	11 ± 1.8 (8–12)	10 ± 2.3 (8–12)	12 ± 0.0 (12–12)	0.182
	WHO 4	11 ± 1.9 (8–12)	10 ± 2.2 (8–12)	12 ± 0.0 (12–12)	0.076
Length of oxygen therapy (days)	total	3 ± 1.2 (2–6)	3 ± 0.8 (2–4)	4 ± 1.3 (2–6)	0.057
	WHO 5	3 ± 0.9 (2–4)	2 ± 0.5 (2–3)	3 ± 0.9 (2–4)	**0.048**
	WHO 4	4 ± 1.3 (2–6)	3 ± 0.8 (2–4)	4 ± 1.6 (2–6)	0.247

WHO – World Health Organization

(every 3 to 7 days) during the outpatient period until 28 days' post administration.

Neither the physical examination, interrogation nor laboratory showed elements compatible with adverse events that motivated his report.

There were no cases of complications, hemodynamic decompensation, deterioration of consciousness, deterioration of respiratory mechanics, or any other cause that could motivate the transfer of a patient to the intensive care unit.

This behaviour did not present differences between both therapeutic groups.

Pharmacokinetics analysis

The 10 patients in the treated group presented detectable plasma concentrations of equine IgG after

Prague Medical Report / Vol. 126 (2025) No. 3, p. 121–138

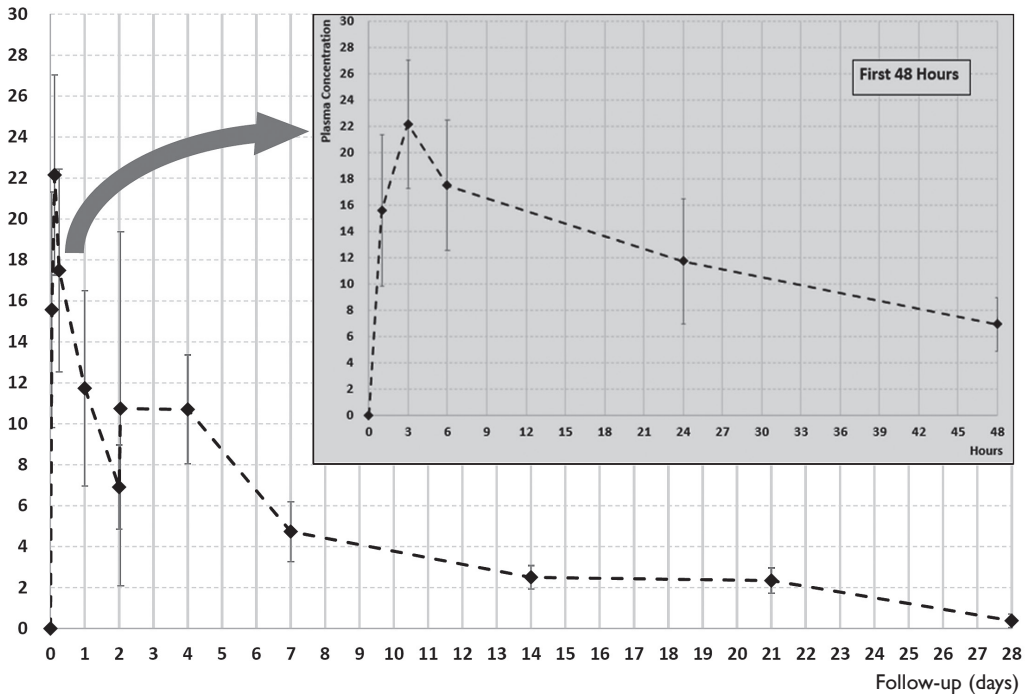

Figure 3: Mean plasma concentration over time.

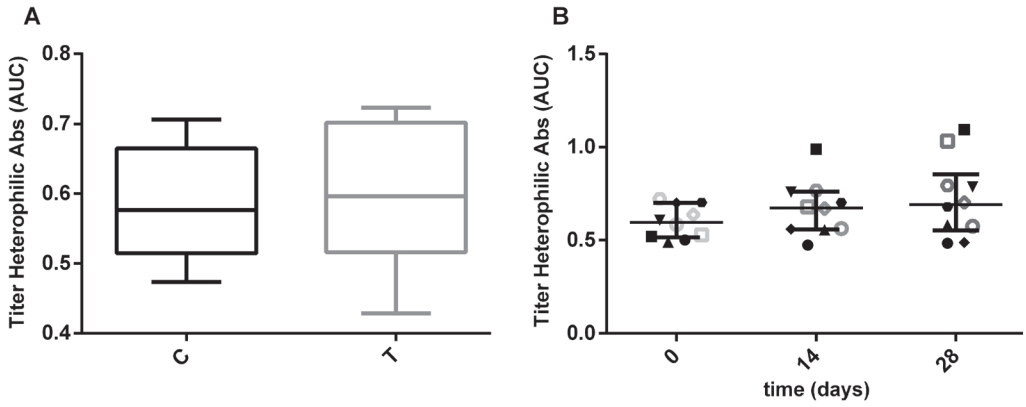

Figure 4: Titter of human heterophilic antibodies against equine immunoglobulins (HHA-HI) in the basal samples.

Table 6: Comparative evolution of heterophilic antibodies titter

	All patients	Control	Treatment				
	basal	basal	basal	day 14		day 28	
Individuals	20	10	10	10	Δ%	10	Δ%
Mean	0.5917	0.5833	0.6002	0.6724	18.67	0.7223	23.48
SD	0.0816	0.0777	0.0886	0.1472	35.80	0.2105	44.70
SEM	0.0182	0.0246	0.0280	0.0465	11.32	0.0666	14.14
Min	0.4734	0.4734	0.4900	0.4748	–20.00	0.4848	–30.50
25% percentile	0.5196	0.5145	0.5162	0.5598	–4.10	0.5540	–3.25
Median	0.5832	0.5764	0.5962	0.6748	5.60	0.6913	10.00
75% percentile	0.6736	0.6645	0.7016	0.7616	37.43	0.8543	45.73
Max	0.7231	0.7062	0.7231	0.9893	89.90	1.0940	110.00
Inferior limit 95% CI	0.5536	0.5278	0.5367	0.5671	–6.94	0.5717	–8.50
Superior limit 95% CI	0.6299	0.6389	0.6636	0.7777	44.28	0.8728	55.46

SD – standard deviation; SEM – standard error of the mean; CI – confidence interval

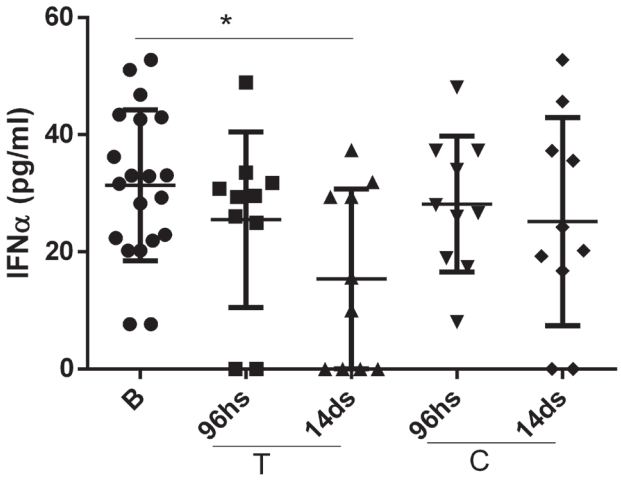

Figure 5: α-IFN concentration compared between groups throughout time.

its administration and up to 21–28 days (Figure 3). The therapeutic product was undetectable in all patients from the control group.

In the treated group, the maximum concentration (C_{max}) was reached between 1 and 3 hours (T_{max}) after the start of administration, with an average C_{max} value of 27.21 ± 7.16 (16.80 to 36.53) mg/ml. The AUC_{0-t} until the last detectable concentration (21 days for 6 patients and 28 days for 4 patients) was 2,903 ± 608 (1,897–3,804) mg/l×h, with a residual area of 22.33 ± 31.67 (0–81.10) mg/l×h and the $AUC_{0-\infty}$ of 1,925 ± 609 (1,897–3,830) mg/l×h. The Ke was quantified at –0.018 ± 0.007 (–0.007 to –0.027), correlating with a terminal elimination half-life (t1/2) of 47 ± 22 (26 to 94) hours (4 or 5 plasma concentrations were used as minimum to Ke estimation). The total clearance was 1.435 ± 0.501 (0.394 to 2.329) ml/min. The apparent volume of distribution (Vd) was 5.33 ± 2.29 (2.36 to 10.62) liters.

Immunopharmacology

The results obtained showed the presence of human heterophilic antibodies against horse IgG (HHA-HI) in the basal samples of the 20 patients analysed (treatment and control groups). Relative titter expressed as mean AUC value of two assays was 0.59 ± 0.08 (0.47 to 0.72). There was no difference between the control and treatment groups (Figure 4, Table 6).

The equine anti-$F(ab')_2$ antibody titter in the patients who received the product was studied as a function of time (Figure 5). Statistical analysis showed no significant differences between study times using ANOVA and Tuckey's multiple comparisons test (Table 6).

Table 7 shows the individual results at each time expressed as the average AUC value of two measurements, and the percentage of the variation of AUC with respect to baseline (Δ%), where: $\Delta\% = ([AUC_{Time} - AUC_{Basal}]/AUC_{Basal})\times 100$. Results showed that 5/10 patients maintained (±10%) post-infusion the levels of anti-equine antibodies detected in basal conditions (P1, P4, P16, P17, and P19), 2/10 (P12 and P13) showed a mild increase around 19–30%, 2/10 showed a greater increase around 95–100% (P7 and P8) and 1/10 (P14) diminished 30% the titter of anti-equine antibodies.

Determination of cytokine plasma levels

Plasma concentrations of IL-6, TNFα and IFNα were assessed at t = 0, t = 96 h and t = 14 days in all patients. The kinetics of plasma IFNα levels may

Table 7: Individual variation of the titter of heterophilic antibodies anti horse over time

Patient code	Basal	14 days		28 days	
	AUC	AUC	Δ%	AUC	Δ%
P01	↓ 0.5019	↓ 0.4748	–5.3	↓ 0.4848	–3.2
P04	0.5843	0.5626	–3.7	0.5760	–1.4
P07	0.5210	↑ 0.9893	+89.9	↑ 1.0940	+110.0
P08	0.5300	0.6790	+75.0	↑ 1.0335	+95.0
P12	↓ 0.4800	↓ 0.5569	+13.7	0.5830	+19.0
P13	0.6081	0.7595	+24.9	0.7863	+29.3
P14	0.7009	0.5608	–20.0	↓ 0.4880	–30.5
P16	0.6387	0.6706	+5.0	0.7032	+10.1
P17	↑ 0.7035	0.7029	+1.0	0.6794	–3.4
P19	↑ 0.7231	↑ 0.7679	+6.2	0.7945	+9.9

The titter of human heterophilic antibodies anti horse IgG (HHA-HI) was expressed as the mean area under the curve (AUC) of the best fit curve of absorbance for 5 serial sample dilutions in indirect ELISA. Arrows point out values below or above of interquartile range. (↑) greater than 75% percentile; (↓) lesser than 25% percentile

Prague Medical Report / Vol. 126 (2025) No. 3, p. 121–138

Table 8: Cytokines determination over time

		α-IFN	IL-6	α-TNF
All (N=20)	basal	31.36 + 12.89 (7.67–52.78)	1.03 + 1.10 (0.40–5.00)	8.60 + 3.09 (4.00–13.79)
Treatment (N=10)	96 h	25.50 + 14.96 (0.00–48.94)	0.63 + 0.11 (0.50–0.88)	8.46 + 2.87 (4.00–12.74)
	14 days	15.38 + 15.37 (0.00–37.40)	0.94 + 0.60 (0.45–2.02)	8.08 + 2.81 (4.00–12.10)
Control (N=10)	96 h	28.16 + 11.61 (8.00–48.08)	0.79 + 0.54 (0.40–2.01)	7.31 + 3.04 (4.00–10.74)
	13 days	25.18 + 17.75 (0.00–52.78)	1.95 + 0.56 (0.40–1.95)	7.22 + 3.43 (4.00–11.33)

mirror the course of the patient's innate antiviral response. Having discriminated between treated and control patients from previous pharmacokinetic (PK) studies, plasma IFNα levels among baseline (B), treated (96 h and 14 days) and controls (96 h and 14 days) were compared. The population distribution of the results is shown in Table 8 and Figure 5. Results showed that the basal levels of IFNα from both groups of patients were similar. In addition, IFNα levels peaked at t = 0 (oscillating between 7.660 pg/ml and 52.779 pg/ml), while for others, it peaked at t = 96 h (maximum value in the treated group: 48.936 pg/ml and in the control group: 48.08 pg/ml). Despite these variations, plasma levels of IFNα in the treated group decreased significantly after 14 days with respect to the baseline ($P<0.05$). The concentration of IFNα remained constant along the study.

The plasmatic levels of IL-6 and TNFα represent markers of systemic inflammatory response in severe cases SARS-Cov2 infection. Table 8 shows the population distribution of plasma levels of IL-6 and TNFα respectively. Data indicated that, in the present cohort, all patients showed low circulating levels of these cytokines, either at baseline or along the study in both groups.

Discussion

Passive immunotherapy is an old tool, and also a well-known, well-studied tool when a new therapy approach is needed to easy to develop a treatment on a larger scale, with properties that are largely known (Pan et al., 2020; Piccoli et al., 2020). This type of therapy includes different variants that can be classified into general groups: use of human convalescent plasma, use of animal polyclonal immunoglobulins, and specific monoclonal antibodies. Convalescent plasma has advantages (species similarity, source study feasibility, lower cost of obtaining), and disadvantages (risk of disease transmission, lower neutralizing titter, higher infusion volumes required, hemodynamic and hypersensitivity adverse effects). At the opposite pole, monoclonals offer great advantages (extremely high specificity and neutralizing power, lower volume requirement, lower risk of disease transmission), and disadvantages (selectivity of the neutralization point that can present mutations and therefore resistance, very high production cost, longer development time, less predictable pattern of adverse effects). Polyclonal antibodies of equine origin present an intermediate pattern between both groups, providing great advantages such as high specificity and neutralizing activity, lower infusion volumes required, combined with the possibility of blocking several points (and less possibility of resistance or phenomena of escape), and lower production cost (compared to monoclonals), possibility of rapid development and scaling of the product. For these reasons, this tool should be taken into account whenever a pathogen spreads rapidly, generating an epidemic and/or pandemic outbreak faster than the development capacity of other new specific therapies (Casadevall, 2002; Hussen et al., 2020).

Although the strategy of using this type of tool has been initially developed by several research groups (250 MEDLINE publications linking the MeSH ("Immunoglobulin Fragments" [Mesh] AND "SARS-CoV-2"[Mesh]), few groups have reached the clinical phase, and none to our knowledge have simultaneously reported pharmacokinetics, clinical effects, immunological effects, and inflammatory markers (Piechotta et al., 2020). This manuscript shows the pharmacological properties of a biological drug based on $F(ab')_2$ fragments of polyclonal antibodies of equine origin with anti-SARS-CoV-2 neutralizing activity, describing pharmacokinetics, clinical efficacy, neutralizing activity, effect on neutralization of nasal swabs, correlation with cytokine concentration, safety and adverse event profile, and immunopharmacology.

The study was able to demonstrate a reduction in time needed to clinical improvement, during 28 days after the assignment in the WHO category 5 subgroup of this small sample of 20 initial patients. The results in this subgroup (statistically significant despite the small initial number of patients) adds important evidence in favour of passive immunotherapy in patients with

severe COVID-19 disease. These findings are in line with what was previously reported, according to which passive immunization strategies seem to provide improvement only in patients with severe symptoms, where it has also been shown that it is necessary to report more data to develop sufficient evidence to make recommendations (Piechotta et al., 2020; Libster et al., 2021).

There was no evidence of shorter duration of oxygen therapy, but there was evidence of improvement in arterial saturation measured between days 3 and 12. This contrasts with studies that showed effects in reducing the duration and severity of some episodes, although our work did not analyse a population with prolonged COVID (Cimellaro et al., 2022).

Time to viral clearance (negative SARS-CoV-2 RT-PCR test) is a marker of great interest to assess the efficacy of antiviral treatment. To our knowledge, this is the first study to show (in a clinical study with $F[ab']_2$ products) a decrease in the proportion of patients with viral RNA detected on days 8 to 11 (Deng et al., 2023), which had been suggested in experimental models with other coronaviruses and in other infections (Zhou et al., 2007; Zhao et al., 2017).

Although, the effects on mortality, use of mechanical ventilation, and other complications were not evaluable due to the absence of similar outcomes in the small group studied, we study and found no evidence of a decrease in hospital stay, like previous studies (Deng et al., 2023).

Pharmacokinetic parameters, including maximum concentration and T_{max} (1 to 3 hours), AUC to last time (21 to 28 days) with low residual area, and terminal elimination half-life (t1/2 = 47 hours) are as expected and reported. Widely with this type of products, in the same way that they allow expecting a sustained therapeutic effect with the dosage regimen used (Deng et al., 2023).

Inflammatory parameters show a gradual post-treatment reduction that is greater for α-IFN in the treated group. Although IL-6 and α-TNF levels also decreased with treatment, the baseline determination was already low and did not correlate with previously reported cases of severity (>30 pg/ml) (Galván-Román et al., 2021). From another point of view, cytokine concentrations are an additional safety parameter, showing that the patients did not present an increase in the profile of pro-inflammatory cytokines analysed (IL-6, TNFα) as a consequence of the administration of the research product (behaving similarly to the untreated control group). While the group of treated patients presented a significant decrease in IFNα plasma levels 14 days after starting treatment, which suggests a favourable evolution of the infectious process (Krämer et al., 2021).

It should be remembered that the research product (obtained from plasma horses) was processed to remove the Fc portion of IgG by pepsin digestion, followed by partial purification of the $F(ab')_2$ fragment, a proven technology used in anti-venom $F(ab')_2$ products with no records of hypersensitivity issues and decades of excellent safety records. The safety of the treatment was actively monitored and showed no differences between arms, similar to studies performed with plasma and monoclonal antibodies (Bal et al., 2015; Deng et al., 2023).

The presence of human heterophile antibodies against horse immunoglobulins (HHA-HI) in healthy individuals, not previously exposed to equine serum derivatives, has been previously demonstrated (Hennig et al., 2000; Herrera et al., 2005; Ayres et al., 2006). The HHA-HI are natural antibodies, capable of reacting against the $F(ab')_2$ fragment and whole horse IgG and correspond mainly to the IgG class (León et al., 2008; Sevcik et al., 2008; Pan et al., 2020). Previously, HHA-HI titter was compared between healthy volunteers and patients who received IgG or $F(ab')_2$ equine antivenom without finding differences before and after immunotherapy or between both groups (Piechotta et al., 2020). Albeit another study (Casadevall, 2002) reported titter increase at 14 and 28 days post immunization, the literature agrees that HHA-HI levels would not be related to anaphylactoid reactions. The increase in anti-equine antibodies in the detected cases does not induce an increase in the formation of immune complexes in a clinically relevant manner. Regarding the expression of the HHA-HI titter, it is worth mentioning that the cited works compare levels of HHA-HI at a single dilution of study serum, while in the present report, the HHA-HI titter is expressed in a more stringent, as AUC from a range of sample dilutions from 1/150 to 1/2,400. The presence of circulating HHA-HI reported in the present study is widely accepted in the literature and agrees with the data reported here on the 20 study patients. Although most patients do not change their HHA-HI levels after the administration of equine $F(ab')_2$, according to the results reported in this study, the production of anti-equine antibodies responds to the individual behaviour of each patient. Lastly, the existence of circulating HHA-HI constitutes a factor to be considered in the interpretation of the results of the study of the plasmatic concentration kinetics of equine $F(ab')_2$ in patients as well as in the neutralizing activity data observed in the same samples.

The emergence of strains with mutations in the spike protein has brought much concern, being able to affect the efficacy observed with monoclonal antibodies and vaccines, although possibly with less possibility of affecting the efficacy of preparations of

polyclonal origin. Even with the current availability of efficacious vaccines, the possibility of having equine antibody products may provide a therapeutic option to save lives in cases of patients with immunosuppression, insufficient immunization, and severe clinical pictures.

Hyperimmune $F(ab')_2$ concentrates are manufactured in existing facilities, using a long-proven platform technology, which could help accelerate the health system response facing an outbreak. The regulatory approval pathway could be simple, considering the existence of antivenoms regularly produced under the same conditions (same active pharmaceutical ingredient).

Limitations of the study

The hyperimmune equine $F(ab')_2$ developed provides high neutralization titters against previous known SARS-CoV-2 strains, meanwhile new strains appear periodically, so neutralizing potency should be reassessed regularly.

Until now, our study used a very small group of patients, appropriate for the pharmacokinetic evaluation and a number of inflammatory mediators and viral presence; however, it remains to continue with the trial and evaluate the effects in a larger number of patients with a multicenter design.

Conclusion

The study was able to include 20 initial patients and verify that although the primary objective has not yet been achieved, the disaggregated analysis shows that it would have been achieved in the WHO category 5 subgroup.

Regarding the secondary objectives: with the evaluated treatment, an acceptable pharmacokinetic and safety profile was verified, and a lower proportion of patients in category 4 and 5 early (day 3 to 5). There was no evidence of shorter duration of oxygen therapy, but there was evidence of improvement in arterial saturation measured between days 3 and 12, and a decrease in the proportion of patients with viral RNA detected on days 8 to 11. The effects on mortality, use of mechanical ventilation, and other complications were not evaluable. There was no evidence of a decrease in hospital stay.

References

Abolghasemi, H., Eshghi, P., Cheraghali, A. M., Imani Fooladi, A. A., Bolouki Moghaddam, F., Imanizadeh, S., Moeini Maleki, M., Ranjkesh, M., Rezapour, M., Bahramifar, A., Einollahi, B., Hosseini, M. J., Jafari, N. J., Nikpouraghdam, M., Sadri, N., Tazik, M., Sali, S., Okati, S., Askari, E., Tabarsi, P., Aslani, J., Sharifipour, E., Jarahzadeh, M. H., Khodakarim, N., Salesi, M., Jafari, R., Shahverdi, S. (2020) Clinical efficacy of convalescent plasma for treatment of COVID-19 infections: Results of a multicenter clinical study. *Transfus. Apher. Sci.* **59(5)**, 102875.

Ahn, J. Y., Sohn, Y., Lee, S. H., Cho, Y., Hyun, J. H., Baek, Y. J., Jeong, S. J., Kim, J. H., Ku, N. S., Yeom, J. S., Roh, J., Ahn, M. Y., Chin, B. S., Kim, Y. S., Lee, H., Yong, D., Kim, H. O., Kim, S., Choi, J. Y. (2020) Use of convalescent plasma therapy in two COVID-19 patients with acute respiratory distress syndrome in Korea. *J. Korean Med. Sci.* **35(14)**, e149.

Ayres, J., Barraviera, B., Calvi, S., Carvalho, R., Peracoli, M. (2006) Antibody and cytokine serum levels in patients subjected to anti-rabies prophylaxis with serum-vaccination. *J. Venom. Anim. Toxins Incl. Trop. Dis.* **12(3)**, 435–455.

Bal, C., Herbreteau, C. H., Buchy, P., Rith, S., Zaid, M., Kristanto, W., Han, V., Reynaud, C., Granjard, P., Lépine, B., Durand, C., Tambyah, P. A. (2015) Safety, potential efficacy, and pharmacokinetics of specific polyclonal immunoglobulin $F(ab')_2$ fragments against avian influenza A (H5N1) in healthy volunteers: A single-centre, randomised, double-blind, placebo-controlled, phase 1 study. *Lancet Infect. Dis.* **15(3)**, 285–292.

Beigel, J. H., Aga, E., Elie-Turenne, M. C., Cho, J., Tebas, P., Clark, C. L., Metcalf, J. P., Ozment, C., Raviprakash, K., Beeler, J., Holley, H. P. Jr., Warner, S., Chorley, C., Lane, H. C., Hughes, M. D., Davey, R. T. Jr.; IRC005 Study Team (2019) Anti-influenza immune plasma for the treatment of patients with severe influenza A: A randomised, double-blind, phase 3 trial. *Lancet Respir. Med.* **7(11)**, 941–950.

Bloch, E. M., Shoham, S., Casadevall, A., Sachais, B. S., Shaz, B., Winters, J. L., van Buskirk, C., Grossman, B. J., Joyner, M., Henderson, J. P., Pekosz, A., Lau, B., Wesolowski, A., Katz, L., Shan, H., Auwaerter, P. G., Thomas, D., Sullivan, D. J., Paneth, N., Gehrie, E., Spitalnik S., Hod, E. A., Pollack, L., Nicholson, W. T., Pirofski, L., Bailey, J. A., Tobian, A. A. (2020) Deployment of convalescent plasma for the prevention and treatment of COVID-19. *J. Clin. Invest.* **130(6)**, 2757–2765.

Cao, W., Liu, X., Bai, T., Fan, H., Hong, K., Song, H., Han, Y., Lin, L., Ruan, L., Li, T. (2020) High-dose intravenous immunoglobulin as a therapeutic option for deteriorating patients with coronavirus disease 2019. *Open Forum Infect. Dis.* **7(3)**, ofaa102.

Casadevall, A. (2002) Passive antibody administration (immediate immunity) as a specific defense against biological weapons. *Emerg. Infect. Dis.* **8(8)**, 833–841.

Chen, L., Xiong, J., Bao, L., Shi, Y. (2020) Convalescent plasma as a potential therapy for COVID-19. *Lancet Infect. Dis.* **20(4)**, 398–400.

Cimellaro, A., Addesi, D., Cavallo, M., Spagnolo, F., Suraci, E., Cordaro, R., Spinelli, I., Passafaro, F., Colosimo, M., Pintaudi, M., Pintaudi, C.; On Behalf Of The CATAnzaro LOng Covid Cataloco Study Group (2022) Monoclonal antibodies and antivirals against SARS-CoV-2 reduce the risk of long COVID: A retrospective propensity score-matched case-control study. *Biomedicines* **10(12)**, 3135.

Davey, R. T. Jr., Fernández-Cruz, E., Markowitz, N., Pett, S., Babiker, A. G., Wentworth, D., Khurana, S., Engen, N., Gordin, F., Jain, M. K., Kan, V., Polizzotto, M. N., Riska, P., Ruxrungtham, K., Temesgen, Z., Lundgren, J., Beigel, J. H., Lane, H. C., Neaton, J. D.; INSIGHT FLU-IVIG Study Group (2019) Anti-influenza hyperimmune intravenous immunoglobulin for adults with influenza A or B infection (FLU-IVIG): A double-blind, randomised, placebo-controlled trial. *Lancet Respir. Med.* **7(11)**, 951–963.

Deng, J., Heybati, K., Ramaraju, H. B., Zhou, F., Rayner, D., Heybati, S. (2023) Differential efficacy and safety of anti-SARS-CoV-2 antibody therapies for the management of COVID-19: A systematic review and network meta-analysis. *Infection* **51(1)**, 21–35.

Duan, K., Liu, B., Li, C., Zhang, H., Yu, T., Qu, J., Zhou, M., Chen, L., Meng, S., Hu, Y., Peng, C., Yuan, M., Huang, J., Wang, Z., Yu, J., Gao, X., Wang, D., Yu, X., Li, L., Zhang, J., Wu, X., Li, B., Xu, Y., Chen, W., Peng, Y., Hu, Y., Lin, L., Liu, X., Huang, S., Zhou, Z., Zhang, L., Wang, Y., Zhang, Z., Deng, K., Xia, Z., Gong, Q., Zhang, W., Zheng, X., Liu, Y., Yang, H., Zhou, D., Yu, D., Hou, J., Shi, Z., Chen, S., Chen, Z., Zhang, X., Yang, X. (2020) Effectiveness of convalescent plasma therapy in severe COVID-19 patients. *Proc. Natl. Acad. Sci. U. S. A.* **117(17)**, 9490–9496.

FDA (2023) *Investigational COVID-19 Convalescent Plasma*. Available at: https://www.fda.gov/regulatory-information/search-fda-guidance-documents/investigational-covid-19-convalescent-plasma (last accessed in September 2024).

Fischer, J. C., Zänker, K., van Griensven, M., Schneider, M., Kindgen-Milles, D., Knoefel, W. T., Lichtenberg, A., Tamaskovics, B., Djiepmo-Njanang, F. J., Budach, W., Corradini, S., Ganswindt, U., Häussinger, D., Feldt, T., Schelzig, H., Bojar, H., Peiper, M., Bölke, E., Haussmann, J., Matuschek, C. (2020) The role of passive immunization in the age of SARS-CoV-2: An update. *Eur. J. Med. Res.* **25(1)**, 16.

Galván-Román, J. M., Rodríguez-García, S. C., Roy-Vallejo, E., Marcos-Jiménez, A., Sánchez-Alonso, S., Fernández-Díaz, C., Alcaraz-Serna, A., Mateu-Albero, T., Rodríguez-Cortes, P., Sánchez-Cerrillo, I., Esparcia, L., Martínez-Fleta, P., López-Sanz, C., Gabrie, L., Del Campo Guerola, L., Suárez-Fernández, C., Ancochea, J., Canabal, A., Albert, P., Rodríguez-Serrano, D. A., Aguilar, J. M., Del Arco, C., de Los Santos, I., García-Fraile, L., de la Cámara, R., Serra, J. M., Ramírez, E., Alonso, T., Landete, P., Soriano, J. B., Martín-Gayo, E., Fraile Torres, A., Zurita Cruz, N. D., García-Vicuña, R., Cardeñoso, L., Sánchez-Madrid, F., Alfranca, A., Muñoz-Calleja, C., González-Álvaro, I.; REINMUN-COVID Group (2021) IL-6 serum levels predict severity and response to tocilizumab in COVID-19: An observational study. *J. Allergy Clin. Immunol.* **147(1)**, 72–80.e8.

Grasselli, G., Pesenti, A., Cecconi, M. (2020) Critical care utilization for the COVID-19 outbreak in Lombardy, Italy: Early experience and forecast during an emergency response. *JAMA* **323(16)**, 1545–1546.

Hennig, C., Rink, L., Fagin, U., Jabs, W. J., Kirchner, H. (2000) The influence of naturally occurring heterophilic anti-immunoglobulin antibodies on direct measurement of serum proteins using sandwich ELISAs. *J. Immunol. Methods* **235(1–2)**, 71–80.

Herrera, M., León, G., Segura, A., Meneses, F., Lomonte, B., Chippaux, J. P., Gutiérrez, J. M. (2005) Factors associated with adverse reactions induced by caprylic acid-fractionated whole IgG preparations: Comparison between horse, sheep and camel IgGs. *Toxicon* **46(7)**, 775–781.

Hussen, J., Kandeel, M., Hemida, M. G., Al-Mubarak, A. I. A. (2020) Antibody-based immunotherapeutic strategies for COVID-19. *Pathogens* **9(11)**, 917.

Kanjilal, S., Mina, M. J. (2019) Passive immunity for the treatment of influenza: Quality not quantity. *Lancet Respir. Med.* **7(11)**, 922–923.

Keith, P., Day, M., Perkins, L., Moyer, L., Hewitt, K., Wells, A. (2020) A novel treatment approach to the novel coronavirus: An argument for the use of therapeutic plasma exchange for fulminant COVID-19. *Crit. Care* **24(1)**, 128.

Klein, E. (1894) The antitoxin treatment of diphtheria: The preparation of Behring's diphtheria antitoxin. *Br. Med. J.* **2(1772)**, 1393–1397.

Ko, J. H., Seok, H., Cho, S. Y., Ha, Y. E., Baek, J. Y., Kim, S. H., Kim, Y. J., Park, J. K., Chung, C. R., Kang, E. S., Cho, D., Müller, M. A., Drosten, C., Kang, C. I., Chung, D. R., Song, J. H., Peck, K. R. (2018) Challenges of convalescent plasma infusion therapy in Middle East respiratory coronavirus infection: A single centre experience. *Antivir. Ther.* **23(7)**, 617–622.

Krämer, B., Knoll, R., Bonaguro, L., ToVinh, M., Raabe, J., Astaburuaga-García, R., Schulte-Schrepping, J., Kaiser, K. M., Rieke, G. J., Bischoff, J., Monin, M. B., Hoffmeister, C., Schlabe, S., De Domenico, E., Reusch, N., Händler, K., Reynolds, G., Blüthgen, N., Hack, G., Finnemann, C., Nischalke, H. D., Strassburg, C. P., Stephenson, E., Su, Y., Gardner, L., Yuan, D., Chen, D., Goldman, J., Rosenstiel, P., Schmidt, S. V., Latz, E., Hrusovsky, K., Ball, A. J., Johnson, J. M., Koenig, P., Schmidt, F. I., Haniffa, M., Heath, J. R., Kümmerer, B. M., Keitel, V., Jensen, B., Stubbemann, P., Kurth, F., Sander, L. E., Sawitzki, B.; Deutsche COVID-19 OMICS Initiative (DeCOI); Aschenbrenner, A. C., Schultze, J. L., Nattermann, J. (2021) Early IFN-α signatures and persistent dysfunction are distinguishing features of NK cells in severe COVID-19. *Immunity* **54(11)**, 2650–2669.e14.

Kruse, R. L. (2020) Therapeutic strategies in an outbreak scenario to treat the novel coronavirus originating in Wuhan, China. *F1000Res.* **9**, 72.

le Fleming, K. (1937) Adult serum in measles. *Br. Med. J.* **2(4003)**, 612–613.

León, G., Segura, A., Herrera, M., Otero, R., França, F. O., Barbaro, K. C., Cardoso, J. L., Wen, F. H., de Medeiros, C. R., Prado, J. C., Malaque, C. M., Lomonte, B., Gutiérrez, J. M. (2008) Human heterophilic antibodies against equine immunoglobulins: Assessment of their role in the early adverse reactions to antivenom administration. *Trans. R. Soc. Trop. Med. Hyg.* **102(11)**, 1115–1119.

Libster, R., Pérez Marc, G., Wappner, D., Coviello, S., Bianchi, A., Braem, V., Esteban, I., Caballero, M. T., Wood, C., Berrueta, M., Rondan, A., Lescano, G., Cruz, P., Ritou, Y., Fernández Viña, V., Álvarez Paggi, D., Esperante, S., Ferreti, A., Ofman, G., Ciganda, Á., Rodriguez, R., Lantos, J., Valentini, R., Itcovici, N., Hintze, A., Oyarvide, M. L., Etchegaray, C., Neira, A., Name, I., Alfonso, J., López Castelo, R., Caruso, G., Rapelius, S., Alvez, F., Etchenique, F., Dimase, F., Alvarez, D., Aranda, S. S., Sánchez Yanotti, C., De Luca, J., Jares Baglivo, S., Laudanno, S., Nowogrodzki, F., Larrea, R., Silveyra, M., Leberzstein, G., Debonis, A., Molinos, J., González, M., Perez, E., Kreplak, N., Pastor Argüello, S., Gibbons, L., Althabe, F., Bergel, E., Polack, F. P.; Fundación INFANT-COVID-19 Group (2021) Early high-titer plasma therapy to prevent severe Covid-19 in older adults. *N. Engl. J. Med.* **384(7)**, 610–618.

Luo, D., Ni, B., Zhao, G., Jia, Z., Zhou, L., Pacal, M., Zhang, L., Zhang, S., Xing, L., Lin, Z., Wang, L., Li, J., Liang, Y., Shi, X., Zhao, T., Zou, L., Wu, Y., Wang, X. (2007) Protection from infection with severe acute respiratory syndrome coronavirus in a Chinese hamster model by equine neutralizing F(ab')2. *Viral Immunol.* **20(3)**, 495–502.

Mair-Jenkins, J., Saavedra-Campos, M., Baillie, J. K., Cleary, P., Khaw, F. M., Lim, W. S., Makki, S., Rooney, K. D., Nguyen-Van-Tam, J. S., Beck, C. R.; Convalescent Plasma Study Group (2015) The effectiveness of convalescent plasma and hyperimmune immunoglobulin for the treatment of severe acute respiratory infections of viral etiology: A systematic review and exploratory meta-analysis. *J. Infect. Dis.* **211(1)**, 80–90.

McGuire, L. W., Redden, W. R. (1918) The use of convalescent human serum in influenza pneumonia – A preliminary report. *Am. J. Public Health (N. Y.)* **8(10)**, 741–744.

Onder, G., Rezza, G., Brusaferro, S. (2020) Case-fatality rate and characteristics of patients dying in relation to COVID-19 in Italy. *JAMA* **323(18)**, 1775–1776.

Pan, X., Zhou, P., Fan, T., Wu, Y., Zhang, J., Shi, X., Shang, W., Fang, L., Jiang, X., Shi, J., Sun, Y., Zhao, S., Gong, R., Chen, Z., Xiao, G. (2020) Immunoglobulin fragment $F(ab')_2$ against RBD potently neutralizes SARS-CoV-2 *in vitro*. *Antiviral Res.* **182**, 104868.

Piccoli, L., Park, Y. J., Tortorici, M. A., Czudnochowski, N., Walls, A. C., Beltramello, M., Silacci-Fregni, C., Pinto, D., Rosen, L. E., Bowen, J. E., Acton, O. J., Jaconi, S., Guarino, B., Minola, A., Zatta, F., Sprugasci, N., Bassi, J., Peter, A., De Marco, A., Nix, J. C., Mele F., Jovic, S., Fernandez Rodriguez, B., Gupta, S. V., Jin, F., Piumatti, G., Lo Presti, G., Franzetti Pellanda, A., Biggiogero, M., Tarkowski, M., Pizzuto, M. S., Cameroni, E., Havenar-Daughton, C., Smithey, M., Hong, D., Lepori, V., Albanese, E., Ceschi, A., Bernasconi, E., Elzi, L., Ferrari, P., Garzoni, C., Riva, A., Snell, G., Sallusto, F., Fink, K., Virgin, H. W., Lanzavecchia, A., Corti, D., Veesler, D. (2020) Mapping neutralizing and immunodominant sites on the SARS-CoV-2 spike receptor-binding domain by structure-guided high-resolution serology. *Cell* **183(4)**, 1024–1042.e21.

Piechotta, V., Iannizzi, C., Chai, K. L., Valk, S. J., Kimber, C., Dorando, E., Monsef, I., Wood, E. M., Lamikanra, A. A., Roberts, D. J., McQuilten, Z., So-Osman, C., Estcourt, L. J., Skoetz, N. (2020) Convalescent plasma or hyperimmune immunoglobulin for people with COVID-19: A living systematic review. *Cochrane Database Syst. Rev*. **7(7)**, CD013600.

Racine, T., Denizot, M., Pannetier, D., Nguyen, L., Pasquier, A., Raoul, H., Saluzzo, J. F., Kobinger, G., Veas, F., Herbreteau, C. H. (2019) *In vitro* characterization and *in vivo* effectiveness of Ebola virus specific equine polyclonal $F(ab')_2$. *J. Infect. Dis.* **220(1)**, 41–45.

Roback, J. D., Guarner, J. (2020) Convalescent plasma to treat COVID-19: Possibilities and challenges. *JAMA* **323(16)**, 1561–1562.

Sevcik, C., Díaz, P., D'Suze, G. (2008) On the presence of antibodies against bovine, equine and poultry immunoglobulins in human IgG preparations, and its implications on antivenom production. *Toxicon* **51(1)**, 10–16.

Tanne, J. H. (2020) Covid-19: FDA approves use of convalescent plasma to treat critically ill patients. *BMJ* **368**, m1256.

Tiberghien, P., de Lamballerie, X., Morel, P., Gallian, P., Lacombe, K., Yazdanpanah, Y. (2020) Collecting and evaluating convalescent plasma for COVID-19 treatment: Why and how? *Vox Sang.* **115(6)**, 488–494.

Wang, X., Ni, B., Du, X., Zhao, G., Gao, W., Shi, X., Zhang, S., Zhang, L., Wang, D., Luo, D., Xing, L., Jiang, H., Li, W., Jiang, M., Mao, L., He, Y., Xiao, Y., Wu, Y. (2005) Protection of mammalian cells from severe acute respiratory syndrome coronavirus infection by equine neutralizing antibody. *Antiviral Ther.* **10(5)**, 681–690.

Ye, M., Fu, D., Ren, Y., Wang, F., Wang, D., Zhang, F., Xia, X., Lv, T. (2020) Treatment with convalescent plasma for COVID-19 patients in Wuhan, China. *J. Med. Virol.* **92(10)**, 1890–1901.

Zhao, Y., Wang, C., Qiu, B., Li, C., Wang, H., Jin, H., Gai, W., Zheng, X., Wang, T., Sun, W., Yan, F., Gao, Y., Wang, Q., Yan, J., Chen, L., Perlman, S., Zhong, N., Zhao, J., Yang, S., Xia, X. (2017) Passive immunotherapy for Middle East Respiratory Syndrome coronavirus infection with equine immunoglobulin or immunoglobulin fragments in a mouse model. *Antiviral Res.* **137**, 125–130.

Zhou, L., Ni, B., Luo, D., Zhao, G., Jia, Z., Zhang, L., Lin, Z., Wang, L., Zhang, S., Xing, L., Li, J., Liang, Y., Shi, X., Zhao, T., Zhou, L., Wu, Y., Wang, X. (2007) Inhibition of infection caused by severe acute respiratory syndrome-associated coronavirus by equine neutralizing antibody in aged mice. *Int. Immunopharmacol.* **7(3)**, 392–400.

Orofacial Infection Number Decrease during COVID-19 Pandemic

Bronislava Dvoranová[1], Michal Vavro[1], Martin Selvek[2], Natália Gurčíková[1], David Med[1], Ladislav Czakó[1]

[1] Department of Oral and Maxillofacial Surgery, Comenius University, University Hospital Bratislava, Slovakia;
[2] Dôvera Insurance Company, Bratislava, Slovakia

Received January 7, 2025; Accepted August 27, 2025.

Key words: Orofacial infection – Odontogenic abscess – COVID-19 – Epidemiology

Abstract: This study analyses trends in orofacial infection hospital admissions at a single department, focusing on the impact of the COVID-19 pandemic. Admission counts fluctuated over the study period, but 2020 (n=65) and 2021 (n=56) showed a statistically significant decrease, falling slightly outside the 95% confidence interval of a linear trend established for 2014–2019. In 2022, the number of admitted patients (n=63) remained below average but within the confidence interval, while 2023 saw an increase to 97 patients. A notable shift in treatment methods was observed during the pandemic years. The proportion of patients treated with extraoral revision increased, with the most pronounced disparity in 2020 (n=40:10, 80%:20% extraoral revision-to-local treatment ratio). Statistical analysis (chi-square test, $p<0.001$) confirmed significant differences across the years. Comparing COVID-19-affected years (2020–2022) with non-COVID years (2014–2019 and 2023), 73% of patients were treated with extraoral revision during the pandemic, compared to 49% in non-COVID years ($p<0.001$). Additionally, only 44 patients were treated with antibiotics alone, whereas 75 would have been expected in the absence of COVID-19-related disruptions. These findings suggest that the pandemic influenced both the number of orofacial infection admissions and the treatment approach.

Mailing Address: MDDr. Michal Vavro, PhD., Department of Oral and Maxillofacial Surgery, Comenius University, University Hospital Bratislava, Ružinovská 6, 826 06 Bratislava, Slovakia; Phone: +421 248 234 865; e-mail: vavromichal@gmail.com

https://doi.org/10.14712/23362936.2025.21

Prague Medical Report / Vol. 126 (2025) No. 3, p. 139–143

Introduction

Infectious disease refers to a clinically evident illness caused by pathogenic microorganisms such as bacteria, viruses, fungi, or parasites (Morens et al., 2004). The aetiology of orofacial infection can be divided into odontogenic and non-odontogenic origin (salivary glands, facial skeleton fracture, osteonecrosis, osteomyelitis).

Odontogenic orofacial infections are most caused by anaerobic bacteria originating from a gangrenous tooth. If left untreated, the infection can spread from the periodontium of the tooth into adjacent subperiosteal and subsequently submucosal area spreading on into deep neck spaces and turning the state of the patient into a life-threatening condition (Figures 1 and 2).

The COVID-19 pandemic, caused by the SARS-CoV-2 virus, was a global health crisis that began in late 2019 and was officially declared a pandemic by the World Health Organization (WHO) on March 11, 2020. Its impact on healthcare systems worldwide was profound, leading to significant restrictions in both outpatient and inpatient care. In Slovakia, as in many other countries, healthcare facilities faced strict infection control measures, which limited access to routine and elective treatments. This disruption affected the management of various medical conditions, including dental care, potentially leading to delayed diagnoses and complications. In response, the Slovak Chamber of Dentists issued recommendations for dental practitioners, emphasizing the prioritization of emergency and urgent care while postponing non-essential procedures – especially any treatment involving spreading of aerosol, e.g. caries preparation. These guidelines aimed to minimize the risk of viral transmission while ensuring that patients with acute dental infections received necessary treatment. All these preventive measures might have potentially resulted in acute exacerbation of many chronic difficulties, e.g. dental caries and pulpitis.

Postponing planned dental care during the COVID-19 pandemic in general resulted in a higher number of odontogenic orofacial infections according to several studies (Long and Corsar, 2020; Visholm et al., 2021; Çelik and Karaaslan, 2023; Louizakis et al., 2024).

At the authors' workplace, Department of Oral and Maxillofacial Surgery, there was a statistically significant decrease of the number of these admissions in the pandemic years (2020–2022).

Aim of this study was to analyse the differences between the years and find a possible explanation for this phenomenon in previously published literature.

Material and Methods

A retrospective study was conducted to analyse patients with orofacial infections admitted to the Department of Oral and Maxillofacial Surgery between 2014 and 2023. The inclusion criterion was a primary admission diagnosis of an orofacial infection. Patients were categorized based on the treatment received: either surgical management involving extraoral revision under general anesthesia with pus evacuation and drainage or conservative treatment, including the removal of the inflammatory cause. Antibiotic therapy was administered to all patients. Statistical analyses were performed using RStudio, with the specific tests used to evaluate statistical significance indicated alongside p-values in the results section.

Figure 1: Pus evacuation during extraoral revision of a submandibular odontogenic abscess.

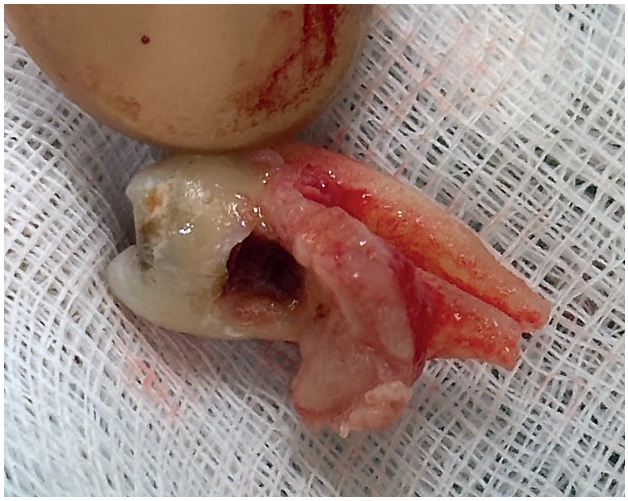

Figure 2: Extracted causal tooth of an orofacial infection.

Results

Total number of patients was n=744, 303 women and 441 men. The mean age was 43.1 years. Average length of hospital stay was 6.81 days. The highest admission count n=101 was noted in 2018. The admission count was quite variable during the study period, however if we assume linear trend for years 2014–2019, then number of patients in 2020 (n=65) and 2021 (n=56) is slightly outside the 95% confidence interval (CI), indicating a drop in patient counts. 63 patients in 2022 are still below average, although within the 95% CI for linear trend. In 2023, the number increased again to 97 admitted orofacial infection patients (Figures 3 and 4).

Regarding treatment method, the share of patients treated by extraoral revision is slightly increasing over the analysed years, with the extraoral revision-local treatment ratio being most uneven in 2020 – n=40:10 (80%:20%). This trend was particularly imminent during the COVID-19 pandemic. Differences between the years are statistically significant (chi-square test, $p<0.001$) (Figure 5). When comparing COVID-19 impacted year (2020–2022) with non-COVID years (2014–2019 and 2023), there is statistically significant difference in the number of patients treated with extraoral revision – 49% of patients were treated in non-COVID years, while in COVID years, 73% of patients were treated by extraoral revision (chi-square test, $p<0.001$). Only 44 patients were treated with

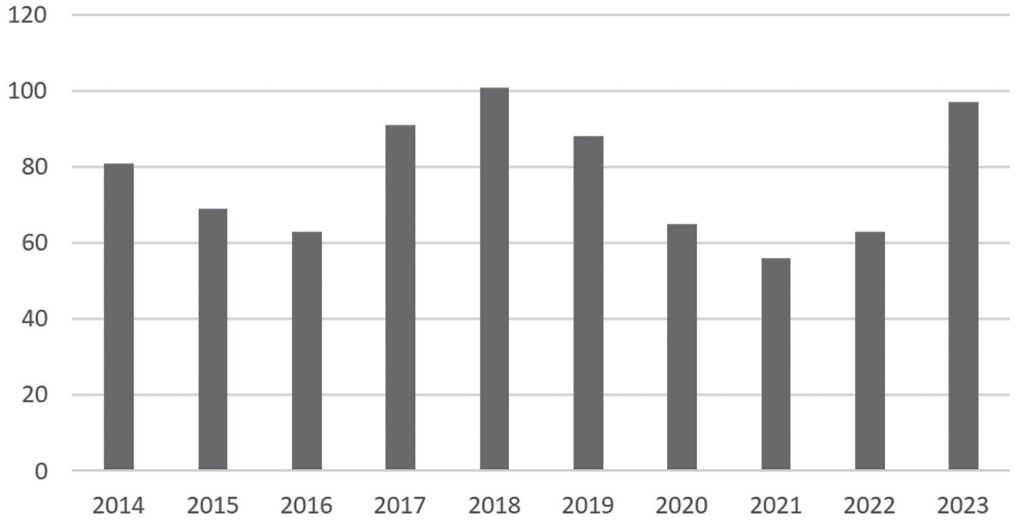

Figure 3: Orofacial infection number over analysed years 2014–2023.

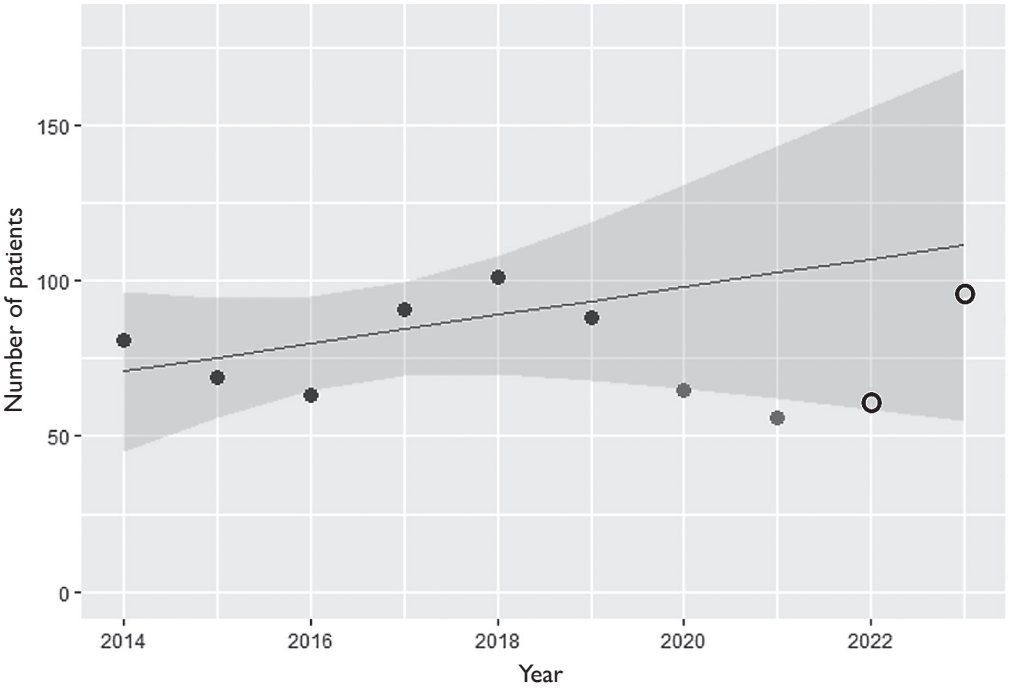

Figure 4: Linear regression of number of patients in years 2014–2023.

Prague Medical Report / Vol. 126 (2025) No. 3, p. 139–143

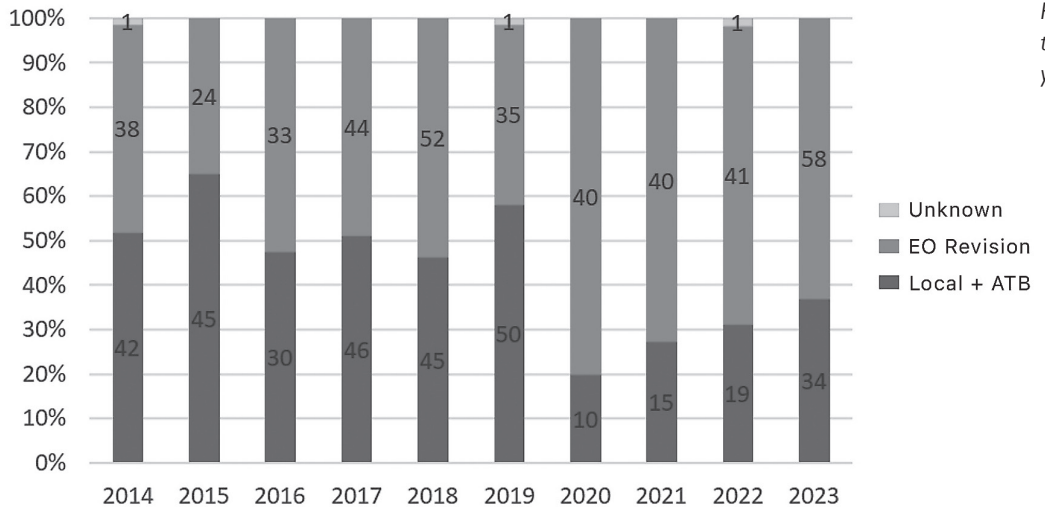

Figure 5: Orofacial infection treatment over analysed years 2014–2023.

antibiotics only, while 75 would be the expected number assuming no difference between COVID and non-COVID years.

Discussion

Deep space orofacial infections represent a potential life-threatening condition in oral and maxillofacial surgery. Epidemiological information about orofacial infection patient count during different world situations help the clinicians to prepare guidelines and educate the public.

Results of this study showed the patient counts in COVID-19 pandemic years 2020 (n=65) and 2021 (n=56) fell slightly outside the 95% confidence interval, indicating a notable decrease. The proportion of patients treated with extraoral revision has shown a slight increase over the analysed years, with the most pronounced disparity in the extraoral revision-to-local treatment ratio observed in 2020 (n=40:10, 80%:20%).

Explanation of this phenomenon is not entirely certain. As previously stated, number of deep space orofacial infection patients requiring hospital admission during the COVID-19 pandemic years increased in many regions (Long and Corsar, 2020; Visholm et al., 2021; Çelik and Karaaslan, 2023; Louizakis et al., 2024).

During the COVID-19 pandemic, treatment management of odontogenic infections varied across countries due to differing healthcare capacities and guidelines. In the United Kingdom (UK), oral and maxillofacial units adopted a more radical approach to managing odontogenic cervicofacial infections. During the first wave of the pandemic in the UK, dental practitioners increasingly opted for early and definitive interventions, such as tooth extractions, to reduce the risk of complications requiring hospital admission. This approach aimed to limit patient exposure to hospital environments and alleviate the burden on healthcare facilities already overwhelmed by COVID-19 cases (Puglia et al., 2021). In contrast, the recommendations issued by the Slovak Chamber of Dentists prioritized emergency and urgent care while deferring non-essential procedures.

In particular, in the United Kingdom, on the 25th March 2020, the Chief Dental Officer (CDO) for England released a statement calling for primary dental care services to cease all routine dental care, as a result the number of dental abscesses presenting to the emergency department decreased, but the number of patients with abscesses requiring admission increased significantly from 35 to 80% (Long and Corsar, 2020).

In Oxford, in the so called "Central Hub", outpatient reviews on the general practitioner referral unit saw an increased number of dental abscesses reviewed ($p=0.0067$). However, there was no statistical significance between the number of dental abscesses admitted between the COVID and non-COVID period (Visholm et al., 2021).

In Turkey, in a paediatric study, the rates of odontogenic cervicofacial infections requiring intravenous antibiotics and abscess drainage in children increased significantly in the second year of the COVID-19 pandemic (Çelik and Karaaslan, 2023).

In a study from Germany, there was an interesting shift in the orofacial infection patient portfolio: despite an overall reduction in the number of patients treated for odontogenic and intraoral abscesses in the first year of the pandemic (298 cases) compared to the two preceding years (663 cases), the severity of infections increased. Specifically, there was a significant rise in the number of advanced cases requiring general anaesthesia ($p<0.001$) (Grill et al., 2023).

A study conducted at Helsinki University Hospital evaluated the effects of the COVID-19 pandemic on the rate of orofacial and respiratory infections in emergency departments. The results showed a significant 37% reduction in patient visits for these infections in 2020 compared to 2018 and 2019 (1,894 cases in 2020 vs. 3,077 and 2,929 in previous years, respectively) (Haapanen et al., 2021).

Most hospitals have reported an increase in orofacial infection patients during the COVID-19 pandemic years (Long and Corsar, 2020; Haapanen et al., 2021; Visholm et al., 2021; Çelik and Karaaslan, 2023; Grill et al., 2023; Louizakis et al., 2024), yet the reasons for the decrease in such patients in Bratislava remain unclear. Several possibilities come into consideration. First, the overall number of patients seeking hospital care declined significantly during the pandemic, which might explain why many infection cases that would typically be referred to specialized departments were treated in outpatient settings, such as emergency dental practices. Another possible explanation for the patient count decrease is the possibility that fear of contracting COVID-19 may have kept people from seeking hospital care until necessary. However, this remains speculative.

In Slovakia, the Slovak Chamber of Dentists issued a statement advising practitioners to minimize aerosol producing treatment to reduce the risk of COVID-19 transmission (https://www.skzl.sk/wp-content/uploads/2021/11/ZUBNE_OSETRENIE_POKYNY_ZL-1.pdf). This directive likely changed the treatment approach for many patients. Traditionally, most dentists favour conservative methods, such as endodontic treatment or trepanation, which allows the problematic tooth to remain in the socket. Due to the issued guidance, dentists might have decided to extract the affected teeth instead. Previous findings (Vavro et al., 2024) indicated that orofacial infection patients admitted with the causal tooth still in the socket represented the largest aetiological group and exhibited the highest levels of inflammation markers, such as C-reactive protein and leukocyte counts.

Conclusion

Less hospital admissions for orofacial infections during the COVID-19 pandemic than in non-pandemic years was reported at the monitored department. However, the number of patients requiring extraoral revision of orofacial infection was significantly higher.

To optimize orofacial infection management during pandemics, early patient presentation and education should be prioritized to prevent complications. A more radical approach, such as immediate tooth extraction in severe cases, can reduce hospitalizations. Strengthening collaboration between dental and medical professionals and ensuring access to essential treatments in outpatient settings can further improve patient outcomes.

References

Çelik, T., Karaaslan, L. (2023) Increase in odontogenic cervicofacial infection requiring hospitalization in children during COVID-19 quarantine: Odontogenic infections in children during COVID-19. *J. Pediatr. Acad*. **4(2)**, 50–53.

Grill, F. D., Rothlauf, P., Ritschl, L. M., Deppe, H., Stimmer, H., Scheufele, F., Schwarz, M., Klaus-Dietrich, W., Fichter, A. M. (2023) The COVID-19 pandemic and its possible impact on the treatment of odontogenic and intraoral abscesses. *Head Face Med*. **19(1)**, 36.

Haapanen, A., Uittamo, J., Furuholm, J., Mäkitie, A., Snäll, J. (2021) Effect of COVID-19 pandemic on orofacial and respiratory infections in ear, nose, and throat and oral and maxillofacial surgery emergency departments: A retrospective study of 7900 patients. *Eur. Arch. Otorhinolaryngol*. **279(3)**, 1615–1620.

Long, L., Corsar, K. (2020) The COVID-19 effect: Number of patients presenting to the Mid Yorkshire Hospitals OMFS team with dental infections before and during the COVID-19 outbreak. *Br. J. Oral Maxillofac. Surg*. **58(6)**, 713–714.

Louizakis, A., Tatsis, D., Paraskevopoulos, K., Antoniou, A., Kyrgidis, A., Vahtsevanos, K. (2024) The effect of the COVID-19 pandemic on odontogenic cervicofacial infections in a single center in Greece. *Cureus* **16(5)**, e61333.

Morens, D. M., Folkers, G. K., Fauci, A. S. (2004) The challenge of emerging and re-emerging infectious diseases. *Nature* **430(6996)**, 242–249.

Puglia, F. A., Ubhi, H., Dawoud, B., Magennis, P., Chiu, G. A. (2021) Management of odontogenic cervicofacial infections presenting to oral and maxillofacial units during the first wave of the COVID-19 pandemic in the United Kingdom. *Br. J. Oral Maxillofac. Surg*. **59(8)**, 875–880.

Vavro, M., Dvoranová, B., Czakó, L., Šimko, K., Gális, B. (2024) Antibiotic susceptibility of orofacial infections in Bratislava: A 10-year retrospective study. *Clin. Oral Investig*. **28(10)**, 538.

Visholm, T. M., Sandhu, N., Dhariwal, D. K. (2021) COVID-19: The oral and maxillofacial surgery experience, Oxford, UK. *Craniomaxillofac. Trauma Reconstr.* **14(4)**, 317–324.

Biofilm-forming Ability of Anaerobic Bacterial Strains Isolated from Patients Diagnosed with Periodontitis

Ivan Skliar[1], Maryna Kryvtsova[1], Yevhen Kostenko[2], Marianna Savenko[1]

[1] Department of Clinical, Laboratory and Morphofunctional Diagnostics, Uzhhorod National University, Uzhhorod, Ukraine;
[2] Department of Orthopaedic Dentistry, Uzhhorod National University, Uzhhorod, Ukraine

Received March 11, 2025; Accepted August 27, 2025.

Key words: Biofilm formation – Periodontal pathogens – Obligate anaerobes – *Slackia exigua*

Abstract: Bacterial biofilms represent the primary causative agents of pathogenic processes within the oral cavity. Biofilm microorganisms exhibit heightened resistance to adverse environmental factors. The objective of this study was to ascertain the biofilm-forming potential of clinical strains of anaerobic microorganisms isolated from the periodontal pocket of patients diagnosed with periodontitis. The study of biofilm formation was carried out by the method (Djordjevic et al., 2002) using flat-bottomed 96-well polystyrene microtitration plates. Biofilm formation was determined by staining with 0.1% crystal violet. The study utilised clinical strains isolated from the periodontal pocket of 61 patients diagnosed with grade III chronic periodontitis. Of these, 30 strains belonging to three bacterial species were selected for further analysis: *Porphyromonas asaccharolytica*, *Slackia exigua*, and *Schaalia odontolytica*. Among the *Porphyromonas asaccharolytica* strains, 80% formed biofilm; the figure for *Slackia exigua* was 90%, and for *Schaalia odontolytica* – 80%. In total, 25 strains were capable of biofilm formation. The results indicate that the isolated strains of *Porphyromonas asaccharolytica*, *Slackia exigua*, and *Schaalia odontolytica* exhibited a significant capacity for biofilm formation (83.3% of the strains formed biofilm), particularly *Slackia exigua* strains, which exhibited the highest number of strains with high biofilm formation ability – 5 (16.6%). It is also noteworthy that these microorganisms exhibited a moderate persistence frequency (16.4% each), of the total sample of microbial biocenoses from inflammatory periodontal soft tissue areas.

Mailing Address: Ivan Skliar, Department of Clinical, Laboratory and Morphofunctional Diagnostics, Uzhhorod National University, 60A Stantsiyna Street, 88000, Uzhhorod, Ukraine; Phone: +380 682 114 707; e-mail: sklarivan728@gmail.com

https://doi.org/10.14712/23362936.2025.22

Introduction

Bacterial biofilms represent the primary causative agents of pathogenic processes within the oral cavity (Marsh and Devine, 2011). These biofilms form on both the surface of the oral mucosa and synthetic materials, resulting in the development of persistent inflammatory processes and a substantial reduction in the service life of dental prostheses and restorative materials (Auschill et al., 2002). Oral biofilms have the capacity to affect the tissues surrounding the tooth, causing gingival inflammation and, if persistent, damage to the alveolar ridge, which can ultimately result in tooth loss (Papapanou et al., 2018).

Biofilms are defined as conglomerates of microorganisms (bacteria, algae and fungi) that attach to biological and non-biological surfaces and are functionally organised in layers (Marsh, 2005). Biofilm microorganisms exhibit enhanced resistance to adverse environmental factors (Chia et al., 2008). The life processes within a biofilm differ significantly from those observed in the planktonic state (Marsh, 2004; Shemesh et al., 2007). In addition to mechanical stability, the formation of biofilms stimulates synergistic interactions, ensures survival during periods of starvation and exposure to antimicrobial agents, and prevents the displacement of extracellular enzymes (Tzu et al., 2004). In this sense, biofilms are not merely conglomerates of microorganisms, but rather well-organised matrix systems with a clear distribution of functions. Individual prokaryotes "communicate" within the system by transmitting signals that modulate gene expression. In addition to this, biofilms perform various functions in order to ensure their own survival (Brown et al., 2005; Shemesh et al., 2010). One of the main functions of biofilms is the secretion of extracellular polymeric substances (EPS) to protect microorganisms from external influences (Flemming and Wingender, 2010).

Okahashi et al. (2011) demonstrated that the predominant primary colonisers of teeth are gram-positive facultative anaerobic cocci and bacilli, including *Streptococcus* and *Actinomyces* species. These bacteria provide the basis for the further development of dental biofilm. After these microorganisms attach to the surface, a mass of biofilm develops through continuous growth and further adsorption of other bacterial species by coagulation. The biofilm-forming microorganisms secrete enzymes and toxins that stimulate the human body to synthesise antibodies and cytokines, which are retained by the biofilm matrix, exacerbating the inflammatory process (Leonteva et al., 2023).

The surface molecules of these primary colonisers allow for the coaggregation of gram-negative bacteria that have a lower level of adhesion to the pelvis, including members of the *Veillonella* and *Fusobacterium* genera. Bacteria belonging to the *Fusobacterium* genus, such as *Fusobacterium nucleatum*, are capable of co-aggregating with both primary and secondary colonisers, hence their name "bridge bacteria", and they are known to contribute to the successful development of dental biofilm. The mechanism by which *F. nucleatum* aggregates with neighbouring bacteria involves surface molecules such as RadD, arginine-inhibitory adhesin, and fusobacterial apoptosis protein Fap2 (Kaplan et al., 2010).

Another study (Mark Welch et al., 2016) utilised a combination of labelling and spectral imaging FISH (CLASI-FISH) to demonstrate that the composition of biofilms was characterised by a complex microbial consortium, termed the "hedgehog structure". This structure consisted primarily of nine taxa arranged in an organised spatial structure, including *Corynebacterium*, *Streptococcus*, *Porphyromonas*, *Haemophilus/Aggregatibacter*, *Neisseriaceae*, *Fusobacterium*, *Leptotrichia*, *Capnocytophaga*, and *Actinomyces*.

It is also known that bacteria in the biofilm exhibit a higher degree of resistance to antibiotics and antimicrobial agents, so the ability to form biofilms is considered one of the factors of pathogenicity (Shahzad et al., 2015). The formation of multispecies biofilms, which include periodontopathogenic microorganisms, has been demonstrated to cause the progression of periodontal diseases through microbial interactions (Meyle and Chapple, 2015; Sanz et al., 2017). Biofilms on the teeth surface, especially on porous hydroxyapatite, have been shown to contribute to the progression of periodontitis by facilitating bacterial attachment and growth (Jaffar et al., 2016).

Objective

The objective of this study was to ascertain the biofilm-forming activity of clinical strains of anaerobic microorganisms isolated from the periodontal pocket of patients diagnosed with periodontitis.

Material and Methods

Strains and cultivation conditions

For the purposes of this study, clinical strains were isolated from the periodontal pocket of 61 patients diagnosed with grade III chronic periodontitis at the Dental Outpatient Clinic of the Dental Faculty of the Uzhhorod National University. The isolation of pure cultures was carried out by the sector sowing method according to Gold using Schaedler agar + 5%

Prague Medical Report / Vol. 126 (2025) No. 3, p. 144–150

defibrinated sheep blood (Condalab, Spain) nutrient medium containing (on a g/l basis): bacteriological agar – 13.5; hemin – 0.01 g/l; peptone mixture – 5; trypto-casein soy broth – 10; dextrose – 5; L-cysteine – 0.4; yeast extract – 5; Tris (hydroxymethyl aminomethane) – 3.To create anaerobic conditions, an anaerobic container with an anaerobic system (AnaeroGen System – "Oxoid", UK) was used. The pure cultures were grown in Schaedler broth (Condalab, Spain) containing (on a g/l basis): casein peptone – 2.5; hemin – 0.01; meat peptone – 2.5; trypto-casein soy broth – 10; dextrose – 5; L-cysteine – 0.4; yeast extract – 5; Tris (hydroxymethyl aminomethane) – 3. The cultures were then subjected to incubation under anaerobic conditions at 37 °C for a period of 48 hours. The identification of the isolated pure cultures was conducted through the utilisation of MALDI-TOF (matrix-assisted laser desorption/ ionisation and time-of-flight mass spectrometry).

Biofilm analysis

The study of biofilm formation was carried out by the method (Djordjevic et al., 2002) using flat-bottomed 96-well polystyrene microtitration plates (Starlab, Ukraine). Prior to plating, the 48-hour cultures of periodontal pathogens were diluted in fresh sterile Schaedler broth to an optical density (OD) of 0.05 at 600 nm. The inoculum was then injected into the wells using a Thermo Scientific F1 multichannel variable volume pipette (Thermo Fisher Scientific, USA), with 200 µl aliquots per well. Sterile Schaedler broth with the same volume was used as a negative control. The inoculated plates were then incubated under stable anaerobic conditions at 37 °C for 72 hours, after which biofilm formation was periodically assessed by visual inspection.

Quantification of biofilm formation

Biofilm formation was determined by staining with 0.1% crystal violet, as described above (Pratt and Kolter, 1998). The microtiter plate containing the biofilm was gently washed several times with distilled water, using sterile Pasteur pipettes (Starlab, Ukraine). The plates were then dried by tapping them on a paper towel. This cleaning procedure was undertaken to ensure the removal of any loosely attached cells or broth residues that might otherwise be stained during the subsequent step. To determine the total biofilm mass, 200 µl of 0.1% crystal violet was added to each well for 30 minutes (Sol et al., 2013). The plate was then gently rinsed with distilled water and allowed to air-dry in an incubator at 37 °C for 15 minutes. The remaining biofilm was then visualised using photography. Following this, the stained biofilm was dissolved for 30 minutes by adding 200 µl of 95% ethanol to each well. The plates were then read using a semi-automatic ELISA analyser with a photometric system for microplates RT-6100 (Rayto, China) at an absorption of 492 nm (Stepanović et al., 2007).

Statistical analysis

The data from a minimum of three independent experiments are presented as mean ± SD (standard deviation). Comparisons were performed by Student's *t*-test using Microsoft Office Excel 2016 software.

Figure 1: Pure culture of Slackia exigua on Schaedler agar + 5% defibrinated sheep blood.

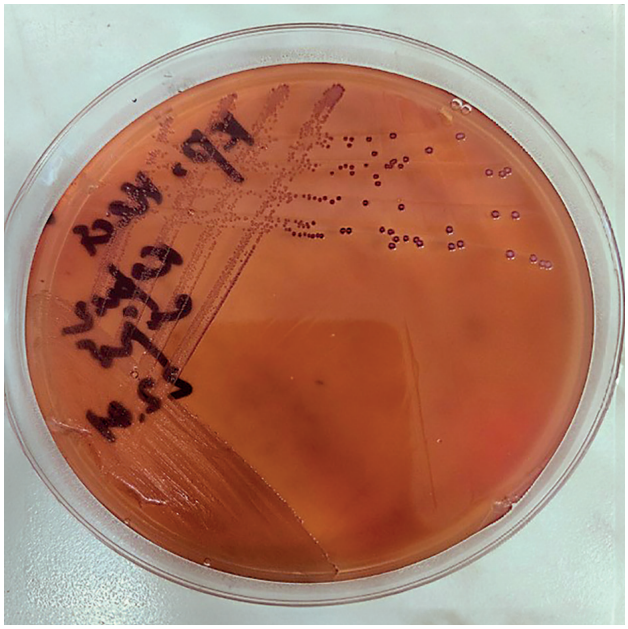

Figure 2: Pure culture of Schaalia odontolytica on Schaedler agar + 5% defibrinated sheep blood.

Results

The present study investigates the formation of biofilm *in vitro* in strains of obligate anaerobes isolated from the inflammatory process in the periodontal pocket of patients diagnosed with periodontitis. A total of 61 patients with grade III chronic periodontitis were included in the study, and material was taken from their periodontal pockets. Of these, 30 bacterial strains belonging to 3 species were selected for further study: *Porphyromonas asaccharolytica*, *Slackia exigua*, and *Schaalia odontolytica* (Figures 1–3). The overall persistence rate of these microorganisms was 16.4% across the entire sample.

In the study, the formation of biofilm was observed in 80% of *Porphyromonas asaccharolytica* strains, 90% of *Slackia exigua* strains, and 80% of *Schaalia odontolytica* strains. The investigation revealed that a total of 25 strains were capable of biofilm formation, as illustrated in Figure 4.

The microtitration plate shown in Figure 5 presents an *in vitro* biofilm from the strains of obligate anaerobes, with the optical density of different strains

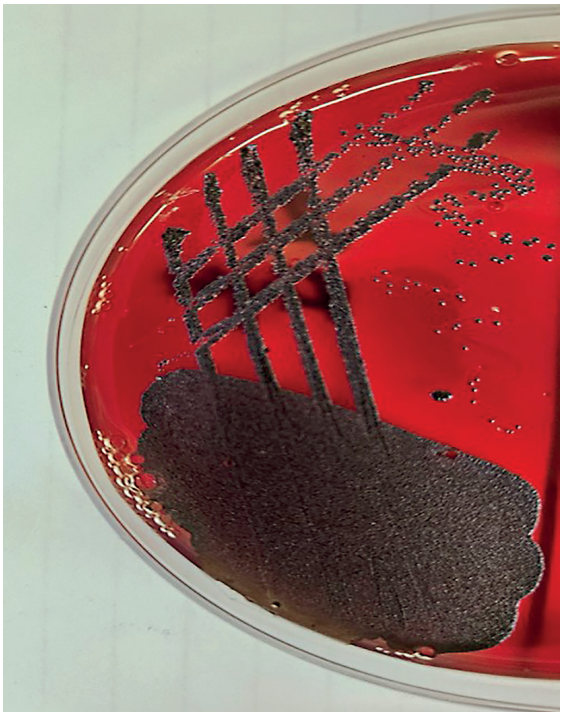

Figure 3: Pure culture of Porphyromonas asaccharolytica on Schaedler agar + 5% defibrinated sheep blood.

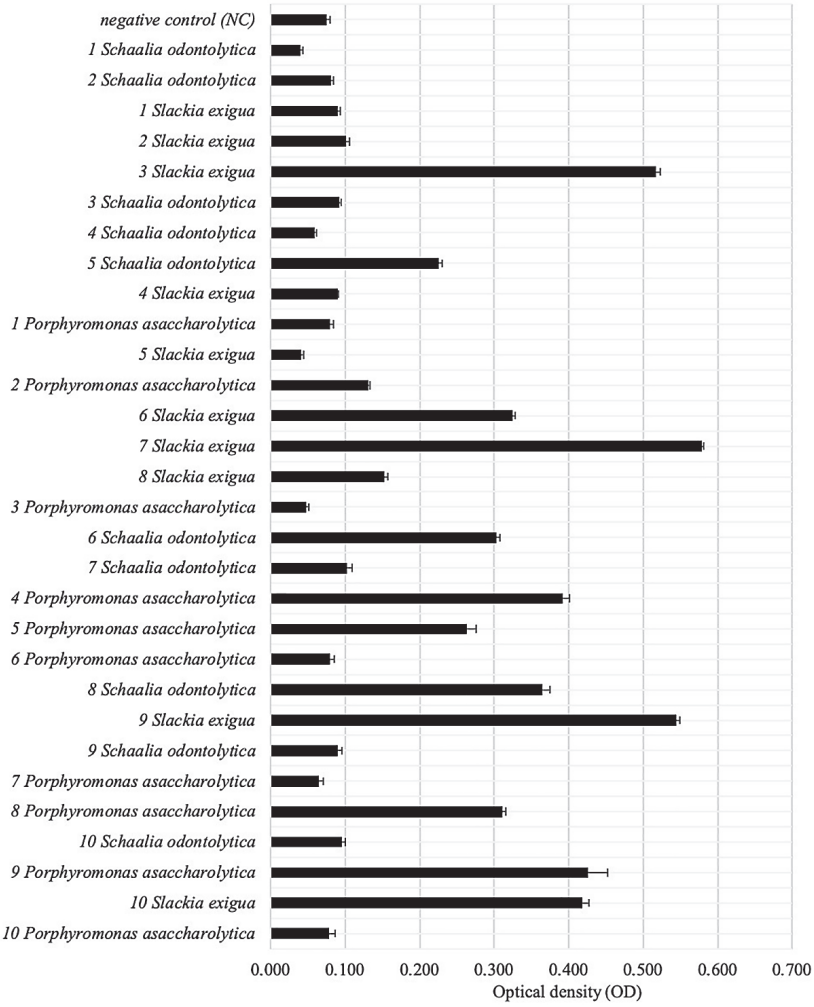

Figure 4: Biofilm indicators of Porphyromonas asaccharolytica, Slackia exigua, and Schaalia odontolytica strains. Sterile Schaedler broth was utilised as a negative control (NC), with a value of 0.075. The mean value is represented by wide bars, whilst the standard deviation (SD) is indicated by error bars.

Prague Medical Report / Vol. 126 (2025) No. 3, p. 144–150

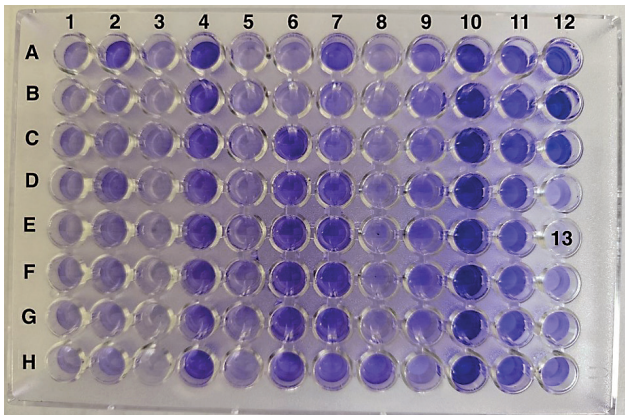

Figure 5: A microtitration plate with biofilm in vitro in strains of obligate anaerobes: **1** *– 9 Schaalia odontolytica;* **2** *– 2 Slackia exigua;* **3** *– 10 Porphyromonas asaccharolytica;* **4** *– 6 Schaalia odontolytica;* **5** *– 7 Schaalia odontolytica;* **6** *– 6 Slackia exigua;* **7** *– 8 Schaalia odontolytica;* **8** *– 10 Schaalia odontolytica;* **9** *– 8 Slackia exigua;* **10** *– 7 Slackia exigua;* **11** *– 8 Porphyromonas asaccharolytica;* **12 (A–D)** *– 9 Porphyromonas asaccharolytica;* **13 (E–H)** *– 2 Porphyromonas asaccharolytica.*

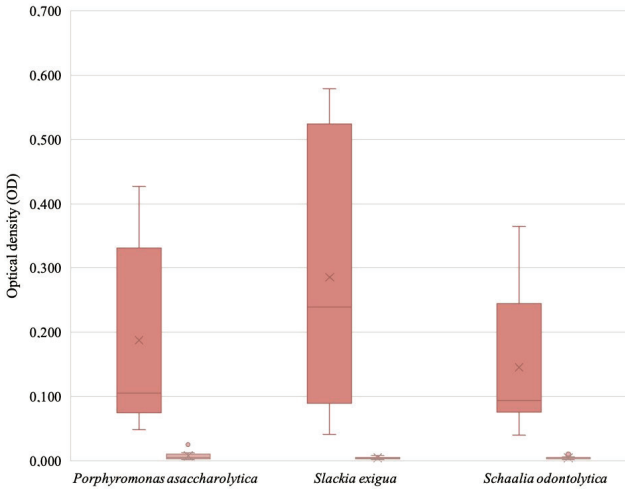

Figure 6: The biofilm formation ability of anaerobic bacteria isolated from the periodontal pocket. Note: The median is indicated by a horizontal line within each block. The error bars represent the minimum and maximum values, and the spread between quartiles represents the variability of the results.

depending on the intensity of staining with 0.1% crystal violet clearly demonstrated.

The following classification system was utilised to interpret the biofilm formation by strains: non-biofilm-forming, low biofilm forming, moderate and high biofilm forming (see Tables 1 and 2 for the data).

OD (strain) ≤ OD (control) = no biofilm formation;
OD (control) ≤ OD (strain) ≤ 2OD (control) = low biofilm formation;
2OD (control) ≤ OD (strain) ≤ 4OD (control) = moderate biofilm formation;
4OD (control) ≤ OD (strain) = high biofilm formation (Stepanović et al., 2007).

A comparative analysis of the optical density of the strains of each species (Figure 6) reveals that *Slackia exigua* strains exhibit the most extensive data scatter and the highest median. This finding suggests that these strains possess the most pronounced biofilm formation ability (within the experimental parameters), with their indicators demonstrating significant variability. In contrast, *Porphyromonas asaccharolytica* exhibited a comparatively diminished data scatter

Table 1: Formation of biofilms by anaerobic periodontal pathogens, distribution by classification (n=30)

Microorganisms	No biofilm formation	Number of biofilm-forming strains		
		low	moderate	high
Porphyromonas asaccharolytica	2	4	1	3
Slackia exigua	1	3	1	5
Schaalia odontolytica	2	5	1	2

Table 2: Optical density of biofilms by anaerobic periodontal pathogens, distribution by classification (n=30)

Microorganisms	Biofilm forming density, in OD		
	low	moderate	high
Porphyromonas asaccharolytica	0.105 ± 0.027	0.263	0.367 ± 0.060
Slackia exigua	0.095 ± 0.006	0.153	0.450 ± 0.145
Schaalia odontolytica	0.092 ± 0.011	0.226	0.334 ± 0.031

OD – optical density

and median, indicative of a less pronounced biofilm-forming capacity that is more stable than that observed in *Slackia exigua*. *Schaalia odontolytica* demonstrated characteristics analogous to those of *Porphyromonas asaccharolytica*, yet with a marginally lower median and a more extensive data scatter. This suggests that while these strains do possess biofilm-forming capabilities, the extent and variability of their responses may vary.

Discussion

The results obtained demonstrate the role of the studied species in the formation of inflammatory periodontal diseases. *S. exigua* has been frequently isolated from periradicular lesions (Sato et al., 1993; Kiryu et al., 1994; Hashimura et al., 2001), as well as from other areas of the oral cavity (Moore et al., 1983; Hill et al., 1987; Wade et al., 1994). In addition, *S. exigua* has been reported to be associated with clinical indicators of periodontal disease (Booth et al., 2004). In one study, two cases of monomicrobial bacteraemia caused by *S. exigua* isolated from two healthcare facilities were reported (Kawasuji et al., 2020); a case of systemic infection caused by obligate anaerobes was also reported: *Dialister pneumosintes* and *Slackia exigua*, arising from an acute periapical abscess (Lee et al., 2016). Bukki et al. (2011) reported the first case of *S. exigua* isolation from cerebrospinal fluid in a patient with suspected enterospinal fistula and subsequent polymicrobial exudative meningitis. A further case of hip prosthesis infection associated with anaerobic gram-positive *Slackia exigua* was also described by Rieber et al. (2019). This was isolated from periprosthetic tissues and prosthesis components after invasive dental procedures, and the patient had not received antibiotic prophylaxis before the dental intervention. A rare instance of bacteremia caused by *Porphyromonas asaccharolytica* in a patient diagnosed with necrotising fasciitis was documented by Cobo et al. (2021). Gupta et al. (2018) delineated the case of a patient with Lemierre's syndrome caused by obligate anaerobe *Porphyromonas asaccharolytica* from the oral cavity. Stašková et al. (2021) investigated the antibiofilm activity of neutralised cell-free supernant (nCFS) of *Streptococcus salivarius* K12 at different concentrations against *Schaalia odontolytica* P10, showing a significant reduction ($p<0.001$) in biofilm formation at nCFS concentrations of 60 and 30 mg/ml (37). In the study conducted by Heller et al. (2016), early dental biofilm samples were analysed from 11 healthy individuals. The semi-quantitative HOMIM method was utilised, resulting in the identification of at least 92 species. Among these, *Slackia exigua* and other species demonstrated a high persistence frequency.

As demonstrated in our previous studies, opportunistic pathogens that persist in the context of chronic inflammation of periodontal tissues have the capacity to form a biofilm (Kryvtsova and Kostenko, 2020). Furthermore, there is evidence to suggest that bacteria of the *Staphylococcus* genus possess genetic determinants associated with biofilm formation. Consequently, determining the bacteria's capacity to form a biofilm is imperative in order to develop a treatment strategy that utilises substances with antibiofilm-forming properties. The capacity of *Porphyromonas asaccharolytica*, *Slackia exigua*, and *Schaalia odontolytica* bacteria isolated from periodontal pockets of patients diagnosed with periodontitis to form biofilms underscores their role in the development of inflammatory periodontal diseases.

Conclusion

The results of this study demonstrate that the isolated strains of *Porphyromonas asaccharolytica*, *Slackia exigua*, and *Schaalia odontolytica* exhibited a notable capacity to form biofilms (83.3% of strains formed biofilms), particularly *Slackia exigua* strains, which exhibited the highest number of strains with high biofilm formation ability – 5 (16.6%). It is also noteworthy that these microorganisms exhibited a moderate frequency of persistence, with 16.4% of the total sample of microbial biocenoses of inflammatory periodontal soft tissues being represented by each. The results of the study suggest the potential for further research and the establishment of the role of these microorganisms in periodontal inflammatory diseases.

References

Auschill, T., Arweiler, N., Brecx, M., Reich, E., Sculean, A., Netuschil, L. (2002) The effect of dental restorative materials on dental biofilm. *Eur. J. Oral Sci.* **110(1)**, 48–53.

Booth, V., Downes, J., Van den Berg, J., Wade, W. G. (2004) Gram-positive anaerobic bacilli in human periodontal disease. *J. Periodontal Res.* **39(3)**, 213–220.

Brown, T., Ahn, S., Frank, R., Chen, Y., Lemos, J., Burne, R. (2005) A hypothetical protein of *Streptococcus mutans* is critical for biofilm formation. *Infect. Immun*. **73(5)**, 3147–3151.

Bukki, J., Huttner, H. B., Lee, D. H., Jantsch, J., Janka, R., Ostgathe, C. (2011) Polymicrobial feculent meningitis with detection of *Slackia exigua* in the cerebrospinal fluid of a patient with advanced rectal carcinoma. *J. Clin. Oncol.* **29**, 852–854.

Chia, N., Woese, C., Goldenfeld, N. (2008) A collective mechanism for phase variation in biofilms. *Proc. Natl. Acad. Sci. U. S. A.* **105(38)**, 14597–14602.

Cobo, F., Pérez-Carrasco, V., Sánchez-Martin, V., García-Salcedo, J.

A., Barrón Martín, E., Navarro-Marí, J. M. (2021) A rare cause of bacteremia due to *Porphyromonas asaccharolytica* in a patient with necrotizing fasciitis. *Anaerobe* **71**, *102442*.

Djordjevic, D., Wiedmann, M., McLandsborough, L. A. (2002) Microtiter plate assay for assessment of *Listeria monocytogenes* biofilm formation. *Appl. Environ. Microbiol.* **68(6)**, 2950–2958.

Flemming, H., Wingender, J. (2010) The biofilm matrix. *Nat. Rev. Microbiol*. **8(9)**, 623–633.

Gupta, M., Annam, R., Bahgat, J., Eng, M. (2018) *Porphyromonas asaccharolytica* as a rare causative agent for Lemierre's syndrome. *Case Rep. Infect. Dis.* **2018**, 3628395.

Hashimura, T., Sato, M., Hoshino, E. (2001) Detection of *Slackia exigua*, *Mogibacterium timidum* and *Eubacterium saphenum* from pulpal and periradicular samples using the polymerase chain reaction (PCR) method. *Int. Endod. J.* **34(7)**, 463–470.

Heller, D., Helmerhorst, E., Gower, A., Siqueira, W., Paster, B., Oppenheim, F. (2016) Microbial diversity in the early *in vivo*-formed dental biofilm. *Appl. Environ. Microbiol.* **82**, 1881–1888.

Hill, G. B., Ayers, O. M., Kohan, A. P. (1987) Characteristics and sites of infection of *Eubacterium nodatum*, *Eubacterium timidum*, *Eubacterium brachy*, and other asaccharolytic eubacteria. *J. Clin. Microbiol.* **25(8)**, 1540–1545.

Jaffar, N., Miyazaki, T., Maeda, T. (2016) Biofilm formation of periodontal pathogens on hydroxyapatite surfaces: Implications for periodontium damage. *J. Biomed. Mater. Res. A* **104(11)**, 2873–2880.

Kaplan, C., Ma, X., Paranjpe, A., Jewett, A., Lux, R., Kinder-Haake, S., Shi, W. (2010) *Fusobacterium nucleatum* outer membrane proteins Fap2 and RadD induce cell death in human lymphocytes. *Infect. Immun*. **78**, 4773–4778.

Kawasuji, H., Kaya, H., Kawamura, T., Ueno, A., Miyajima, Y., Tsuda, T., Taniguchi, H., Nakamura, M., Wada, A., Sakamaki, I., Niimi, H., Yamamoto, Y. (2020) Bacteremia caused by *Slackia exigua*: A report of two cases and literature review. *J. Infect. Chemother.* **26(1)**, 119–123.

Kiryu, T., Hoshino, E., Iwaku, M. (1994) Bacteria invading periapical cementum. *J. Endod.* **20(4)**, 169–172.

Kryvtsova, M., Kostenko, Y. (2020) Dominant microbial associations of oral cavity at periodontitis and features of their sensitivity to antibacterial drugs. *Studia Biologica* **14(1)**, 51–62.

Lee, M. Y., Kim, Y. J., Gu, H. J., Lee, H. J. (2016) A case of bacteremia caused by *Dialister pneumosintes* and *Slackia exigua* in a patient with periapical abscess. *Anaerobe* **38**, 36–38.

Leonteva, A., Pototskaya, L., Chervinets, Y. (2023) Mechanisms of oral microbial biofilm formation in healthy people and patients with chronic generalized periodontitis. *Parodontologiya* **3**, *208–217*.

Mark Welch, J. L., Rossetti, B. J., Rieken, C. W., Dewhirst, F. E., Borisy, G. G. (2016) Biogeography of a human oral microbiome at the micron scale. *Proc. Natl. Acad. Sci. U. S. A.* **113(5)**, E791–E800.

Marsh, P. (2004) Dental plaque as a microbial biofilm. *Caries Res.* **38(3)**, 204–211.

Marsh, P. (2005) Dental plaque: Biological significance of a biofilm and community life-style. *J. Clin. Periodontol*. **32(6)**, 7–15.

Marsh, P., Devine, D. (2011) How is the development of dental biofilms influenced by the host? *J. Clin. Periodontol*. **38(11)**, 28–35.

Meyle, J., Chapple, I. (2015) Molecular aspects of the pathogenesis of periodontitis. *Periodontol. 2000* **69(1)**, 7–17.

Moore, W. E. C., Holdeman, L. V., Cato, E. P., Smibert, R. M., Burmeister, J. A., Ranney, R. R. (1983) Bacteriology of moderate (chronic) periodontitis in mature adult humans. *Infect. Immun.* **42(2)**, 510–515.

Okahashi, N., Nakata, M., Terao, Y., Isoda, R., Sakurai, A., Sumitomo, T., Yamaguchi, M., Kimura, R., Oiki, E., Kawabata, S., Ooshima, T. (2011) Pili of oral *Streptococcus sanguinis* bind to salivary amylase and promote the biofilm formation. *Microb. Pathog*. **50(3–4)**, 148–154.

Papapanou, P., Sanz, M., Buduneli, N., Dietrich, T., Feres, M., Fine, D., Flemmig, T., Garcia, R., Giannobile, W., Graziani, F., Greenwell, H., Herrera, D., Kao, R., Kebschull, M., Kinane, D., Kirkwood, K., Kocher, T., Kornman, K., Kumar, P., Loos, B., Machtei, E., Meng, H., Mombelli, A., Needleman, I., Offenbacher, S., Seymour, G., Teles, R., Tonetti, M. (2018) Periodontitis: Consensus report of workgroup 2 of the 2017 World Workshop on the Classification of Periodontal and Peri-implant Diseases and Conditions. *J. Clin. Periodontol*. **89(1)**, 173–182.

Pratt, L. A., Kolter, R. (1998) Genetic analysis of *Escherichia coli* biofilm formation: Roles of flagella, motility, chemotaxis and type I pili. *Mol. Microbiol.* **30(2)**, 285–293.

Rieber, H., Frontzek, A., Schmitt, H. (2019) *Slackia exigua*, an anaerobic Gram-positive rod and part of human oral microbiota associated with periprosthetic joint infection of the hip: First case and review of the literature. *Anaerobe* **56**, 130–132.

Sanz, M., Beighton, D., Curtis, M., Cury, J., Dige, I., Dommisch, H., Ellwood, R., Giacaman, R., Herrera, D., Herzberg, M., Könönen, E., Marsh, P., Meyle, J., Mira, A., Molina, A., Mombelli, A., Quirynen, M., Reynolds, E., Shapira, L., Zaura, E. (2017) Role of microbial biofilms in the maintenance of oral health and in the development of dental caries and periodontal diseases: Consensus report of group 1 of the Joint EFP/ORCA workshop on the boundaries between caries and periodontal disease. *J. Clin. Periodontol.* **44**, S5–S11 (Suppl. 18).

Sato, T., Hoshino, E., Uematsu, H., Noda, T. (1993) Predominant obligate anaerobes in necrotic pulps of human deciduous teeth. *Microb. Ecol. Health Dis.* **6(6)**, 269–275.

Shahzad, M., Millhouse, E., Culshaw, S., Edwards, C., Ramage, G., Combet, E. (2015) Selected dietary polyphenols inhibit periodontal pathogen growth and biofilm formation. *Food Funct.* **6(3)**, 719–729.

Shemesh, M., Tam, A., Steinberg, D. (2007) Differential gene expression profiling of *Streptococcus mutans* cultured under biofilm and planktonic conditions. *Microbiology (Reading)* **153(Pt 5)**, 1307–1317.

Shemesh, M., Tam, A., Aharoni, R., Steinberg, D. (2010) Genetic adaptation of *Streptococcus mutans* during biofilm formation on different types of surfaces. *BMC Microbiol*. **10**, 51.

Sol, A., Ginesin, O., Chaushu, S., Karra, L., Coppenhagen-Glazer, S., Ginsburg, I., Bachrach, G. (2013) LL-37 opsonizes and inhibits biofilm formation of *Aggregatibacter actinomycetemcomitans* at subbactericidal concentrations. *Infect. Immun.* **81(10)**, 3577–3585.

Stašková, A., Sondorová, M., Nemcová, R., Kačírová, J., Maďar, M. (2021) Antimicrobial and antibiofilm activity of the probiotic strain *Streptococcus salivarius* K12 against oral potential pathogens. *Antibiotics (Basel)* **10(7)**, *793*.

Stepanović, S., Vuković, D., Holá, V., Bonaventura, G., Djukić, S., Cirkovic, I., Růžička, F. (2007) Quantification of biofilm in microtiter plates: Overview of testing conditions and practical recommendations for assessment of biofilm production by staphylococci. *APMIS* **115(8)**, 891–899.

Tzu, L., Hall-Stoodley, L., Costerton, J., Stoodley, P. (2004) Bacterial biofilms: From the natural environment to infectious diseases. *Nat. Rev. Microbiol*. **2(2)**, 95–108.

Wade, W. G., Lewis, M. A., Cheeseman, S. L., Absi, E. G., Bishop, P. A. (1994) An unclassified *Eubacterium* taxon in acute dento-alveolar abscess. *J. Med. Microbiol.* **40(2)**, 115–117.

Glucocorticoid Remediable Aldosteronism in a Family with a Strong History of Cerebral Aneurysms and Hypertension

Jan Zeman[1,2], Crystal Kamilaris[3]

[1] Department of Medicine, University of Connecticut, Farmington, Connecticut, USA;
[2] Institute of Biology and Medical Genetics, First Faculty of Medicine, Charles University and General University Hospital in Prague, Prague, Czech Republic;
[3] Department of Endocrinology, NIH, Maryland, USA

Received November 26, 2024; Accepted August 27, 2025.

Key words: Glucocorticoid remediable aldosteronism – Familial hyperaldosteronism type 1 – Primary aldosteronism – Hypertension – Cerebral aneurysm – Genetic testing – Mineralocorticoid receptor antagonist

Abstract: Glucocorticoid remediable aldosteronism (GRA) also known as familial hyperaldosteronism type 1 (FH1) is a rare genetic form of primary aldosteronism characterized by aldosterone overproduction regulated by adrenocorticotropic hormone (ACTH). We present the case of a 54-year-old woman with severe hypertension and hypokalemia. Genetic testing confirmed GRA by identifying a chimeric gene involving CYP11B1 and CYP11B2. This case highlights the importance of considering GRA in patients with resistant hypertension and a family history of cerebral aneurysms. Management involved glucocorticoid therapy and mineralocorticoid receptor antagonists, leading to significant improvement in blood pressure control.

Mailing Address: Jan Zeman, MD., Institute of Biology and Medical Genetics, First Faculty of Medicine, Charles University and General University Hospital in Prague, Albertov 4, 128 00 Prague 2, Czech Republic; e-mail: jan.zeman94@gmail.com

https://doi.org/10.14712/23362936.2025.23

Prague Medical Report / Vol. 126 (2025) No. 3, p. 151–154

Introduction

Glucocorticoid remediable aldosteronism (GRA) also known as familial hyperaldosteronism type 1 (FH1) is a rare, autosomal dominant form of primary aldosteronism (PA) caused by a chimeric gene resulting from unequal crossing-over between the CYP11B1 and CYP11B2 genes on chromosome 8q24.3. This genetic anomaly leads to aldosterone overproduction regulated by adrenocorticotropic hormone (ACTH), resulting in hypertension and hypokalemia typically presenting in early adulthood. GRA is associated with an increased risk of cerebral aneurysms and hemorrhagic strokes due to vascular remodeling effects of aldosterone (Dluhy and Lifton, 1999; Tan et al., 2023). Early diagnosis and management are crucial to prevent complications. We report a case of GRA in a patient with a significant family history of hypertension and cerebral aneurysms.

Case report

A 54-year-old woman was referred to our clinic for evaluation of severe hypertension and hypokalemia. She was diagnosed with hypertension at the age of 23 after experiencing episodes of light-headedness. Over the years, she had been treated with various antihypertensive medications, including atenolol 50 mg daily, hydralazine 100 mg three times daily, lisinopril 20 mg daily, hydrochlorothiazide 25 mg daily, a combination of amlodipine 10 mg and benazepril 40 mg daily, and chlorthalidone 25 mg daily, without achieving adequate blood pressure control. At the time of examination, the patient was taking atenolol 50 mg daily and amlodipine 10 mg daily and thanks to this major interactions of medications with laboratory testing were avoided. Spironolactone, eplerenone, or amiloride had not been previously tried.

Family history

The patient's family history was significant for hypertension and cerebral aneurysms (Figure 1). Her mother and father both died of ruptured cerebral aneurysms at ages 54 and 56, respectively. A maternal uncle and aunt also had cerebral aneurysms. Multiple family members were diagnosed with hypertension at a young age.

Laboratory investigations

On examination, her blood pressure was 180/100 mm Hg. Laboratory tests revealed:

- Serum potassium: 3.4 mmol/l (reference range: 3.5–5.0 mmol/l)
- Plasma renin activity: undetectable
- Serum aldosterone concentration: 17.6 ng/dl (reference range: 1–16 ng/dl)
- Aldosterone-to-renin ratio: 105 (reference range: <30)
- Adrenocorticotropic hormone (ACTH): 89 pg/ml

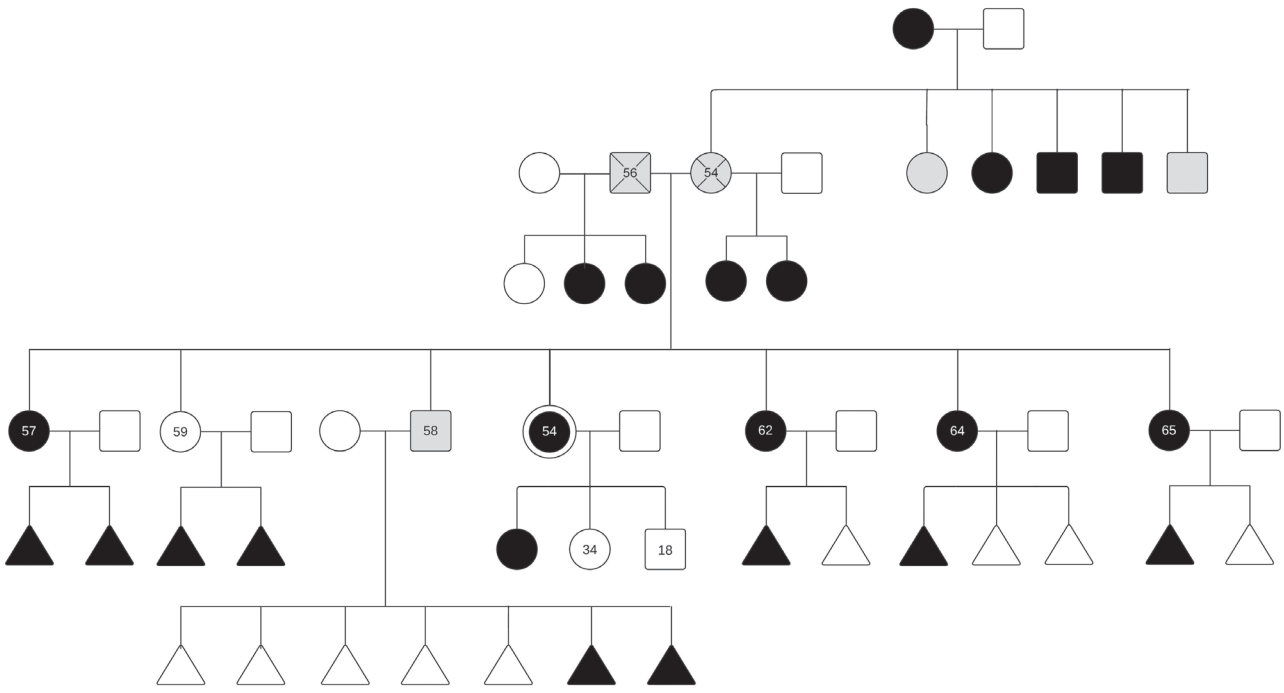

Figure 1: Genogram depicting the family history of hypertension and cerebral aneurysms.
White – no known hypertension or brain aneurysm; grey – known hypertension and brain aneurysm; black – known hypertension and no known brain aneurysm. Numbers signify the age in years of the patient and her family members at the time of evaluation.

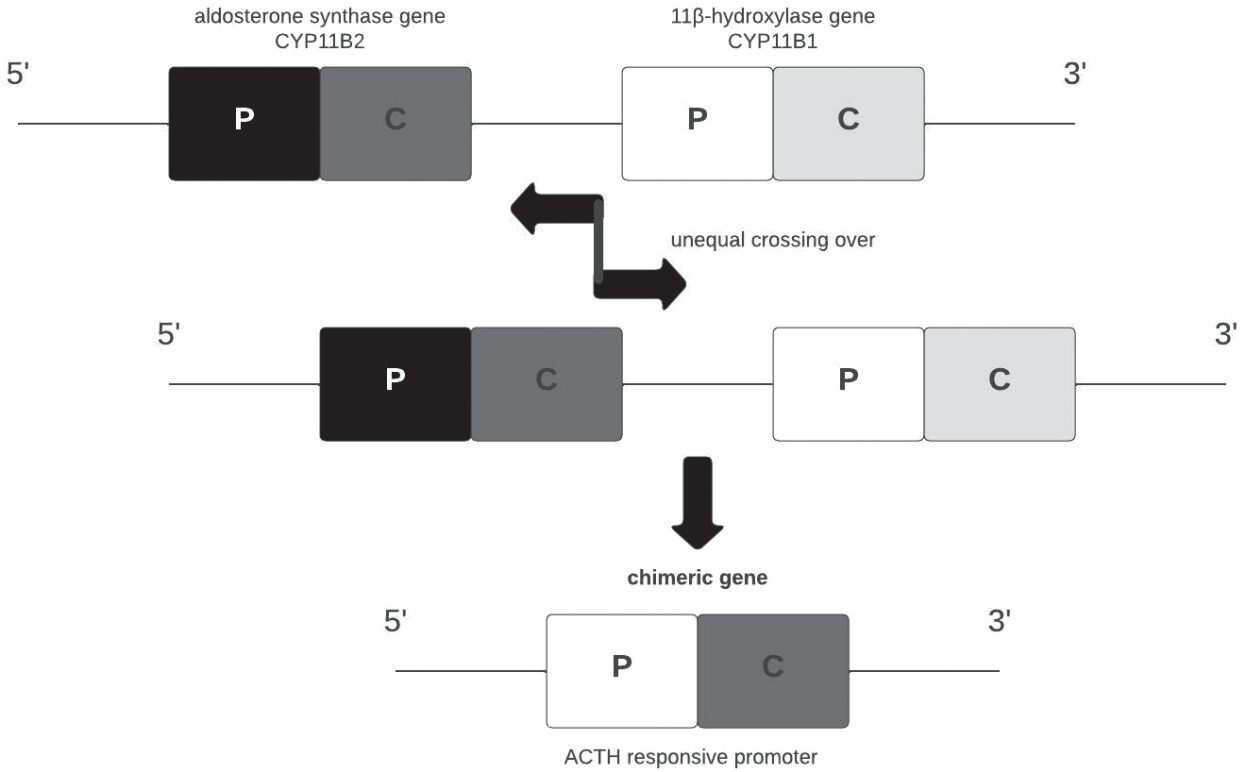

Figure 2: Chimeric gene.
P – promoter sequence; C – coding sequence.

A saline infusion test confirmed PA, with insuppressible aldosterone levels of 24 ng/dl, 21 ng/dl, and 18 ng/dl at 0, 1, and 4 hours post-infusion, respectively. An overnight 1 mg dexamethasone suppression test showed adequate cortisol suppression with a serum cortisol level of 1.0 µg/dl, ruling out cortisol-producing conditions. Serum metanephrines were normal.

Given the family history and laboratory findings, genetic testing was performed using polymerase chain reaction, revealing a chimeric CYP11B1/CYP11B2 gene (Figure 2), confirming the diagnosis of GRA.

Treatment

Initially, the patient was started on low-dose dexamethasone to suppress ACTH production, leading to improved blood pressure control. However, she experienced significant insomnia as a side effect. Spironolactone was then initiated but caused recurrent hyperkalemia. Eplerenone, a selective mineralocorticoid receptor antagonist, was introduced at 25 mg daily and gradually increased to 50 mg daily.

Outcome and follow-up

The patient's systemic blood pressure stabilized at around 130/80 mm Hg with eplerenone monotherapy. Serum potassium levels normalized to 4.0 mmol/l. Regular follow-up appointments were scheduled to monitor blood pressure, electrolyte levels, and potential medication side effects. ACTH levels were unfortunately not repeated following the initiation of the treatment.

Given the strong family history of cerebral aneurysms, magnetic resonance angiography (MRA) of the cerebral vessels was performed, which did not reveal any aneurysms. Genetic counselling was provided, and first-degree relatives were advised to undergo screening for GRA and cerebral aneurysms.

Discussion

This case underscores the importance of considering GRA in patients with resistant hypertension and a family history of early-onset hypertension or cerebrovascular events. The patient's presentation with severe hypertension and hypokalemia aligns with typical manifestations of GRA, a condition caused by a chimeric CYP11B1/CYP11B2 gene resulting in aldosterone overproduction under ACTH regulation (Lifton et al., 1992; Dluhy and Lifton, 1999; Tan et al., 2023). Interestingly in general patients with FH1 tend to be younger, more commonly female, have lower plasma aldosterone concentration, higher plasma renin activity, and less frequent hypokalemia compared to those with

sporadic primary aldosteronism (Araujo-Castro et al., 2024). The prevalence of FH1 ranges from 0.2 to 0.7% in various primary aldosteronism cohorts and may reach up to 4% in selected populations (Mulatero et al., 2011; Araujo-Castro et al., 2025). Genetic testing confirmed the diagnosis, consistent with findings by Lifton et al. (1992), who identified this genetic marker as definitive for GRA.

Treatment with low-dose glucocorticoids like dexamethasone effectively suppresses ACTH, reducing aldosterone production and managing hypertension (McMahon and Dluhy, 2004). However, our patient experienced significant side effects, necessitating the use of mineralocorticoid receptor antagonists. Eplerenone was preferred over spironolactone due to a better side effect profile, leading to marked improvement in blood pressure and normalization of potassium levels (Funder et al., 2016).

The association between GRA and an increased risk of cerebral aneurysms is well-documented (Litchfield et al., 1998; Mohan et al., 2015; Shahrrava et al., 2016). Excess aldosterone may contribute to vascular remodelling and arterial wall weakening, predisposing patients to aneurysm formation (Al Romhain et al., 2015). Given the patient's family history, screening for cerebral aneurysms using imaging modalities like MRA is essential. Early detection allows for timely intervention, potentially reducing morbidity and mortality.

Effective management of GRA requires a multidisciplinary approach involving endocrinologists, geneticists, and other specialists. Regular monitoring of blood pressure, electrolytes, and potential medication side effects is crucial for optimal patient care. Genetic counselling is recommended for family members, as early diagnosis can lead to preventive measures and improved outcomes.

Conclusion

GRA should be considered in patients with resistant hypertension and a strong family history of hypertension and cerebral aneurysms. Early diagnosis through genetic testing allows for targeted therapy, improving outcomes and preventing complications. Awareness of the increased risk of cerebral aneurysms in GRA patients highlights the importance of appropriate screening and preventive measures.

References

Al Romhain, B., Young, A. M., Battacharya, J. J., Suttner, N. (2015) Intracranial aneurysm in a patient with glucocorticoid-remediable aldosteronism. *Br. J. Neurosurg.* **29**, 715–717.

Araujo-Castro, M., Parra, P., Martín Rojas-Marcos, P., Paja Fano, M., González Boillos, M., Pascual-Corrales, E., García Cano, A. M., Ruiz-Sanchez, J. G., Vicente Delgado, A., Gómez Hoyos, E., Ferreira, R., García Sanz, I., Recasens Sala, M., Barahona San Millan, R., Picón César, M. J., Díaz Guardiola, P., Perdomo, C. M., Manjón-Miguélez, L., García Centeno, R., Rebollo Román, Á., Gracia Gimeno, P., Robles Lázaro, C., Morales-Ruiz, M., Calatayud, M., Furio Collao, S. A., Meneses, D., Sampedro Nuñez, M., Escudero Quesada, V., Mena Ribas, E., Sanmartín Sánchez, A., Gonzalvo Diaz, C., Lamas, C., Del Castillo Tous, M., Serrano Gotarredona, J., Michalopoulou Alevras, T., Moya Mateo, E. M., Hanzu, F. A. (2024) Differences in the clinical and hormonal presentation of patients with familial and sporadic primary aldosteronism. *Front. Endocrinol. (Lausanne)* **15**, 1336306.

Araujo-Castro, M., Ruiz-Sánchez, J. G., Gonzalvo, C., Lamas, C., Parra Ramírez, P., Martín Marcos-Rojas, P., Paja, M., Robles Lázaro, C., Michalopoulou, T., Tous, M., Gonzalez-Boillos, M., Recio-Córdova, J. M., Casteras, A., Fernández-Álvarez, P., Barca Tierno, V., Mulatero, P. (2025) Genetic testing for primary aldosteronism in SPAIN: Results from the SPAIN-ALDO Registry and review of the literature. *J. Clin. Endocrinol. Metab.* **110(5)**, e1573–e1579.

Dluhy, R. G., Lifton, R. P. (1999) Glucocorticoid-remediable aldosteronism. *J. Clin. Endocrinol. Metab.* **84(12)**, 4341–4344.

Funder, J. W., Carey, R. M., Mantero, F., Murad, M. H., Reincke, M., Shibata, H., Stowasser, M., Young, W. F. Jr. (2016) The management of primary aldosteronism: Case detection, diagnosis, and treatment: An Endocrine Society Clinical Practice Guideline. *J. Clin. Endocrinol. Metab.* **101(5)**, 1889–1916.

Lifton, R. P., Dluhy, R. G., Powers, M., Rich, G. M., Cook, S., Ulick, S., Lalouel, J. M. (1992) A chimaeric 11β-hydroxylase/aldosterone synthase gene causes glucocorticoid-remediable aldosteronism and human hypertension. *Nature* **355(6357)**, 262–265.

Litchfield, W. R., Anderson, B. F., Weiss, R. J., Lifton, R. P., Dluhy, R. G. (1998) Intracranial aneurysm and hemorrhagic stroke in glucocorticoid-remediable aldosteronism. *Hypertension* **31**, 445–450.

McMahon, G. T., Dluhy, R. G. (2004) Glucocorticoid-remediable aldosteronism. *Cardiol. Rev.* **12**, 44–48.

Mohan, D., Munteanu, V., Coman, T., Ciurea, A. V. (2015) Genetic factors involved in intracranial aneurysms – Actualities. *J. Med. Life* **8**, 336–341.

Mulatero, P., Tizzani, D., Viola, A., Bertello, C., Monticone, S., Mengozzi, G., Schiavone, D., Williams, T. A., Einaudi, S., La Grotta, A., Rabbia, F., Veglio, F. (2011) Prevalence and characteristics of familial hyperaldosteronism: the PATOGEN study (Primary Aldosteronism in TOrino-GENetic forms). *Hypertension* **58**, 797–803.

Shahrrava, A., Moinuddin, S., Boddu, P., Shah, R. (2016) A case of glucocorticoid remediable aldosteronism and thoracoabdominal aneurysms. *Case Rep. Endocrinol.* **2016**, 2017571.

Tan, S. T., Boyle, V., Elston, M. S. (2023) Systematic review of therapeutic agents and long-term outcomes of familial hyperaldosteronism type 1. *Hypertension* **80(7)**, 1517–1525.

Intussusception by Colonic Lipoma in a 51-year-old Patient – A Case Report

Marija Zubčić[1], Florian Stephan Bienenfeld[2], Alessio Sciacqua[3], Manuela Montatore[3], Gianmichele Muscatella[3], Giuseppe Guglielmi[3,4,5]

[1] Radiology Unit, Zadar General Hospital, Zadar, Croatia;
[2] St. Johannes Hospital, Dortmund, Germany;
[3] Department of Clinical and Experimental Medicine, Foggia University School of Medicine, Foggia, Italy;
[4] Radiology Unit, "Dimiccoli" Hospital, Barletta, Italy;
[5] Radiology Unit, "IRCCS Casa Sollievo della Sofferenza" Hospital, San Giovanni Rotondo, Italy

Received November 21, 2024; Accepted August 27, 2025.

Key words: Bowel-within-bowel sign – Computed tomography (CT) – Colocolic – Giant intussusception – Lipoma

Abstract: Intussusception is a rare condition in adults, and often presents with non-specific symptoms. Lipoma, a benign tumour of adipose tissue, is an infrequent cause of intussusception. Standard diagnostic methods include computed tomography (CT) imaging, with typical radiological features such as "bowel-within-bowel" sign enabling a prompt diagnosis with a high sensitivity and specificity. This case report describes a 51-year-old female patient who presented to the emergency department with abdominal pain caused by intussusception, with a gastrointestinal lipoma as the lead point, diagnosed through CT imaging. The article highlights the rarity of colonic lipoma, its potential to cause intussusception and the importance of timely diagnosis to avoid complications like bowel obstruction or necrosis.

Mailing Address: Prof. Giuseppe Guglielmi, MD., Department of Clinical and Experimental Medicine, Foggia University School of Medicine, Viale L. Pinto 1, 71121, Foggia, Italy; e-mail: giuseppe.guglielmi@unifg.it

https://doi.org/10.14712/23362936.2025.24

Prague Medical Report / Vol. 126 (2025) No. 3, p. 155–158

Introduction

By definition, intestinal intussusception presents the invagination of an intestinal loop with a mesenteric fold (intussusceptum) in the lumen of an immediately adjacent segment of the bowel (intussuscipiens) following peristalsis (Balzano et al., 2024).

Lipoma, a benign tumour of adipose tissue, is an uncommon cause of intussusception in contrast to colonic cancer (Busa et al., 2022).

It is more common in pediatric than in adult patients and therefore represents a challenge to be diagnosed in adult groups (Goyal et al., 2023).

Colocolic intussusception caused by lipoma affects female patients more often, typical age being between the fifth and sixth decade of life (Niazi et al., 2023).

It is mainly characterized by non-specific signs and symptoms; most commonly tenderness, followed by abdominal distension joined with abdominal pain, altered bowel movements and low gastrointestinal bleeding (Niazi et al., 2023).

The most common location of gastrointestinal lipoma is the ascending colon (45%) and the rarest is the transverse colon (9%) (Niazi et al., 2023).

Standard diagnostic procedures for identifying lipoma include computed tomography (CT) and magnetic resonance imaging (MRI) (Niazi et al., 2023).

In this report, we present a case of a 51-year-old female patient with gastrointestinal lipoma causing intussusception that was diagnosed via CT imaging.

Case report

A 51-year-old female patient was admitted to the emergency department with non-specific abdominal pain in the lower left quadrant lasting for five days.

Physical examination revealed a soft abdomen with mild tenderness in the lower left quadrant.

Laboratory blood tests showed elevated CRP (C-reactive protein) of 29.3 (mg/l) and leukocytes of 10.34 (thou/µl), while renal and liver function tests were within normal values.

Due to the previous findings, clinicians suspected acute abdomen and requested a CT.

Hydro-CT of the abdomen with native and contrast venous phase revealed a thickening of up to 3 cm of the colon transversum with a "bowel-within-bowel" sign (Figure 1). The wall of the colon showed no enhancement of contrast agent. These findings were indicative of colocolic intussusception.

Aboral of the invagination a mass measuring 3.2×3.9×4 cm (AP [anteroposterior] × CC [craniocaudal] × LL [laterolateral]), mostly consisting of adipose tissue, was found (Figures 2 and 3). The small intestine showed no signs of dilatation. Additionally, there was no evidence of passage disruption. Pericolic fat stranding in the region of intussusception was observed.

Furthermore, two lymph nodes in the surrounding area of the mass were detected, the bigger one measuring 0.7×0.6 cm. No signs of free air or free fluids were seen.

A colonoscopy was performed the next day which confirmed a mass suspicious of colon carcinoma causing the invagination. A histopathologic study afterward was not able to confirm the dignity of the lesion.

A laparoscopic resection of the bowel was performed: the histopathological report described a colon segment with a completely removed submucosal lipoma measuring 3.5 cm, no positivity for CD117 (c-kit), no reaction to CK 7 and no evidence of malignancy.

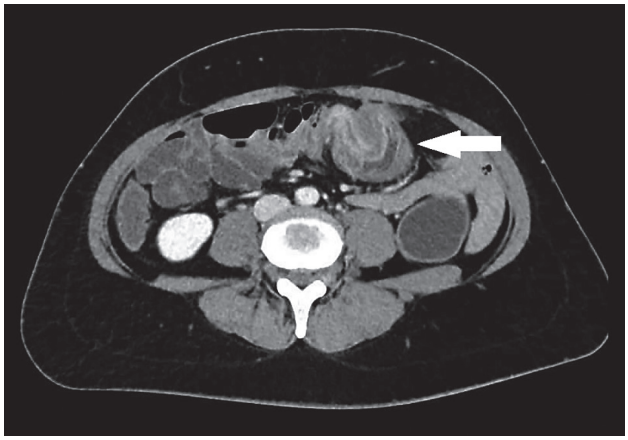

Figure 1: Abdominal hydro-computed tomography, venous phase, axial view. The "bowel-within-bowel" configuration of transversal colon, in which the layers of the bowel are duplicated forming concentric rings.

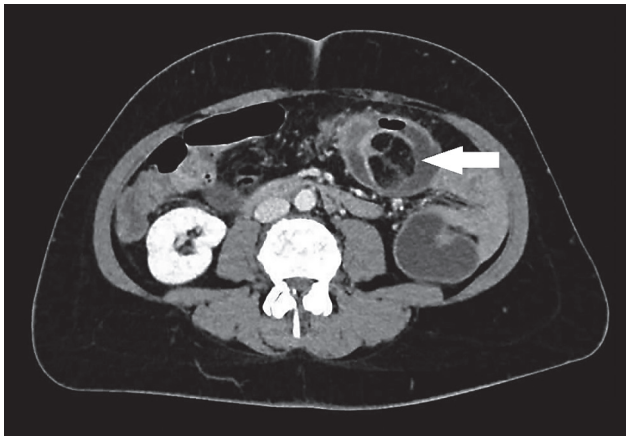

Figure 2: Abdominal hydro-computed tomography, venous phase, axial view. The lipomatous mass lesion aborally to the intussusception showed as a well-defined, fat-density lesion.

Figure 3: Abdominal hydro-computed tomography, venous phase, coronal view. The pedunculated lipomatous mass as the leading point of the intussusception.

Discussion

While intussusception represents a common condition in pediatric patients with 95% of all intussusception cases, it is a rare finding among adults with the remaining 5%, affecting mainly female patients with a typical age being between 40 and 70 years (Goyal et al., 2023; Niazi et al., 2023).

The incidence rate of colonic lipoma is reported to be between 0.2 and 4.5% worldwide, with only 17% resulting in colocolic intussusception (Panagiotakis et al., 2017; Niazi et al., 2023). They are the third most common benign tumours found in the large intestine, following hyperplastic and adenomatous polyps (Panagiotakis et al., 2017).

Smaller lipomas are mostly asymptomatic, while lipomas larger than 2 cm, even though they are rare, can cause abdominal pain, intussusception, change in bowel habits and gastrointestinal bleeding (Abu-Khalaf et al., 2024).

A literature review indicates that larger lipomas are associated with an increased risk of intussusception, with many sources using the term "giant lipoma", although a clear definition is not established.

Some authors use the term giant lipoma for lipomatous masses that exceed 4.5, some define the limit to be 5 cm, while Yaman et al. (2013) define it as a lesion with a measurement of at least 10 cm in one dimension or a minimum weight of a 1,000 g (Panagiotakis et al., 2017; Abu-Khalaf et al., 2024).

A few pathophysiological mechanisms have been proposed to lead to this condition: a tumour may act as a foreign body, inducing intense peristalsis that allows the contracted bowel to slip into the dilated section. Furthermore, the tumour can inhibit muscle function or be pulled forward by traction (Mouaqit et al., 2013).

In 90% of the cases, the lipomas of the colon are submucosal (Kim et al., 2006).

Characteristic signs of lipoma seen on CT include the "pillow mark", which is a soft lesion that shows a cushion-like indentation in the mucosa when pressed with closed biopsy forceps and the "bare fat mark" which refers to the leakage of fat following a biopsy (Niazi et al., 2023).

Additionally, if a lesion has a fat-equivalent density (–40 to –120 Hounsfields units [HU]) and sharp margins, there is a strong suspicion that it is a lipomatous lesion (Mouaqit et al., 2013).

The invagination of the intussusceptum into the intussuscipiens presents as a "target" sign due to the alternating patterns of intestinal walls and mesenteric fat when viewed in a plane perpendicular to the main axis of the affected segment (Balzano et al., 2024).

A pathognomonic sign, also observed in our case, is the "bowel-within-bowel" configuration, where the bowel layers overlap, resulting in a circular formation (Kim et al., 2006).

The appearance of intussusception is influenced by factors such as the presence of a lead point, the configuration of the lead mass, the extent of bowel walls edema, and the amount of invaginated mesenteric fat. When bowel wall edema occurs due to compromised circulation in the mesenteric vessels, thickened bowel loops can complicate the distinction between a lead mass and inflammation, as the lead mass may present as amorphous (Kim et al., 2006).

The sensitivity of CT scans for diagnosing intussusception ranges from 71.4 to 87.5%, with a specificity of 100% (Mouaqit et al., 2013; Panagiotakis et al., 2017). Therefore, CT continues to be the diagnostic modality of choice for intussusception as it can precisely identify the intussusceptive tissue and the lead point (Goyal et al., 2023).

Endoscopy offers insight into the external features of a lesion, but without a biopsy, it is not a diagnostic procedure by itself, as it can misidentify lipomas as adenomas (Busa et al., 2022; Abu-Khalaf et al., 2024).

The importance of prompt diagnosis in this condition lies in its potential to lead to obstruction of the inner passage, which can affect the mesentery, impair blood flow, and ultimately cause tissue damage.

Prague Medical Report / Vol. 126 (2025) No. 3, p. 155–158

This can result in various further complications, such as intestinal blockage, necrosis, and sepsis (Goyal et al., 2023). Additionally, large internal lipomas can cause abdominal pain, kidney failure and other systemic issues, and they may even undergo sarcomatous transformation (Yaman et al., 2013).

Approximately two-thirds of colonic intussusceptions result from primary adenocarcinoma. Consequently, if a lipoma is not identified before surgery, as in our case, it should be managed as if it were cancer, necessitating the removal of a significant portion of the colon (Niazi et al., 2023).

Conclusion

The diagnosis of intussusception caused by lipoma is challenging, given the rarity and non-specific symptoms of the condition.

Given that abdominal pain is one of the most frequent reasons for emergency room visits, it is crucial to consider it as a possible differential diagnosis in these patients.

The emphasis is on a detailed diagnostic approach, centered around CT imaging, to prevent potential complications.

Our case report is an ideal example of intussusception caused by lipoma that was recognized promptly using CT diagnostics.

Additional reports on intussusception are needed to enhance the diagnostic approach for this rare condition.

References

Abu-Khalaf, R., Abu-Khalaf, L., Abu-Khalaf, S., Abu-Khalaf, A. (2024) A large sigmoid pseudo-pedunculated lipoma mimicking an adenoma: A report of a rare case and literature review. *Cureus* **16(8)**, e67419.

Balzano, R. F., Lattanzio, F., Fascia, G., Montatore, M., Balbino, M., Masino, F., Mannatrizio, D., Guglielmi, G. (2024) Idiopathic enterocolic intussusception: Imaging findings in an abdominal emergency. *Digital Diagnostics* **5(2)**, 354–360.

Busa, V., Bandaru, S. S., Mahat, R., Janga, C. (2022) A rare case of colo-colonic intussusception caused by colonic submucosal lipoma. *Cureus* **14(3)**, e23600.

Goyal, M. K., Gupta, Y. K., Mehta, V., Singh, A., Sood, A. (2023) Colonic lipoma: A rare cause of intussusception. *Cureus* **15(10)**, e48074.

Kim, Y. H., Blake, M. A., Harisinghani, M. G., Archer-Arroyo, K., Hahn, P. F., Pitman, M. B., Mueller, P. R. (2006) Adult intestinal intussusception: CT appearances and identification of a causative lead point. *Radiographics* **26(3)**, 733–744.

Mouaqit, O., Hasnai, H., Chbani, L., Oussaden, A., Maazaz, K., Amarti, A., Taleb, K. A. (2013) Pedunculated lipoma causing colo-colonic intussusception: A rare case report. *BMC Surg.* **13**, 51.

Niazi, S. A. K., Raza, M. S., Mukhtar, M. U., Hassan, R., Nasir, M. U. (2023) Colonic lipoma mimicking malignancy and presenting as an intussusception: A rare case report. *Int. J. Surg. Case Rep.* **109**, 108611.

Panagiotakis, G. I., Andreou, A. G., Petrakis, I. E., Tzardi, M., Daskalogiannaki, M., Chalkiadakis, G. E. (2017) Laparoscopic resection of a sigmoid colon lipoma in a young female patient: A case report and review of the literature. *Oncol. Lett.* **13(3)**, 1303–1306.

Yaman, İ., Derici, H., Demirpolat, G. (2013) Giant colon lipoma. *Ulus. Cerrahi Derg.* **31(2)**, 102–104.

Unveiling the Enigma: Plasma Cell Leukaemia Presenting with Flower-like Cells, Mimicking Adult T-cell Leukaemia – A Rare Diagnostic Conundrum

Anurag Singh[1], Gyanendra Singh[2]

[1] Department of Pathology, King George's Medical University, Lucknow, Uttar Pradesh, India;
[2] Department of Pathology, All India Institute of Medical Sciences, Rajkot, Gujarat, India

Received May 8, 2024; Accepted August 27, 2025.

Key words: Plasma cell – Plasma cell leukaemia – Leukaemia/lymphoma adult T-cell

Abstract: Peripheral plasma cell leukaemia (PCL) is a rare hematologic malignancy that can pose diagnostic challenges due to its resemblance to other conditions such as adult T-cell leukaemia/lymphoma (ATLL) or dissemination lymphoma in peripheral blood. We present a case report of a 40-year-old male with symptoms of fatigue, irregular heartbeat, weight loss, and bone pain, whose peripheral blood examination revealed hyperleukocytosis with atypical lymphoid cells exhibiting flower-shaped nuclei, reminiscent of adult T-cell leukaemia/lymphoma. Further investigations including bone marrow aspiration and biopsy confirmed the diagnosis of primary PCL. Immunophenotyping revealed expression of plasma cell antigens CD38 and CD138. This case underscores the importance of recognizing morphological variants and employing comprehensive immunophenotypic analysis for accurate diagnosis of PCL, especially when atypical nuclear features mimic other hematologic malignancies.

Mailing Address: Gyanendra Singh, MD., Department of Pathology, AIIMS Rajkot, village Khanderi, Parapipaliya, 360001, Gujarat, India; e-mail: gyanendra002@gmail.com

https://doi.org/10.14712/23362936.2025.25

Prague Medical Report / Vol. 126 (2025) No. 3, p. 159–161

Introduction

Peripheral clonal plasma cells with a count greater than 2×10^9/l are considered to be indicative of plasma cell leukaemia (PCL), an uncommon condition that can develop independently of or as part of plasma cell myeloma (García-Sanz et al., 1999). Plasma cell leukaemia with abnormal plasma cells and nuclear characteristics in the form of flower-like cells has been reported previously. Because "flower cells" or clover-leaf lymphocytes are usually described in human T-cell lymphotropic virus type 1 (HTLV-1) induced adult T-cell leukaemia and very infrequently in B-cell lymphoma, these morphological characteristics can create diagnostic challenges and can mimic lymphoma (Singh et al., 2017). We describe a case of primary PCL that mimicked adult T-cell leukaemia or lymphoma and presented with nuclei in the form of flowers. This is a really informative case report about a patient with multiple myeloma who had flower-shaped nuclear characteristics and aberrant plasma cells.

Case report

A 40-year-old man presented with complaints of fatigue, an irregular heartbeat, weight loss, and bone pain for the last three months. There was no medical history for the patient. Family history was also inconclusive. During the physical examination, neither splenomegaly nor lymphadenopathy were found. On routine blood examination, the total blood count showed hyperleukocytosis, with a count of 112×10^9/l, 97% atypical lymphoid cells, haemoglobin 9.2 g/dl, and a platelet count of 150×10^9/l. Viral markers were negative. The serum biochemical test showed elevated levels of beta-2 microglobulin (19.5 mg/l), lactate dehydrogenase (4,328 IU/l), and hypercalcemia (3.93 mmol/l). C-reactive protein was less than 2.8 mg/l. A renal function test showed a mild elevation of serum creatinine, and a liver function test showed moderately elevated transaminase. Peripheral blood smear examination shows medium to large, profoundly basophilic, coarsely clumped chromatin, medium to large size, and occasionally perinuclear clearing of the highly pleomorphic atypical lymphoid cells. Like adult T-cell leukaemia/lymphoma (ATLL) flower cells, the nuclear morphology was highly asymmetrical and frequently polylobulated (Figure 1A). Based on peripheral smear findings, a differential diagnosis of either an ATLL or a PCL was considered. On bone marrow aspiration and biopsy, there was hypercellularity with >90% of the same large atypical cells as seen in the peripheral blood smear (Figure 1B and C). On initial immunophenotyping, both B-cell and T-cell lineage markers were negative, but with an extended panel of markers, the plasma cell antigens CD38 and CD138 were found to be expressed by these atypical cells (Figure 1D). Serum immunofixation revealed the presence of lambda light chains but not heavy chains. Light chains in the urine were not studied. The study's findings on HTLV-1 or 2 infections were unfavourable. Based on these findings, a primary diagnosis of primary plasma cell leukaemia was made.

Discussion

Flower-shaped nuclei, although typically associated with adult T-cell leukaemia/lymphoma, have also

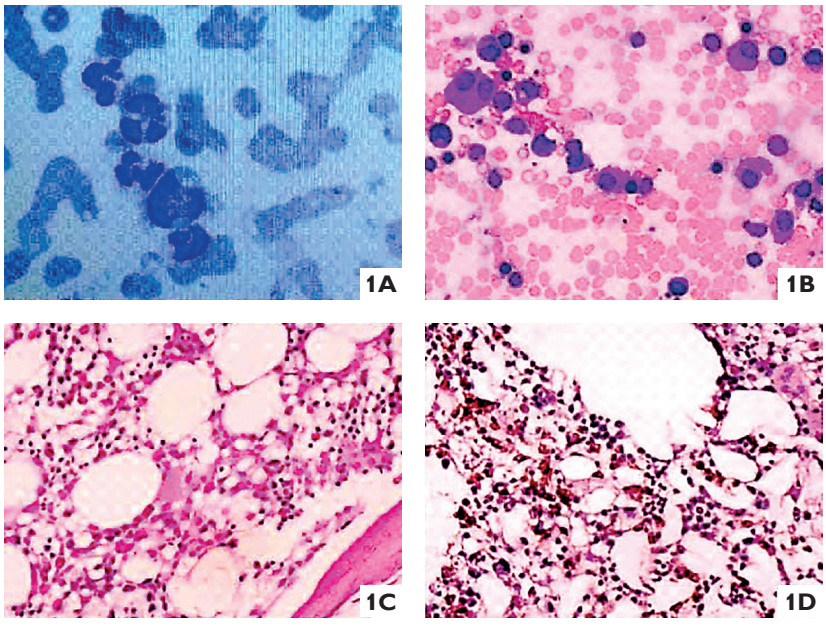

Figure 1: A) Abnormal flower-shaped cells with lobes, numerous nuclear convolutions, and basophilic cytoplasm (arrow), Wright-Giemsa stain, 1000× magnification. B and C) Bone marrow aspiration and biopsy images show many plasma cells with a few binucleated forms, May-Grünwald Giemsa (MGG) stain, and haematoxylin and eosin stain, 100× image. D) Atypical plasma cells show immunopositivity for CD138, 100× image.

been observed as an unusual morphological finding in plasma cell leukaemia. These cases can pose diagnostic challenges due to overlapping features with lymphoid neoplasms. In fact, rare instances of PCL presenting with flower-like nuclei have been misinterpreted as ATLL based on morphology alone have been described in the literature (Shibusawa, 2020; De Miguel Sánchez et al., 2021). Condensed chromatin, on the other hand, may make flower-shaped plasma cells resemble lymphocytes. Whether these cells were flower-like plasma cells or flower-like lymphocytes could have been determined by CD20 or CD138 immunocytochemistry, as reported earlier (Kobayashi et al., 2015; Sall et al., 2021). There have also been reports of a few instances of morphological variants of PCL, such as plasmoblastic or megakaryocytic, mimicking acute leukaemia (Liu et al., 2020). Flow cytometry remains an excellent tool for identifying clonal plasma cells from normal or reactive ones. In PCL, abnormal plasma cells often lack CD19 and CD20 expression while being positive for CD28, CD117, CD56, and CD33. They also have light chain restriction and are clonally positive for either kappa or lambda immunoglobulin, distinguishing them from polyclonal plasma cells. This immunophenotypic profile offers important diagnostic clarity in confusing instances (Flores-Montero et al., 2016). Patients with adult T-cell leukaemia or lymphoma are characterised by the appearance of flower-like lymphocytes in their peripheral blood, however their morphological mimickers can also be seen in PCL as in present case (Dahmoush et al., 2002).

Conclusion

Plasma cell leukaemia indeed presents a diagnostic challenge, especially when encountering unusual features like the presence of flower-like cells, which can lead to confusion with other hematological malignancies such as adult T-cell leukaemia/lymphoma. Immunophenotyping plays a crucial role in accurately diagnosing such cases. Prompt and correct diagnosis is critical in plasma cell leukaemia, as it determines subsequent treatment options such as chemotherapy, targeted therapy, immunomodulatory medications, or stem cell transplantation, depending on disease stage, patient age, and overall health state.

References

Dahmoush, L., Hijazi, Y., Barnes, E., Stetler-Stevenson, M., Abati, A. (2002) Adult T-cell leukemia/lymphoma: A cytopathologic, immunocytochemical, and flow cytometric study. *Cancer* **96(2)**, 110–116.

De Miguel Sánchez, C., Robles de Castro, D., Pisón Herrero, C., Pérez Persona, E., Salcedo Cuesta, L., Guinea de Castro, J. M. (2021) Primary plasma cell leukaemia presenting with flower-shaped nuclei. *Br. J. Haematol*. **193(4)**, 689.

Flores-Montero, J., de Tute, R., Paiva, B., Perez, J. J., Böttcher, S., Wind, H., Sanoja, L., Puig, N., Lecrevisse, Q., Vidriales, M. B., van Dongen, J. J., Orfao, A. (2016) Immunophenotype of normal vs. myeloma plasma cells: Toward antibody panel specifications for MRD detection in multiple myeloma. *Cytometry B Clin. Cytom*. **90(1)**, 61–72.

García-Sanz, R., Orfão, A., González, M., Tabernero, M. D., Bladé, J., Moro, M. J., Fernández-Calvo, J., Sanz, M. A., Pérez-Simón, J. A., Rasillo, A., Miguel, J. F. (1999) Primary plasma cell leukemia: Clinical, immunophenotypic, DNA ploidy, and cytogenetic characteristics. *Blood* **93(3)**, 1032–1037.

Kobayashi, M., Horikawa, M., Uehara, T., Honda, T., Kobayashi, T., Sakai, H. (2015) Flower-like/clover leaf lymphocytes appear in various diseases: Cerebrospinal fluid cytology case with review of the literature. *Diagn. Cytopathol*. **43**, 88–90.

Liu, K., Song, H., Shi, J., Zhang, W., Mu, R., Li, L. (2020) Rare case of plasma cell myeloma with megakaryoblastic morphology mimicking acute leukemia. *Indian J. Pathol. Microbiol*. **63(3)**, 485–487.

Sall, A., Seck, M., Samb, D., Faye, B., Gadji, M., Diop, S., Touré, A. O. (2021) Flower-like plasma cell nuclei in multiple myeloma. *Turk. J. Haematol*. **38(2)**, 153–154.

Shibusawa, M. (2020) Plasma cell leukaemia presenting as flower-shaped plasma cells mimicking adult T-cell leukaemia or lymphoma. *Lancet Haematol*. **7**, e270.

Singh, N., Gandhi, J., Agrawal, N., Panaych, A., Tejwani, N., Mehta, A. (2017) Diagnostic dilemma in the morphological detection of flower cells in lymphomas. *Indian J. Hematol. Blood Transfus*. **33(4)**, 614–616.

Factitiously Low Total Creatine Kinase Activity in Severe Rhabdomyolysis: A Case Series

Ariff Aizzat Abdul Razak[1,2], **Wan Mohd Saifuhisam Wan Zain**[2,3], **Wan Azman Wan Norlina**[2,3]

[1] Pathology Unit, Faculty of Medicine, Universiti Sultan Zainal Abidin, Kuala Terengganu, Terengganu, Malaysia;
[2] Department of Chemical Pathology, School of Medical Sciences, Universiti Sains Malaysia, Kubang Kerian, Kelantan, Malaysia;
[3] Hospital Pakar Universiti Sains Malaysia, Kubang Kerian, Kelantan, Malaysia

Received February 4, 2025; Accepted August 27, 2025.

Key words: Creatine kinase – Rhabdomyolysis – Analytical interference – Clinical chemistry – Laboratory medicine

Abstract: Factitiously low total creatine kinase (CK) activity can occur in severe rhabdomyolysis, potentially causing misdiagnosis and inappropriate patient management. We hereby describe 2 cases of severe rhabdomyolysis with falsely low total CK activity. Case 1 was a 61-year-old lady with underlying diabetes mellitus diagnosed with severe rhabdomyolysis secondary to severe pneumonia. Case 2 was a 77-year-old man with underlying diabetes mellitus diagnosed with severe rhabdomyolysis secondary to recurrent pyogenic spondylodiscitis. Both cases showed unexpectedly low total CK activity (<7 U/l N: 26–192 U/l). Post-dilution procedures showed markedly elevated total CK activity for case 1 (18,364 U/l [1:11]) and case 2 (15,217 U/l [1:11]). Unfortunately, both patients succumbed despite optimized medical treatment due to multi-organ failures. Measurement of CK in blood is considered as a diagnostic marker for rhabdomyolysis and its severity. Most of the laboratory nowadays measures total CK activity using enzymatic coupled with spectrophotometry method. However, substrate depletion can occur in severe rhabdomyolysis in which creatine phosphate is consumed by high concentration of CK in sample before the kinetic measurement is initiated, leading to factitiously low total CK activity. Sample dilution can be done to obtain the accurate total CK activity, avoiding result reporting error and possibility misdiagnosis of rhabdomyolysis. Good communication between clinical and laboratory personnel is vital to prevent the error and safeguard patient management.

Mailing Address: Dr. Wan Mohd Saifuhisam Wan Zain, Department of Chemical Pathology, School of Medical Sciences, Universiti Sains Malaysia Health Campus, Jalan Raja Perempuan Zainab 2, 16150, Kubang Kerian, Kelantan, Malaysia; Phone: +609 767 64 90; e-mail: wansaifu1985@usm.my

https://doi.org/10.14712/23362936.2025.26

Introduction

Rhabdomyolysis is a medical condition associated with rapid dissolution of damaged skeletal muscle (Torres et al., 2015). Measurement of creatine kinase (CK) in blood is considered as a diagnostic marker for rhabdomyolysis and its severity as disruption of skeletal muscle integrity leads to the release of CK as part of intracellular muscle components as well as myoglobin, lactate dehydrogenase and electrolytes into bloodstream (Nance and Mammen, 2015; Torres et al., 2015). Although rhabdomyolysis is most commonly caused by direct traumatic injury, uncommonly it can be secondary to severe infections (Torres et al., 2015; Zhao and Zheng, 2019). Postulated mechanisms for rhabdomyolysis secondary to infection include tissue hypoxia due to sepsis, dehydration, toxin, direct invasion by microorganisms, pyrexia associated or rigors (Torres et al., 2015).

Case report

Case 1

A 61-year-old Malay lady with underlying diabetes mellitus presented with productive cough associated with shortness of breath for 3 days. No chest pain, no history of contact with sick individual, no history of traveling and no history of trauma. Upon arrival at the emergency department she was alert, conscious,

Table 1: Case 1 laboratory investigations

Test		Result	Unit	Reference range
Complete full blood count	WBC	18.1×10^9	/l	4.38–10.00
	RBC	5.07×10^9	/l	3.91–5.30
	Hb	11.6	g/dl	11.24–15.07
	Hct	35.5	%	33.80–45.22
	MCV	69.4	fl	78.03–94.96
	MCH	27.2	pg	24.45–31.49
	MCHC	32.4	g/dl	30.65–33.75
	Plt	219×10^9	/l	198–405
Coagulation profile	PT	13.7	s	12.61–15.72
	INR	1.0		0.86–1.14
	APTT	41.8	s	30.00–45.80
Liver function tests profile	Total protein	50	g/l	66–87
	Albumin	24	g/l	39.7–49.4
	AST	1049	U/l	10–35
	ALT	246	U/l	10–35
	ALP	170	U/l	35–104
	Total bilirubin	11	µmol/l	≤ 15
Renal function tests profile	Urea	17.4	mmol/l	2.76–8.07
	Sodium	138.0	mmol/l	136–145
	Potassium	6.1	mmol/l	3.5–5.1
	Chloride	98.0	mmol/l	98–107
	Creatinine	601.0	µmol/l	44–80
Creatine kinase		< 7	U/l	26–192
		18364 (post dilution 1:11)		
		306.68 (post dilution 1:11)	µkat/l	0.43–3.21
LDH		367	U/l	135–214
Urinalysis (dipstick)	Leukocytes	negative		negative
	Nitrite	negative		negative
	Urobilinogen	normal		normal
	Protein	negative		negative
	pH	5.1		4.7–7.8
	Red blood cell	negative		negative
	SG	1.007		1.005–1.030
	Ketone	negative		negative
	Bilirubin	negative		negative
	Glucose	negative		negative

WBC – white blood cells; RBC – red blood cells; Hb – haemoglobin; Hct – haematocrit; MCV – mean corpuscular volume; MCH – mean corpuscular haemoglobin; MCHC – mean corpuscular haemoglobin concentration; Plt – platelet; PT – prothrombin time; INR – international normalized ratio; APTT – activated partial thromboplastin time; AST – aspartate aminotransferase; ALT – alanine aminotransferase; ALP – alkaline phosphatase; LDH – lactate dehydrogenase; SG – specific gravity

Prague Medical Report / Vol. 126 (2025) No. 3, p. 162–166

pink, tachypneic and lethargic looking. Her vital signs were as followed: blood pressure of 89/70 mm Hg, pulse rate of 113 beats/min, respiratory rate of 32 breaths/min, temperature of 37 °C and oxygen saturation of 55% under room air. Respiratory examinations showed coarse crepitation on right side of the lung. Other systematic examinations showed no significant findings. She was intubated due to severe hypoxia and started on inotropic supports due to haemodynamically unstable. She was diagnosed with septicaemic shock secondary to severe community acquired pneumonia and admitted to intensive care unit (ICU) for further management and monitoring. While in the ICU she became oliguric and passed out brownish coloured urine. Thus, the diagnosis of myoglobinuria secondary to rhabdomyolysis was considered. However, her total CK activity showed persistently very low results despite samples were repeated 12 hours apart, prompting the treating clinician to contact laboratory. Sample dilution was done and post-dilution procedures showed markedly elevated total CK activity. The samples were not diluted, not haemolysed, not icteric and not lipaemic. No other CK samples of different patients showed similar very low results on the same day of testing. Her renal and liver profiles showed features of acute kidney injury and liver impairment, respectively. Urine myoglobin was not offered by our laboratory. Her final diagnosis was severe rhabdomyolysis secondary to severe pneumonia. Unfortunately, her conditions worsened and she succumbed despite optimized medical treatment due to multi-organ failures. Her laboratory results were summarized in Table 1.

Case 2

A 77-year-old Malay man with underlying diabetes mellitus and recurrent L4-L5 pyogenic spondylodiscitis presented with fever associated with back pain and spasm for 4 days. No cough, no abdominal pain, no vomiting, no loose stool, no history of contact with sick individual, no history of traveling and no history of trauma. Upon arrival at the emergency department he was alert, conscious, pink and lethargic looking. His vital signs were as followed: blood pressure of 85/79 mm Hg, pulse rate of 110 beats/min, respiratory rate of 17 breaths/min and temperature of 38 °C. Examination at the back showed tenderness

Table 2: Case 2 laboratory investigations

Test		Result	Unit	Reference range
Complete full blood count	WBC	15.3×10^9	/l	4.68–9.70
	RBC	5.07×10^9	/l	4.43–6.09
	Hb	14.00	g/dl	13.0–16.8
	Hct	42.50	%	40.14–51.77
	MCV	80.40	fl	79.10–94.70
	MCH	29.70	pg	24.81–31.10
	MCHC	31.70	g/dl	30.52–33.97
	Plt	203×10^9	/l	169–372
Coagulation profile	PT	12.70	s	12.61–15.72
	INR	1.03		0.86–1.14
	APTT	39.80	s	30.0–45.8
Liver function tests profile	Total protein	48	g/l	66–87
	Albumin	25	g/l	39.7–49.4
	AST	1379	U/l	10–50
	ALT	285	U/l	10–50
	ALP	73	U/l	40–129
	Total bilirubin	17	µmol/l	≤ 24
Renal function tests profile	Urea	24.1	mmol/l	2.76–8.07
	Sodium	139.0	mmol/l	136–145
	Potassium	5.4	mmol/l	3.5–5.1
	Chloride	105.0	mmol/l	98–107
	Creatinine	427.0	µmol/l	62–106
Creatine kinase		< 7	U/l	39–308
		15217 (post dilution 1:11)		
		254.12 (post dilution 1:11)	µkat/l	0.43–3.21
LDH		348	U/l	135–225

WBC – white blood cells; RBC – red blood cells; Hb – haemoglobin; Hct – haematocrit; MCV – mean corpuscular volume; MCH – mean corpuscular haemoglobin; MCHC – mean corpuscular haemoglobin concentration; Plt – platelet; PT – prothrombin time; INR – international normalized ratio; APTT – activated partial thromboplastin time; AST – aspartate aminotransferase; ALT – alanine aminotransferase; ALP – alkaline phosphatase; LDH – lactate dehydrogenase

at L4-L5 region with no wound and neurological deficit. Other systematic examinations showed no significant findings. He was started on inotropic supports due to haemodynamically unstable. He was diagnosed with septicaemic shock secondary to possible recurrent L4-L5 pyogenic spondylodiscitis and admitted to ICU for further management and monitoring. While in the ICU he complained of intense muscle spasm and pain thus, the diagnosis of rhabdomyolysis was considered. He also became oliguric. Nevertheless, his total CK activity showed persistently very low results despite samples were repeated 12 hours apart, prompting the treating clinician to contact laboratory. Sample dilution was done and post-dilution procedures showed markedly elevated total CK activity. The samples were not diluted, not haemolysed, not icteric and not lipaemic. No other CK samples of different patients showed similar very low results on the same day of testing. His renal and liver profiles showed features of acute kidney injury and liver impairment, respectively. Magnetic resonance image (MRI) of spine was done and confirmed the diagnosis of pyogenic spondylodiscitis. His final diagnosis was severe rhabdomyolysis secondary to recurrent pyogenic spondylodiscitis. Unfortunately, his conditions worsened and he succumbed despite optimized medical treatment due to multi-organ failures. His laboratory results were summarized in Table 2.

Discussion

These 2 cases illustrated the falsely low total CK activity in severe rhabdomyolysis. Total CK is the most sensitive marker for myocyte injury (Nanda et al., 2016). A 5-fold increase of total CK activity from normal level is diagnostic of rhabdomyolysis and its activity is directly proportional to the degree of muscle injury (Nanda et al., 2016).

There are different causes to be considered for falsely low total CK activity in rhabdomyolysis which can be classified into errors in pre-analytical, analytical and post-analytical (Nanda et al., 2016). Pre-analytical errors accounted for 32 to 75% of total errors followed by analytical 13 to 32 % and post-analytical 13 to 40% (Nanda et al., 2016). Although pre-analytical errors are more frequent, analytical errors could lead to more severe consequences for patient management (Nanda et al., 2016).

Pre-analytical errors include wrong patient identification, insufficient sample volume, diluted sample and wrong timing of measurement. Diluted sample can cause dilutional effect as in aggressive fluid resuscitation which can dilute CK activity leading to falsely low total CK activity. Diluted sample is usually indicated by hyponatremia and low urea which were not present in both cases. Correct timing of measurement is important as CK activity rises within 2–12 hours, peaked in 3–5 days and started to decline in 6–10 days after the onset of muscle injury (Nance and Mammen, 2015). Measuring CK too early or late from this window period may result in falsely low activity. Both the cases had CK samples repeated within 12 hours apart and yet the results still persistently very low thus, eliminating wrong timing of measurement as the causing factor.

Analytical errors include interferences in method measurement, faulty calibration and internal quality control and malfunctioning instrument. Most of the laboratory nowadays measures total CK activity using enzymatic coupled with spectrophotometry method (Lopez et al., 2012). Creatine phosphate and adenosine diphosphate (ADP) serve as substrates and CK will catalyse these substrates, triggering subsequent reactions leading to formation of nicotinamide adenine dinucleotide phosphate (NADPH) which can be measured spectrophotometrically through absorbance at wavelength 340 nm (Lopez et al., 2012; Pant, 2022). The rate of increase in NADPH absorbance is directly proportional to the CK activity present in serum (Lopez et al., 2012; Pant, 2022). Total CK activity of both cases were analysed by Roche Cobas c503 chemistry analyser. In severe rhabdomyolysis, interference can occur as creatine phosphate is consumed by high concentration of CK causing substrate exhaustion before the kinetic measurement is initiated, leading to falsely low total CK activity (Nanda et al., 2016). This mechanism is most probable to occur in both cases. The measuring range of the kit used to determine CK is 7–2,000 U/l (0.12–33.4 μkat/l). Dilution of 1:11 as recommended by manufacturer was done for both cases to get the correct values for CK activity. Clinically rhabdomyolysis was suspected by the treating physician and fortunately, both cases were discussed with chemical pathologist. Thus, immediate actions were taken which dilutions of the samples were performed, true results were reported and informed to the physician and appropriate treatment was commenced. Based on the experience by the 2 cases our laboratory had set up automated dilution procedures for CK activity which fall outside the measuring range, updated our laboratory workflow process and provided training for our laboratory staffs regarding this issue to prevent the similar errors from recurring. Other interferences include haemolysed, icteric and lipaemic samples. Bilirubin shows high absorbance at wavelengths 340–500 nm

(Cano-Corres et al., 2023). NADPH absorbance wavelength falls within this range thus, icteric sample may cause spectrophotometric interference leading to falsely low total CK activity. Lipaemic sample also may cause spectrophotometric interference due to light scattering effect, affecting NADPH absorbance and also resulting in falsely low total CK activity (Farrell and Carter, 2016). Haemolysed samples mostly will cause falsely high total CK due to positive interference by enzyme adenylate kinase in red blood cells (Farrell and Carter, 2016). The samples of both cases were not haemolysed, not icteric and not lipaemic as mentioned. Faulty calibration, faulty internal quality control and malfunctioning instrument usually will cause error of measurement in batches of samples not one or two particular sample. This was ruled out in both cases as no other CK samples of different patients showed similar very low results on the same day of testing.

Post-analytical errors include transcription errors especially in manual result entry system, wrong result interpretation, wrong unit conversion, inappropriate sample storage and others. In the current era of automation in clinical laboratory system which include automated result entry, these errors are less probable to occur (Bakan and Bakan, 2021).

In both cases, the results of other tests also supported the diagnosis of rhabdomyolysis. Abnormal liver function tests are commonly seen in severe rhabdomyolysis showing elevation of transaminases (aspartate aminotransferase [AST] and alanine aminotransferase [ALT]) especially AST as it is also found in skeletal muscle (Lim, 2020). ALT is more liver specific but also found in skeletal muscle in lower concentrations (Lim, 2020). Both cases showed evidence of liver impairment as there were elevation of AST more than 10 times of the upper limit normal (ULN) and elevation of ALT more than 5 times of the ULN. Acute kidney injury (AKI) is one of the most serious complications of rhabdomyolysis (Torres et al., 2015). CK activity of > 5,000 U/l can predict the likelihood of patient developing kidney injury in rhabdomyolysis (Torres et al., 2015). Both cases showed evidence of AKI based on Kidney Disease: Improving Global Outcomes (KDIGO) definition (Makris and Spanou, 2016) as clinically oliguric and elevation of serum creatinine ≥ 1.5 times from baseline (both patients had normal baseline serum creatinine prior the illness). Hypoalbuminemia has been linked to increased morbidity and mortality related to AKI in severe rhabdomyolysis (Wiedermann et al., 2017). Hyperkalaemia and elevated lactate dehydrogenase (LDH) were expected in both cases as potassium and LDH are intracellular analytes which will be released into blood due to myocyte injury in severe rhabdomyolysis.

Conclusion

The low total creatine kinase activity can occur factitiously in severe rhabdomyolysis due to analytical interference of substrate exhaustion in which creatine phosphate is consumed by high concentration of CK in sample before the kinetic measurement is initiated. Sample dilution can be done to obtain the accurate total CK activity, avoiding result reporting error and possibility misdiagnosis of rhabdomyolysis. Good communication between clinical and laboratory personnel is vital to prevent the error and safeguard patient management.

Acknowledgements: Appreciation for the family members of both patients for their consent and cooperation in completing this case report.

References

Bakan, E., Bakan, N. (2021) Prevention of extra-analytical phase errors by non-analytical automation in clinical laboratory. *Turk. J. Biochem.* **46(3)**, 235–243.

Cano-Corres, R., Sole-Enrech, G., Aparicio-Calvente, M. I. (2023) Definition of icteric interference index for six biochemical analytes. *Biochem. Med. (Zagreb)* **33(2)**, 020702.

Farrell, C. J., Carter, A. C. (2016) Serum indices: Managing assay interference. *Ann. Clin. Biochem.* **53(5)**, 527–538.

Lim, A. K. (2020) Abnormal liver function tests associated with severe rhabdomyolysis. *World J. Gastroenterol.* **26(10)**, 1020–1028.

Lopez, J., Burtis, C. A., Ashwood, E. R., Bruns, D. E. (2012) *Tietz Textbook of Clinical Chemistry and Molecular Diagnosis*, 5th Edition. Elsevier, St. Louis.

Makris, K., Spanou, L. (2016) Acute kidney injury: Definition, pathophysiology and clinical phenotypes. *Clin. Biochem. Rev.* **37(2)**, 85–98.

Nance, J. R., Mammen, A. L. (2015) Diagnostic evaluation of rhabdomyolysis. *Muscle Nerve* **51(6)**, 793–810.

Nanda, S. K., Dinakaran, A., Ray, L. (2016) Is dilution important: Factitious total creatine kinase in case of rhabdomyolysis? *J. Clin. Diagn. Res.* **10(10)**, BD01–BD02.

Pant, V. (2022) Importance of observing the progress curve during enzyme assay in an automated clinical chemistry analyzer: A case study. *EJIFCC* **33(1)**, 56–62.

Torres, P. A., Helmstetter, J. A., Kaye, A. M., Kaye, A. D. (2015) Rhabdomyolysis: Pathogenesis, diagnosis, and treatment. *Ochsner J.* **15(1)**, 58–69.

Wiedermann, C. J., Wiedermann, W., Joannidis, M. (2017) Causal relationship between hypoalbuminemia and acute kidney injury. *World J. Nephrol.* **6(4)**, 176–187.

Zhao, B., Zheng, R. (2019) Community-acquired pneumonia complicated by rhabdomyolysis: A clinical analysis of 11 cases. *World J. Clin. Cases* **7(24)**, 4218–4225.

Navigating Diagnostic Complexity in Hailey-Hailey Disease: A Case Report with Clinical-histopathological Correlation

Parth R. Goswami[1], Gyanendra Singh[1], Varniraj Patel[2], Yashdeep Singh Pathania[3]

[1] Department of Pathology, All India Institute of Medical Sciences, Rajkot, Gujarat, India;
[2] Department of Dermatology, Vedantaa Institute of Medical Sciences, Palghar, Maharashtra, India;
[3] Department of Dermatology, Venereology and Leprosy, All India Institute of Medical Sciences, Rajkot, Gujarat, India

Received February 6, 2025; Accepted August 27, 2025.

Key words: Hailey-Hailey disease – Bullous skin lesion – Pemphigus – Dermatopathology

Abstract: Hailey-Hailey disease (HHD), also known as benign familial pemphigus, is a rare autosomal dominant genodermatosis caused by mutations in the *ATP2C1* gene. These mutations impair keratinocyte adhesion and disrupt calcium homeostasis, leading to characteristic clinical and histopathological findings. Herein, we present the case of a 50-year-old male with a ten-year history of recurrent, pruritic, erythematous erosions and maceration in the left axilla and groin. Clinical examination revealed no systemic comorbidities or relevant family history. Histopathological analysis of skin biopsy demonstrated hallmark features, including epidermal hyperkeratosis, suprabasal and intraepidermal clefting, and acantholysis with the distinctive "dilapidated brick wall" appearance, confirming the diagnosis of HHD. Differential diagnoses, including intertrigo, Darier disease, and pemphigus vegetans, were excluded based on clinical and histological findings. The patient was managed with immunomodulators and topical antibiotics, with follow-up care focused on symptom alleviation and infection prevention. This case underscores the importance of correlating clinical and histopathological findings in diagnosing HHD and differentiating it from other intertriginous dermatoses. Despite its chronic and recurrent nature, timely and accurate diagnosis, coupled with individualized management, significantly enhances patient outcomes. This report also highlights the unique histological feature of acantholysis resembling a "dilapidated brick wall", pivotal in distinguishing HHD. Advances in understanding the molecular pathogenesis of ATP2C1 mutations hold promise for the development of targeted therapies, offering hope for more effective management of this challenging condition in the future.

Mailing Address: Gyanendra Singh, MD., Department of Pathology, AIIMS Rajkot, village Khanderi, Parapipaliya, 360001, Gujarat, India; e-mail. gyanendra002@gmail.com

https://doi.org/10.14712/23362936.2025.27

Prague Medical Report / Vol. 126 (2025) No. 3, p. 167–170

Introduction

Hailey-Hailey disease (HHD), commonly known as benign familial pemphigus, is an uncommon genetic dermatological condition characterized by an autosomal dominant inheritance pattern. It was first recognized by the Hailey brothers in 1939 (Michel, 1982). The condition results from a mutation in the *ATP2C1* gene. This gene aids in preserving cellular adhesion within the epidermis. A mutation in this gene disrupts desmosome activity, leading to disease manifestation (Prateek et al., 2016). Hailey-Hailey illness primarily affects the flexural regions, including the groin, neck, and axilla. It presents as blisters that rupture, leading to painful fissures, erosions, or plaques. Maceration and subsequent infections are common consequences (Sharma and Sharma, 2018). We documented a case of a 50-year-old male who exhibited itchy, erythematous erosions in the left axilla and left groin, subsequently identified as Hailey-Hailey disease through clinical and histological evaluation.

Case report

A 50-year-old man presented to the outpatient department of dermatology with a complaint of multiple erosions accompanied by itching, primarily in the flexural areas, for the past 12–13 years. On examination, erosions with crusting and maceration were observed over the lower abdomen and groin, while the bilateral axillae exhibited mainly post-inflammatory hyperpigmentation with very few erosions. (Figures 1 and 2 showing gross clinical appearance of Hailey-Hailey disease hyperpigmentation crust and erosion.) The patient reported that his symptoms worsened primarily during the summer. No involvement of other systems was noted, and there was no family history of a similar condition.

Figure 1: Clinical image of Hailey-Hailey disease showing hyperpigmentation and maceration and erosion over genital area.

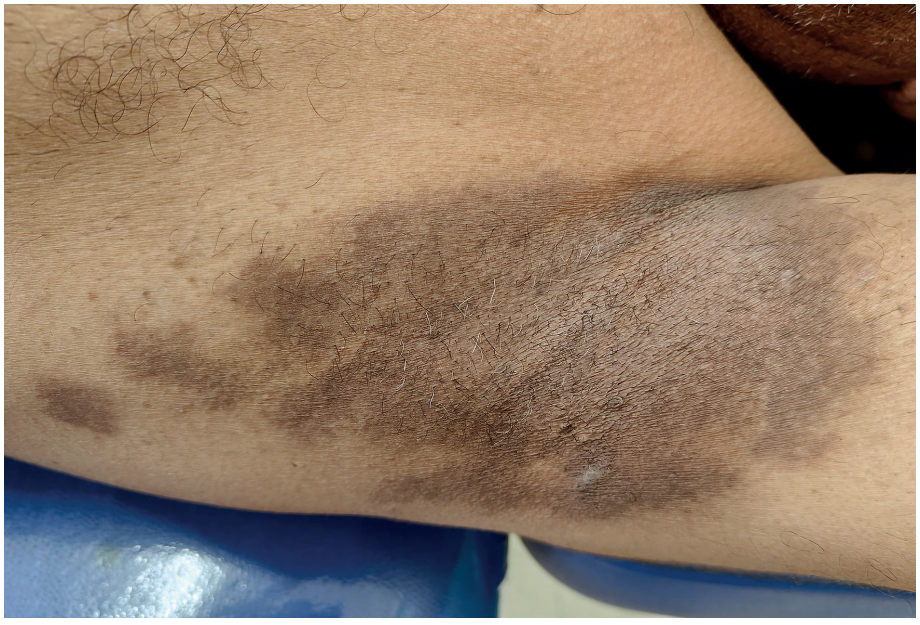

Figure 2: Clinical image of Hailey-Hailey disease showing hyperpigmentation and maceration and erosion over arm cubital fossa area.

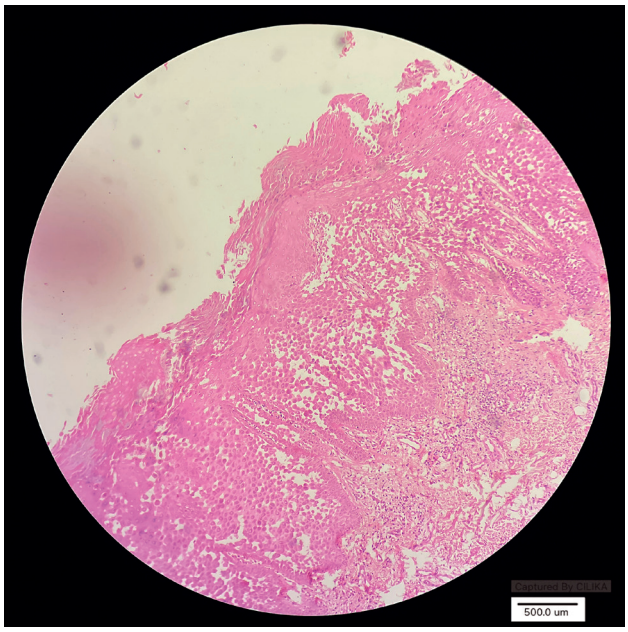

Figure 3: Photomicrograph of Hailey-Hailey disease showing hyperkeratosis, parakeratosis, regular acanthosis, dyskeratotic keratinocyte and acantholysis with dilapidated brick wall appearance (10× view, haematoxylin and eosin stain).

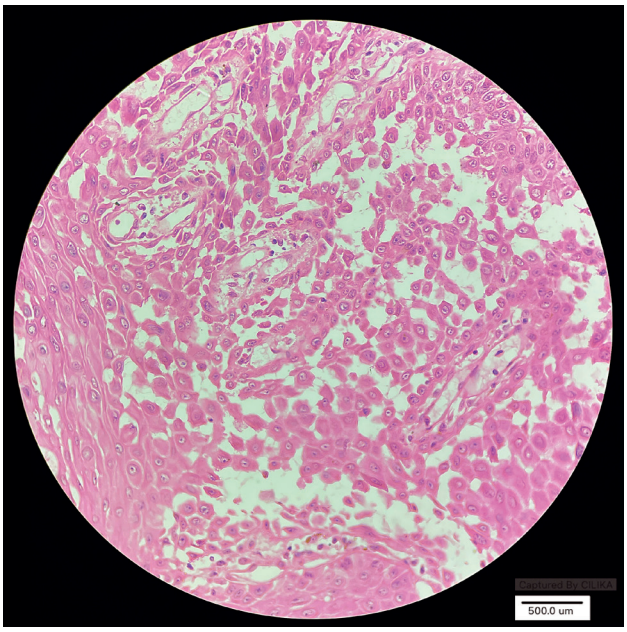

Figure 4: Photomicrograph of Hailey-Hailey disease showing hyperkeratosis, parakeratosis, regular acanthosis, dyskeratotic keratinocyte and acantholysis with dilapidated brick wall appearance (10× view, haematoxylin and eosin stain).

The patient's primary concern was pruritus. Routine blood investigations were within normal limits. There was no history of diabetes mellitus, fungal infections, or medication use. All standard hematological assessments were within normal parameters. There are no significant regards in the family history. A skin biopsy measuring 0.6×0.4 cm was obtained from the erosive areas of the left axilla and groin, and subsequently sent to the histopathology laboratory at the IPD complex for diagnostic evaluation. The term "IPD complex" refers to the in-patient department (IPD) complex, where admitted patients receive medical care and procedures such as skin biopsies are performed. Sections exhibit skin histology that includes epidermal hyperkeratosis, parakeratosis, and regular acanthosis. Supra-basal and intra-epidermal clefting is seen. A small number of dyskeratotic cells are also observed. Acantholytic keratinocytes exhibit a look suggestive of a dilapidated brick wall appearance. The superficial dermis has mild perivascular chronic inflammation. Skin appendages preserved. A diagnosis of Hailey-Hailey disease was established based on the clinical and histological findings. (Figures 3 and 4 showing photomicrograph microscopic appearance of Hailey-Hailey disease acantholytic keratinocytes with classical dilapidated brick wall appearance.)

He was counselled about the natural course of the disease and advised to wear loose clothing and avoid friction. Treatment with topical corticosteroids and oral antihistamines was initiated. The patient showed significant improvement within one month.

Discussion

Hailey-Hailey disease typically develops in early adulthood, often during the third or fourth decade of life, though it can occur at any age. The illness is quite rare, with a frequency of roughly 1 in 50,000, and around two-thirds of patients possess a familial history of the disorder (Burge, 1992; Ikeda et al., 1993; Calonje et al., 2020).

The transmembrane protein ATP2C1 is ubiquitous across all tissues, with high expression in keratinocytes. It functions as an ATPase responsible for transporting Ca^{2+} and Mn^{2+} into the Golgi apparatus, facilitating calcium influx into this organelle while lowering its cytoplasmic concentration. Mutations in the *ATP2C1* gene disrupt this ion gradient, causing cytosolic calcium accumulation, which leads to altered synthesis of junctional proteins, resulting in acantholysis, decreased mitochondrial ATP levels, leading to disruption of adherens junctions and increased reactive oxygen species, impairing keratinocyte proliferation and differentiation (Micaroni et al., 2016; Muncanovic et al., 2019).

Diagnosis is mainly based on clinical presentations, positive family history and characteristic histopathology which shows "dilapidated brick wall" appearance and negative immunofluorescent studies. Differential diagnosis includes intertrigo, eczema, Darier disease (DD) and pemphigus vegetans (Calonje et al., 2020).

Intertrigo and Hailey-Hailey disease can be distinguished by their clinical and histological

Prague Medical Report / Vol. 126 (2025) No. 3, p. 167–170

characteristics. Intertrigo presents as erythematous, macerated, and moist lesions in skin folds, usually resulting from friction and moisture, whereas Hailey-Hailey disease is characterized by recurrent painful erosions, vesicles, and fissures that may become superinfected. Histopathologically, intertrigo exhibits nonspecific abnormalities such as spongiosis and mild inflammation, while Hailey-Hailey disease is marked by acantholytic changes that resemble a "dilapidated brick wall". Intertrigo is mostly caused by mechanical irritation and subsequent infection, while Hailey-Hailey disease is a genetic disorder associated with mutations in the *ATP2C1* gene, leading to impaired calcium homeostasis in keratinocytes (Romanelli et al., 2023).

Hailey-Hailey disease and Darier disease are clinically distinguished by the characteristics and distribution of their lesions, as well as their histological features. HHD is characterized by recurrent, vesicular, and erosive lesions predominantly in flexural regions, while DD is identified by keratotic papules and plaques in seborrheic areas. Histologically, HHD exhibits suprabasal acantholysis resembling a "dilapidated brick wall", whereas DD demonstrates acantholytic dyskeratosis characterized by huge ronds and grains (Kositkuljorn and Suchonwanit, 2019).

Pemphigus vegetans and Hailey-Hailey disease can be distinguished by their clinical and histological characteristics. Pemphigus vegetans generally manifests as vegetative plaques in intertriginous regions, frequently associated with oral mucosal involvement, while HHD is distinguished by vesicles and erosions absent of mucosal involvement. Pemphigus vegetans histologically demonstrates intraepidermal acantholysis with eosinophilic infiltration and pseudoepitheliomatous hyperplasia, unlike the "dilapidated brick wall" acantholysis observed in HHD (Jayapriya et al., 2021).

Management techniques encompass topical or systemic steroids, frequently combined with antibacterial medicines, to mitigate symptoms and avert infections. Notwithstanding advancements in treatment, the illness continues to pose management challenges because to its recurring and chronic characteristics (Ikeda et al., 1993).

Conclusion

This case highlights the clinical and histopathological features of Hailey-Hailey disease, emphasizing its distinct presentation and the critical role of histopathology in confirming the diagnosis. The characteristic "dilapidated brick wall" pattern of acantholysis remains a cornerstone for differentiation from other intertriginous dermatoses. Direct immunofluorescence (DIF) should be performed in the differential diagnosis of Hailey-Hailey and pemphigus vegetans (and other autoimmune bullous diseases), if available. DIF is negative in Hailey-Hailey disease.

Despite its chronic and recurrent nature, timely diagnosis and individualized management strategies, as demonstrated in this case, can alleviate symptoms and improve patient outcomes. Continued research into the molecular pathogenesis of ATP2C1 mutations offers hope for more targeted and effective therapies in the future.

References

Burge, S. M. (1992) Hailey-Hailey disease: The clinical features, response to treatment and prognosis. *Br. J. Dermatol*. **126**, 275–282.

Calonje, E., Brenn, T., Lazar, A. J., Billings, S. D. (2020) *McKee's Pathology of the Skin with Clinical Correlations*, 5th Edition. Elsevier, Edinburgh.

Ikeda, S., Suga, Y., Ogawa, H. (1993) Successful management of Hailey-Hailey disease with potent topical steroid ointment. *J. Dermatol. Sci*. **5(3)**, 205–211.

Jayapriya, R., Chaudhary, M., Uma Maheswari, T. N., Muthukrishnan, A. (2021) Mucocutaneous pemphigus vegetans – A rare case report. *J. Indian Acad. Oral Med. Radiol*. **33(2)**, 222–225.

Kositkuljorn, C., Suchonwanit, P. (2019) Darier's disease: Report of a case with facial involvement. *Case Rep. Dermatol*. **11(3)**, 327–333.

Micaroni, M., Giacchetti, G., Plebani, R., Xiao, G. G., Federici, L. (2016) *ATP2C1* gene mutations in Hailey-Hailey disease and possible roles of SPCA1 isoforms in membrane trafficking. *Cell Death Dis*. **7(6)**, e2259.

Michel, B. (1982) "Familial benign chronic pemphigus" by Hailey and Hailey, April 1939. Commentary: Hailey-Hailey disease, familial benign chronic pemphigus. *Arch. Dermatol*. **118(10)**, 774–783.

Muncanovic, D., Justesen, M. H., Preisler, S. S., Pedersen, P. A. (2019) Characterization of Hailey-Hailey disease-mutants in presence and absence of wild type SPCA1 using *Saccharomyces cerevisiae* as model organism. *Sci. Rep*. **9(1)**, 12442. Erratum (2020) *Sci. Rep*. **10(1)**, 9347.

Prateek, K., Banwarilal, M. R., Chaudhary, S. S., Garg, M. (2016) Hailey-Hailey disease – A rare case report. *Int. J. Res. Dermatol*. **2**, 36–39.

Romanelli, M., Voegeli, D., Colboc, H., Bassetto, F., Janowska, A., Scarpa, C., Meaume, S. (2023) The diagnosis, management and prevention of intertrigo in adults: A review. *J. Wound Care* **32(7)**, 411–420.

Sharma, R. L., Sharma, R. (2018) Hailey-Hailey disease: Case report of a rare disease. *IAIM* **5(7)**, 94–98.

Dual Roots of Origin of Inferior Alveolar Nerve and "Vagal Ansa" Cervicalis: Surgical and Anaesthetic Implications

Dibakar Borthakur, Arthi Ganapathy, Kamalesh Saravanan, Jayanta Biswas, Saroj Kaler Jhajhria

Department of Anatomy, All India Institute of Medical Sciences, New Delhi, India

Received January 21, 2025; Accepted August 27, 2025.

Key words: Ansa cervicalis – Infratemporal fossa – Inferior alveolar nerve – Vagus nerve

Abstract: During routine cadaveric dissection for undergraduate medical teaching, we observed dual roots of origin of the inferior alveolar nerve (IAN) on the right infratemporal fossa in an elderly male cadaver. The IAN originated by two roots encircling the second part of the maxillary artery (MA). The superior root of the ansa cervicalis (AC) originated from the ipsilateral vagus nerve and two independent muscular branches of the right vagus provided additional innervations to the anterior neck muscles. Awareness about the dual roots of origin of IAN is imperative for anaesthesiologists and dentists, while administering local anaesthesia. A prior knowledge about the vagal origin of AC is essential to prevent iatrogenic damage during surgeries.

Mailing Address: Prof. Saroj Kaler Jhajhria, MBBS., MD., Department of Anatomy, Teaching Block, Room No. 1017, All India Institute of Medical Sciences, Ansari Nagar, New Delhi, 110029, India; e-mail: sarojkaler@gmail.com

https://doi.org/10.14712/23362936.2025.28

Prague Medical Report / Vol. 126 (2025) No. 3, p. 171–174

Introduction

The anatomy of the infratemporal fossa (ITF) is of tremendous clinical relevance as a number of important neurovascular structures are located in the compact region that too amidst the masticatory muscles (Anil et al., 2003). The branches of the maxillary artery (MA) and mandibular nerve (MN) are notable structures in the ITF. The inferior alveolar nerve (IAN) arises from the posterior division of the MN deep to the lateral pterygoid muscle and then descends over the medial pterygoid muscle to enter into the mandibular foramen. The nerve terminates as incisive and the mental branches and supplies the lower jaw (Wolf et al., 2016). The nerve to mylohyoid arises from the IAN and courses medial to the main IAN and supplies the mylohyoid muscle. The MA is usually found lateral to the IAN, lingual and the buccal nerves in the ITF. Anatomic variations of the IAN such as accessory IAN, split IAN and aberrant communication of IAN with other branches of the MN are known. However, there are very few reports of IAN arising by two roots and encircling the 2nd part of the MA in the ITF (Nayak et al., 2020). The ansa cervicalis (AC) is a nerve loop formed by the first three cervical spinal nerves i.e. C1 to C3 spinal nerves over the carotid sheath. The nerve loop consists of two roots: the superior and the inferior root. The superior root is formed by C1 spinal nerve fibres that travels along the hypoglossal nerve and descends to join the inferior root which in turn is formed from the C2 and C3 spinal nerve fibres. AC innervates usually all the infrahyoid muscles (except thyrohyoid) which act as depressor of the hyoid bone and thus are involved in the important functions of stabilization of neck, swallowing and vocalization (Shvedavchenko et al., 2019).

Case report

During routine dissections of the head and neck region for undergraduate teaching, we found anatomical variation in the origin of the IAN and in the formation of AC on the right side of a 74-year-old male cadaver. The IAN originated by two roots from the posterior division of the MN which encircled the second part of the MA. The MA was deep to the buccal nerve and superficial to the lingual nerve. The length of the deep and the superficial roots were 1.35 cm and 1.41 cm respectively. The main IAN thus formed further descended for 3.15 cm and entered into the mandibular foramen (Figure 1A and B). The nerve to mylohyoid originated from the IAN 1.50 cm inferior to its formation.

On the right anterior triangle of the neck, the AC is formed over the bifurcation of the common carotid artery whose superior root originated from the right vagus nerve and the inferior root was formed by the C2 and C3 spinal nerves. The AC loop supplied the

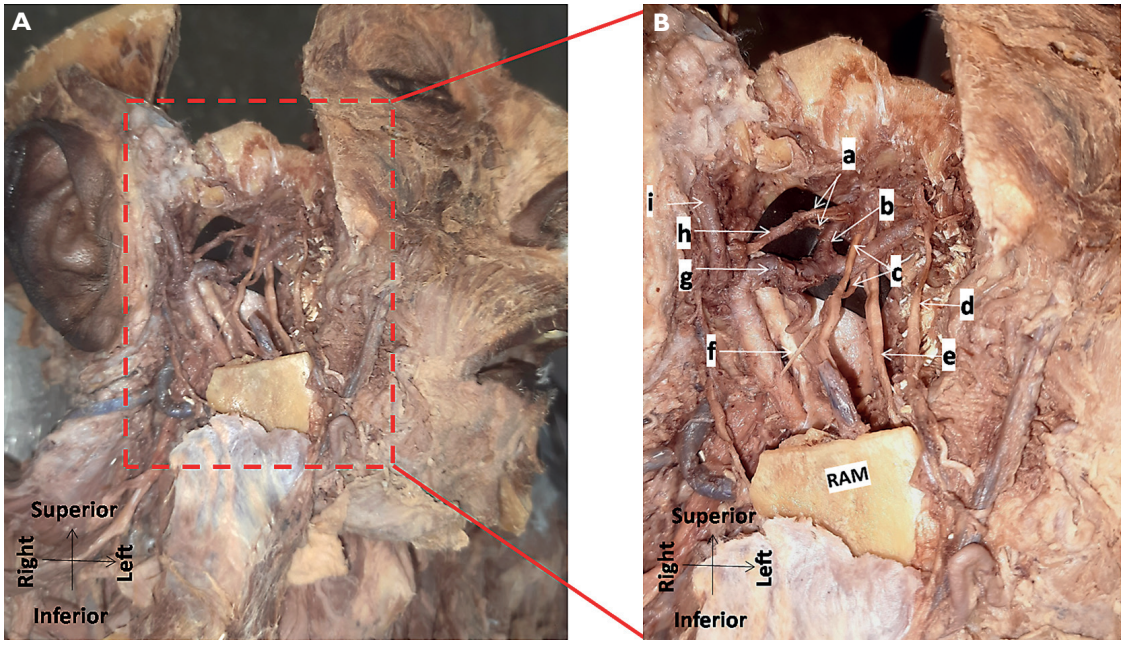

Figure 1: A) Photograph of the part of dissected infratemporal fossa on the right side showing the two roots of origin of the inferior alveolar nerve. B) The same region in close up view. a – two roots of the auriculotemporal nerve; b – middle meningeal artery arising from the maxillary artery; c – the two roots of the inferior alveolar nerve; d – buccal nerve; e – lingual nerve; f – nerve to mylohyoid; g – 2nd part of the maxillary artery; h – auriculotemporal nerve; i – superficial temporal artery; RAM – ramus of the mandible.

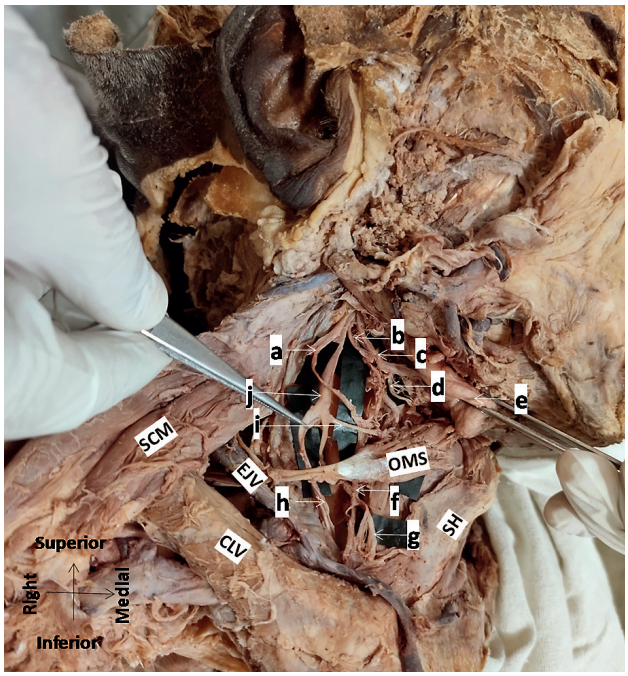

Figure 2: Photograph of the part of the dissected anterior triangle of the neck on the right side showing ansa cervicalis and its formation by the vagus nerve. a – inferior root of the ansa cervicalis; b – superior root of the ansa cervicalis; c – hypoglossal nerve; d – C1 fibre passing with the hypoglossal nerve supplying the thyrohyoid muscle; e – submandibular gland; f – muscular branches arising from ansa cervicalis to the sternohyoid and sternothyroid; g – muscular branches arising from the vagus nerve to the sternohyoid and sternothyroid; h – continuation of the vagus nerve to the thorax; i – muscular branch of the vagus to superior belly of omohyoid; j – vagus nerve within the carotid sheath; SCM – sternocleidomastoid; EJV – external jugular vein; OMS – superior belly of omohyoid; CLV – clavicle; SH – sternohyoid.

sternohyoid, sternothyroid and omohyoid muscles. In addition to that, two independent medial branches were seen arising from the right vagus which supplied the superior belly of omohyoid, sternohyoid and the sternothyroid muscle (Figure 2). The remainder of the vagus nerve descended and entered the thorax following its normal course.

Discussion

One of the common causes for failure to achieve adequate local anaesthesia for routine dental procedures in spite of correct technique is anatomical variations of the MN. These variations are also important as they are prone for iatrogenic injuries (Anil et al., 2003). The ITF is a site for lateral approach during skull base surgeries, which can be challenging in the presence of anatomical variation of IAN (Roy et al., 2002). Bifid IAN is reported where one of the branches enters the mandible through the accessory mandibular foramen. During the local anaesthetic block of IAN, one of the branches can get skipped leading to insufficient anaesthesia. Connection between the IAN and the lingual or auriculotemporal nerve has been reported in the ITF (Wolf et al., 2016). The other notable variation of IAN is MA piercing the IAN (Nayak et al., 2020). Furthermore, the two roots of the IAN encircling the MA mimic the two roots of the auriculotemporal nerve encircling the middle meningeal artery and can confuse surgeons. The 2nd part of the MA may get compressed between the two roots of the IAN. The sensory fibres of the IAN if compressed and irritated by the pulsating MA might give symptoms of mandibular neuralgia (Roy et al., 2002). The origin of the IAN by two roots encircling the MA might necessitate adopting an alternate method for administering local anaesthetic drugs for IAN blocks. Additionally, this type of anatomic variation when undergoing entrapment can present with symptoms similar to mandibular neuralgia.

Table 1: Prevalence of "vagal ansa" cervicalis observed in recent studies

Authors	Population, study type and samples studied	Findings of the study
Jelev (2013)	Bulgarian, cadaveric, 20 cases	2 cases of aberrant formation of AC were observed. In the first case, 3 separate roots of origin of AC from vagus, hypoglossal and cervical ventral rami forming two neural loops. In the second, 2 anterior branches of vagus supplied the anterior neck muscles bilaterally.
Pillay et al. (2012)	South Africa, cadaveric, 40 foetuses	Formation of the superior root of AC from the vagus and the hypoglossal nerve and it was termed vago-hypoglossal-AC.
Kikuta et al. (2019)	American, cadaveric case	Superior root of the AC arose from the vagus and the hypoglossal nerves on the right side.
Gopalakrishnan et al. (2015)	Canadian, clinical case	Superior root of the AC originated from the vagus nerve which also supplied the sternocleidomastoid muscle via separate muscular branches.
Sonne (2019)	American, cadaveric case	Non looping superior root of the AC originated from the vagus nerve and aberrant innervation of the omohyoid muscle by the spinal accessory nerve.

AC – ansa cervicalis

The superior root of AC can arise from the vagus or the spinal accessory nerve instead of the normal hypoglossal nerve and sometimes the superior root can have dual roots of origin from vagus and hypoglossal (Jelev, 2013). The "vagal AC" as found in our case resembles closely with some of the recently reported studies presented in Table 1. The AC in the present case is thus termed as "vagal AC" as coined by several authors and matches with type-IV variety according to Jelev's classification system (Jelev, 2013). However, in our case two additional anterior branches of the right vagus were observed which innervated anterior neck muscles. The reported prevalence of "vagal AC" in foetuses was around 3% (Pillay et al., 2012). Branches of AC are an ideal choice for non-selective reinnervation of the recurrent laryngeal nerve (RLN) by direct end-to-end anastomosis and/or neurorrhaphy procedure. RLN palsy is a clinical condition characterized by denervation of the laryngeal muscles and results in immobilization of the vocal cord, lateralization or inadequate approximation of the vocal cords, impaired phonation, aspirations, breathlessness, dysphagia etc. (Yeole et al., 2024). RLN palsy usually occurs following radical neck dissections, penetrating trauma to the neck etc. The important surgical procedures that commonly lead to RLN injury are thyroid surgery and oesophageal cancer surgery in adults (Kikuta et al., 2019) and patent ductus arteriosus (PDA) closure operation in children. It has been observed that non selective reinnervation of the laryngeal muscles by AC effectively restores voice quality (Zhou et al., 2024). The branches of "vagal AC" may be another excellent alternative for laryngeal reinnervation and hence becomes clinically relevant.

Conclusion

This case highlights rare anatomical variations presenting dual roots of the inferior alveolar nerve encircling the maxillary artery, and a "vagal ansa" cervicalis supplying the anterior neck muscles. Such variations have important implications in dental anaesthesia and neck surgeries. Awareness of these anomalies can help avoid failed nerve blocks, misdiagnosis of neuralgia, and iatrogenic nerve injuries during surgical procedures.

References

Anil, A., Peker, T., Turgut, H. B., Gulekon, I. N., Liman, F. (2003) Variations in the anatomy of the inferior alveolar nerve. *Br. J. Oral Maxillofac. Surg*. **41(4)**, 236–239.

Gopalakrishnan, C. V., Kestle, J. R. W., Connolly, M. B. (2015) The "vagal ansa": A source of complication in vagus nerve stimulation. *J. Neurosurg. Pediatr*. **15(5)**, 535–538.

Jelev, L. (2013) Some unusual types of formation of the ansa cervicalis in humans and proposal of a new morphological classification. *Clin. Anat*. **26(8)**, 961–965.

Kikuta, S., Iwanaga, J., Kusukawa, J., Tubbs, R. S. (2019) An unusual superior root of the ansa cervicalis. *Cureus* **11(4)**, 10–12.

Nayak, U., Vadgaonkar, R., Pai, M. M., Murlimanju, B. V. (2020) A case of inferior alveolar nerve encircling the arteria maxillaris. *Anat. Cell Biol*. **53(2)**, 240–243.

Pillay, P., Partab, P., Lazarus, L., Satyapal, K. S. (2012) The ansa cervicalis in fetuses. *Int. J. Morphol*. **30(4)**, 1321–1326.

Roy, T. S., Sarkar, A. K., Panicker, H. K. (2002) Variation in the origin of the inferior alveolar nerve. *Clin. Anat*. **15(2)**, 143–147.

Shvedavchenko, A. I., Oganesyan, M. V., Hammer, C. M., Paulsen, F., Bakhmet, A. A. (2019) Ansa cervicalis – A new classification approach. *Ann. Anat*. **222**, 55–60.

Sonne, J. W. H. (2019) Report of a non-looped variant of ansa cervicalis with omohyoid innervation from accessory nerve branch and omohyoid attachment to mastoid process. *Eur. Arch. Otorhinolaryngol*. **276**, 2105–2108.

Wolf, K. T., Brokaw, E. J., Bell, A., Joy, A. (2016) Variant inferior alveolar nerves and implications for local anesthesia. *Anesth. Prog*. **63(2)**, 84–90.

Yeole, U., Damiano, G., Marengo, R. L., Socolovsky, M. (2024) Laryngeal reinnervation in recurrent laryngeal neuropathy with ansa cervicalis – RLN end-to-end neurorrhaphy. *Neurol. India* **72(4)**, 725–727.

Zhou, S., Liu, L., Yang, Y., Mo, H., Wei, L., Xu, D., Yang, Y., Luo, R., Hu, J., Fang, H. (2024) A meta-analysis on the improvement of vocal function in unilateral vocal cord paralysis by reinnervation of the recurrent laryngeal nerve. *Lin Chuang Er Bi Yan Hou Tou Jing Wai Ke Za Zhi* **38(10)**, 928–934. (in Chinese)

Urachus Remnant: Importance of Early Diagnosis in Preventing Complications

Bruna Suda Rodrigues[1], Giulia Gadia Leme La Guardia[2], Élcio Roberto Duarte[1], Márcio Luís Duarte[3,4]

[1] Irmandade da Santa Casa de Misericórdia de Santos, Santos (SP), Brazil;
[2] Universidade Metropolitana de Santos, Santos (SP), Brazil;
[3] Universidade de Ribeirão Preto – Campus Guarujá, Guarujá (SP), Brazil;
[4] Diagnósticos da América S. A., São Paulo (SP), Brazil

Received March 22, 2024; Accepted August 27, 2025.

Key words: Remnant of the urachus – Ultrasonography – Urachus

Abstract: The urachus remnant is a vestigial structure that results from incomplete involution of the cloaca and allantois, forming a duct between the bladder and the umbilical scar. Normally, it obliterates to form the middle umbilical ligament. Despite its rarity and often nonspecific symptoms, it can be incidentally discovered during imaging tests or due to complications, such as infections or neoplasms. The first diagnostic test usually ordered is an ultrasound, followed by computed tomography or magnetic resonance imaging for a more detailed evaluation. Early diagnosis and appropriate management, which may include surgical resolution, are important to prevent complications. This report discusses the case of a 4-year-old female presenting with abdominal pain, fever, and constipation, who was diagnosed with a urachus remnant through ultrasound. The patient responded well to antibiotic therapy for a urinary tract infection and was advised to follow-up with ultrasound for the urachus remnant. The article reviews the potential complications, diagnostic methods, and treatment options for urachus remnants, highlighting the importance of early detection in preventing more severe outcomes, including malignancies.

Mailing Address: Dr. Márcio Luís Duarte, Universidade de Ribeirão Preto (UNAERP) – Campus Guarujá, Av. D. Pedro I, 3.300, Enseada, Guarujá (SP), 11440-003, Brazil; Phone: 005 513 981 112 799; e-mail: marcioluisduarte@gmail.com

https://doi.org/10.14712/23362936.2025.29

Prague Medical Report / Vol. 126 (2025) No. 3, p. 175–177

Introduction

The remnant of the urachus is a vestigial structure originating from the involution of the cloaca and allantois, forming a duct between the bladder and the umbilical scar, which normally obliterates to form the middle umbilical ligament (Parada Villavicencio et al., 2016). Despite its rarity and nonspecific or absent symptomatology, it may be incidentally diagnosed during imaging tests or due to developed complications, with the most common complications being infections and neoplasms of the urachus (Buddha et al., 2019).

The first test usually ordered when a remnant of the urachus is suspected for diagnosis is an ultrasound of the urinary tract, but computed tomography (CT) or magnetic resonance imaging (MRI) of the pelvis are excellent tests to better characterize this structure (Buddha et al., 2019). The importance of early diagnosis of the urachus remnant lies in avoiding the occurrence of complications and indicating, if necessary, surgical resolution of this remnant (Parada Villavicencio et al., 2016).

Herein, we report the case of a 4-year-old female patient with abdominal pain and fever (38.8 °C) for one day. Informed consent was obtained from the patient's parents.

Case report

A 4-year-old female patient presented with abdominal pain and fever (38.8 °C) for one day, accompanied by constipation for three days. The patient's mother denied any allergies, use of medications, or previous surgeries, but reported a urinary tract infection six months prior, which was treated with oral antibiotic therapy.

Upon physical examination, the patient exhibited a flaccid abdomen and was painless upon palpation. Ultrasound revealed an oval image in the anterior wall of the bladder, consistent with a remnant of the urachus (Figure 1). A urine test confirmed the diagnosis of urinary tract infection.

The patient was treated with trimethoprim-sulfamethoxazole, resulting in resolution of the symptoms within three days. She was instructed to undergo ultrasound follow-up for the urachus remnant.

Discussion

The urachus remnant is a structure that arises from incomplete involution and persistence of embryonic structures. During pregnancy, the urachus connects the fetal urinary bladder to the allantois, and at birth, it undergoes obliteration to become the middle umbilical ligament (Buddha et al., 2019). More specifically, in the third week of embryonic life, the allantois is formed from the yolk sac as a diverticulum, which enlarges until it joins the cloaca. Subsequently, as segments of the cloaca form the fetal bladder while still connected to the allantois, these structures continue to develop into the navel. By the fourth month of gestation, involution of the allantois occurs, resulting in the formation of the urachus, which ultimately obliterates to form the middle umbilical ligament (Buddha et al., 2019).

Anomalies of the urachus are less prevalent in women than in men, with an incidence of about 1 in 5,000 adults (Parada Villavicencio et al., 2016).

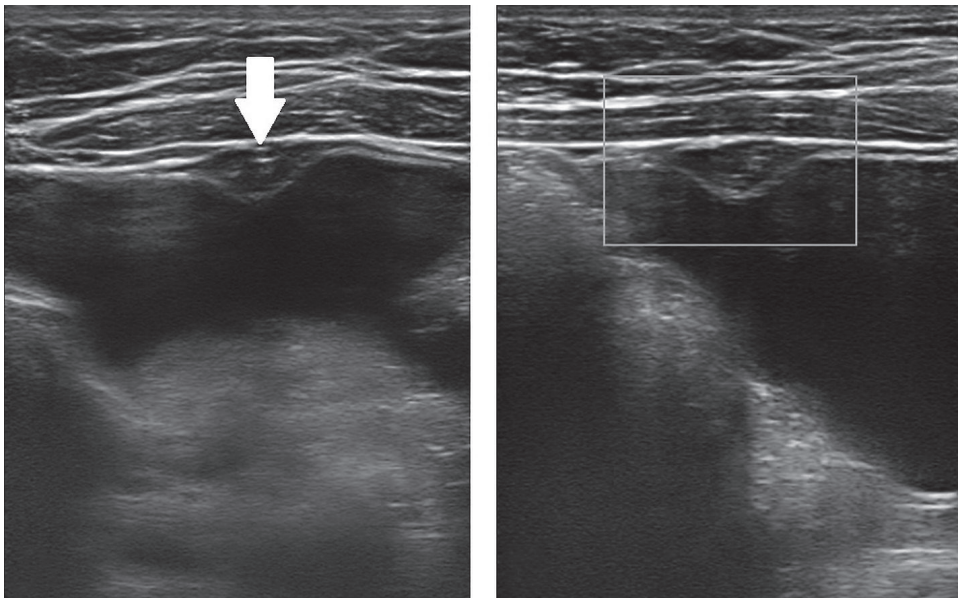

Figure 1: Bladder ultrasound detecting an oval image in the anterior wall of the bladder compatible with a remnant of the urachus (white arrow in A) without vascularization on Doppler study (B).

In autopsies, this condition is observed in only 3% of the general population. Due to either the absence of symptoms or the presence of nonspecific symptoms such as abdominal pain, urinary retention, and fluid drainage through the umbilical scar (Galati et al., 2008), and because it is a rare condition in the general population, the urachus remnant is most often detected incidentally during imaging studies or surgical procedures (Upadhyay and Kukkady, 2003).

There are five ways the urachus remnant can manifest itself (Upadhyay and Kukkady, 2003):

- Complete patent urachus
- Umbilical urachus sinus
- Alternating sinus
- Vesico-urachal diverticulum
- Urachal cyst

The completely patent urachus, also known as urachal fistula, is a tubular structure that connects the navel to the urinary bladder. The "umbilical sinus of the urachus" results in fusiform dilation of the urachus proximal to the navel, and when this dilation periodically empties (either into the urinary bladder or navel), it is referred to as an "Alternating Sinus". A vesico-urachal diverticulum occurs in the suprabladder portion of the urachus, causing the formation of a pouch from the anterosuperior portion of the urinary bladder. Lastly, the urachal cyst forms due to obliteration of the bladder and the umbilical end of the urachus (Buddha et al., 2019).

The increased availability and demand for medical imaging tests in everyday medical practice have made it more common to identify the urachus remnant as an incidental finding. However, several imaging techniques are useful for diagnosing this condition. These include ultrasonography (US), CT, MRI, voiding cystourethrogram, and cystogram. Generally, ultrasonography is initially used to identify and locate the structure, as it is easily accessible and cost-effective (Parada Villavicencio et al., 2016). CT and MRI are capable of assessing the extent of the disease and detecting any complications related to the urachus remnant (Parada Villavicencio et al., 2016; Buddha et al., 2019). Additionally, MRI plays an important role in staging urachal neoplasms. Finally, voiding cystourethrogram and cystogram are contrast-enhanced imaging tests that assist in the detection of vesico-urachal diverticulum and urachal cysts (Buddha et al., 2019).

The complications of the urachus remnant vary according to the age of the patient. In infants, the most common complications include infection of this structure, as reported in the case, and when associated with other changes of the genitourinary tract, such as vesicoureteral reflux, hypospadias, and stenosis of the meatus, among others. In adults, complications may include infection and the development of malignancy of the urachus remnant (Parada Villavicencio et al., 2016).

The choice of treatment for the urachus remnant primarily depends on the age and symptomatology of the patient. For patients under one-year-old, it is recommended to monitor the case and wait for spontaneous resolution, as many remnants of the urachus involute with age. Surgical excision of the structure may be considered for children or those with significant symptoms. In asymptomatic adults, prophylactic excision of the urachus remnant is typically recommended to prevent complications (Parada Villavicencio et al., 2016).

Conclusion

Although urachal anomalies are uncommon, it is important to recognize them. This recognition enables diagnosis in patients presenting with typical changes on imaging exams or symptoms associated with the condition. Early diagnosis is crucial to prevent complications, such as the development of malignancies involving this structure.

References

Buddha, S., Menias, C. O., Katabathina, V. S. (2019) Imaging of urachal anomalies. *Abdom. Radiol. (N. Y.)* **44(12)**, 3978–3989.

Galati, V., Donovan, B., Ramji, F., Campbell, J., Kropp, B. P., Frimberger, D. (2008) Management of urachal remnants in early childhood. *J. Urol.* **180(4 Suppl.)**, 1824–1826; discussion 1827.

Parada Villavicencio, C., Adam, S. Z., Nikolaidis, P., Yaghmai, V., Miller, F. H. (2016) Imaging of the urachus: Anomalies, complications, and mimics. *Radiographics* **36(7)**, 2049–2063.

Upadhyay, V., Kukkady, A. (2003) Urachal remnants: An enigma. *Eur. J. Pediatr. Surg.* **13(6)**, 372–376.

Prague Medical Report / Vol. 126 (2025) No. 3, p. 178–179

Instructions to Authors

Prague Medical Report is an English multidisciplinary biomedical journal published quarterly by the First Faculty of Medicine of the Charles University. Prague Medical Report (Prague Med Rep) is indexed and abstracted by Index-medicus, MEDLINE, PubMed, EuroPub, CNKI, DOAJ, EBSCO, and Scopus.

Articles issued in the journal

a) Primary scientific studies on the medical topics (not exceeding 30 pages in standardized A4 format – i.e. 30 lines and 60–65 characters per line – including tables, graphs or illustrations)
b) Short communications
c) Case reports
d) Reviews
e) Lectures or discourses of great interest
f) Information about activities of the First Faculty of Medicine and other associated medical or biological organizations

Layout of the manuscript

a) Title of the study (brief and concise, without abbreviations)
b) Information about the author(s) in the following form:
   - first name and surname of the author(s) (without scientific titles)
   - institution(s) represented by the author(s)
   - full corresponding (mailing) author's reference address (including first name, surname and scientific titles, postal code, phone/fax number and e-mail)
c) Abstract (maximum 250 words)
d) Key words (4–6 terms)
e) Running title (reduced title of the article that will appear at the footer (page break), not more than 50 typewritten characters including spaces)
f) Introduction
   - The use of abbreviations should be restricted to SI symbols and those recommended by the IUPAC-IUB. Abbreviations should be defined in brackets on first appearance in the text. Standard units of measurements and chemical symbols of elements may be used without definition.
g) Material and Methods
h) Results
i) Discussion
j) Conclusion
k) References
   - All the sources of relevant information for the study should be cited in the text (citations such as "personal communication" or "confidential data" are not accepted).
   - It is not permitted to cite any abstract in the References list.
   - References should be listed alphabetically at the end of the paper and typed double-spaced on separate pages. First and last page numbers must be given. Journal names should be abbreviated according to the Chemical Abstract Service Source Index. All co-authors should be listed in each reference (et al. cannot be used).
   - Examples of the style to be used are:
     Yokoyama, K., Gachelin, G. (1991) An Abnormal signal transduction pathway in CD4–CD8– double-negative lymph node cells of MRL *lpr/lpr* mice. *Eur. J. Immunol.* **21**, 2987–2992.
     Loyd, D., Poole, R. K., Edwards, S. W. (1992) *The Cell Division Cycle. Temporal Organization and Control of Cellular Growth and Reproduction.* Academic Press, London.
     Teich, N. (1984) Taxonomy of retroviruses. In: *RNA Tumor Viruses,* eds. Weiss, R., Teich, N., Varmus, H., Coffin, J., pp. 25–207, Cold Spring Harbor Laboratory, Cold Spring Harbor, New York.
     References in the text should be cited as follows: two authors, Smith and Brown (1984) or (Smith and Brown, 1984); three or more authors, Smith et al. (1984) or (Smith et al., 1984). Reference to papers by the same author(s) in the same year should be distinguished in the text and in the reference list by lower-case letters, e.g. 1980a, or 1980a, b.
l) tables, figures, illustrations, graphs, diagrams, photographs, etc. (incl. legends)

Technical instructions

a) Manuscripts (in UK English only) must be delivered in the electronic form via Online Manuscript Submission and Tracking system (http://www.praguemedicalreport.org/). In case of problems, contact the Prague Medical Report Office (medical.report@lf1.cuni.cz). The online submission has to

include the complete version of the article in PDF format, separately the manuscript as a MS Word file and a cover letter. The detailed version of the Instructions to Authors can be found at: http://www.praguemedicalreport.org/download/instructions_to_authors.pdf.

b) Text should be written in MS WORD only. We accept only documents that have been spell-checked with UK English as a default language.
c) Please, write your text in Times New Roman script, size 12, and line spacing 1.5.
d) Text should be justified to the left, with no paragraph indent (use Enter key only); do not centre any headings or subheadings.
e) Document must be paginated-numbered beginning with the title page.
f) Tables and graphs should represent extra files, and must be paginated too.
g) Edit tables in the following way: Make a plain text, indent by Tab (arrow key) all the data belonging to a line and finish the line by Enter key. For all the notes in table, use letter x, not *.
h) Make your graphs only in black-and-white. Deliver them in electronic form in TIFF or JPG format only.
i) Deliver illustrations and pictures (in black-and-white) in TIFF or JPG format only. The coloured print is possible and paid after agreement with the Prague Medical Report Office.
j) Mark all the pictures with numbers; corresponding legend(s) should be delivered in an extra file. Mark the position of every picture (photo) in the manuscript by the corresponding number, keep the order 1, 2, 3...

Authors' Declaration

The corresponding (or first author) of the manuscript must print, fill and sign by his/her own hand the Authors Declaration and fax it (or send by post) to the Prague Medical Report Office. Manuscript without this Declaration cannot be published. The Authors' Declaration can be found by visiting our web pages: http://pmr.lf1.cuni.cz or web pages of Prague Medical Report Online Manuscript Submission and Tracking system: http://www.praguemedicalreport.org/.

Editorial procedure

Each manuscript is evaluated by the editorial board and by a standard referee (at least two expert reviews are required). After the assessment the author is informed about the result. In the case the referee requires major revision of the manuscript, it will be sent back to the author to make the changes. The final version of the manuscript undergoes language revision and together with other manuscripts, it is processed for printing.

Concurrently, proofs are electronically sent (in PDF format) to the corresponding (mailing) author. Author is to make the proofs in PDF paper copy and deliver it back to the editorial office by fax or as a scanned file by e-mail. Everything should be done in the required time. Only corrections of serious errors, grammatical mistakes and misprints can be accepted. More extensive changes of the manuscript, inscriptions or overwriting cannot be accepted and will be disregarded. Proofs that are not delivered back in time cannot be accepted.

Article processing charge

Authors do not pay any article processing charge.

Open Access Statement

Copyright Statement

Editorial Office
Prague Medical Report
Kateřinská 32, 121 08 Prague 2
Czech Republic
e-mail: medical.report@lf1.cuni.cz
Phone: +420 224 964 570
Fax: +420 224 964 574